Activation mechanism of mixed-lineage-kinase-like proteins in plants

Inaugural Dissertation

Zur
Erlangung des Doktorgrandes
der Maththemetisch-Naturawissenschafttlichen Fakultaet
der Unievrsitaet zu Köln

vorgelegt von

Keiichi Hasegawa
Aus
Kobe, Japan

Köln
2023

Die vorliegende Arbeit wurde am Max Planck Institut für Pflanzenzüchtungsforschung in Köln Arbeitsgruppe Prof. Dr. Jijie Chai and Dr. Takaki Maekawa.

The work described in this thesis was conducted under the supervision of Prof. Dr. Jijie Chai and Dr. Takaki Maekawa at the Max Planck Institute for Plant Breeding Research

Referees/Gutachter: Prof. Dr. Jijie Chai

Prof. Dr. Bart Thomma

Chair of Defence/ Prüfungsvorsitz: Prof. Dr. Alga Zuccaro

Tag der letzten mündlichen Prüfung: 11.01.2023

Table of Contents

List of Abbreviations

Abbreviation	Full Description
2',3'-cAMP	Adenosine-2′, 3′-cyclic monophosphate
ADPr-ATP	ADP-ribosylated adenosine tri-phosphates
ADPr-ATP	ADP-ribosylated adenosine tri-phosphates
ADR1	Activated Disease Resistance 1
ALS	Amyotrophic Lateral Sclerosis
*At*MLKLs	Arabidopsis MLKLs
BAK1	Brassinosteroid Insenstive1-Associated receptor Kinase 1
cGMP	Guanosine-2′,3′-cyclic monophosphate
CNL	Coilded-coil NLR
cNMP	Cyclic Nucleotide MonoPhosphate
DAMP	Damage-Associated Molecular Patterns
diADPR	ADP-ribosylated ADPR
dOCRL	Drosophila Melanogaster orthologue of human oculocerebrorenal syndrome of Lowe
EDS1	Enhance Disease Susceptibility 1
EHM	ExtraHaustorial Membrane
ETI	Effector-Triggered Immunity
FLS2	FLagellin Sensing 2
MAMP	Microbe-Associated Molecular Patterns
MAPK	Mitogen-Activated Protein Kinase
MLKL	Mixed Lineage Kinase domain-Like
NAD	Nicotinamide Adenine Dinucleotide
Nec	Necrostatin
NLR	Nucleotide binding Leucine Rich repeats
NRG1	N-Requirement Gene 1
NSA	NecroSulfonAmide
PAD4	PhytoAlexin Deficient 4
PAMP	Pattern-Associated Molecular Patterns
PCD	Programmed Cell Death
PEG	PolyEthylene Glycols
Pep	Plant Elicitor Peptide
PepR	Pep-Receptor
PFD	Prion-Forimg Domain

PIP	PhosphatidylInositil Phosphate
pRib-AMP/ADP	2´-(5´´-phophoribosyl)-5 ádenosine mono-/di-phosphates
PRR	Pattern Recognition Receptors
PTI	Pattern-Triggered Immunity
PVX	Potato Virus X
R	Resistance
RBA1	Response to HopBA1
RIPK1	Receptor Interacting Protein Kinase-1
RIPK3	Receptor Interacting Protein Kinase-3
RK	Receptor Kinases
RLCK	Receptor-Like Cytoplasmic Kinase
RLP	Receptor-Like Proteins
RNL	RPW8-like coiled-coil NLR
ROQ1	Recognition of XopQ1
ROS	Reactive Oxygen Species
RPM1	Resistance to Pseudomonas syringae pv. maculicola 1
RPP1	Recognition of Peronspora parasitica 1
RPS2	Resistance to Pseudomonas syringae 2
RPS5	Resistance to Pseudomonas syringae 5
RPW8.2	Resistance to Powdery Mildew 8.2
SAG101	Senescence-Associated Gene 101
SNC1	Suppressor of npr1-1 constitutive 1
TIR	Toll/Interleukin-1 Receptor
TLR5	Toll-Like Receptor 5
TNL	TIR NLR

Abstract

Plants and animals have similarities in their immune system. A new protein family was reported to be conserved across seed plants that structurally resembles animal mixed lineage kinase domain-like (MLKL), a mediator of necroptotic cell death. The *Arabidopsis* MLKLs (*At*MLKLs) play a role in disease resistance mediated by TIR-type nucleotide binding–leucine-rich repeats (NLRs). Cryo-EM structures of *Arabidopsis* MLKLs (*At*MLKLs) reveal a tetrameric configuration in contrast with the monomeric structure of animal MLKL. To understand the biological meaning of the *At*MLKL tetramer, I performed a structure-guided study. Together with a newly established disease resistance assay in *N. benthamiana*, the data imply that the *At*MLKL tetramers represent an auto-repressed conformation of plant MLKLs and the exposure of the N-terminal HeLo-domain from the tetramer is an important activation step, which could be mediated by a phosphorylation in the activation loop of the pseudokinase domain. To elucidate the genetic relationship between helper NLRs and plant MLKLs, the disease resistance activities of *At*MLKL1 variants were examined in helper NLR null background and *eds1 pad4 sag101* null background. The plant MLKL-mediated immunity was partially retained in the *helperless* mutant background but no longer retained in the *eds1 pad4 sag101* mutant in *N. benthamiana*. It was found that the *At*MLKL1 HeLo domain elicits Ca^{2+} influx in human cell line and in *N. benthamiana*. These data demonstrate that plant and animal MLKLs commonly utilize the N-terminal HeLo-domain as a signaling domain for immune responses. Furthermore, to study the activation step, I purified N-terminal HeLo domain of *At*MLKL1 and a gain-of-function variant of *At*MLKL1 carrying a phosphomimetic mutation in the activation loop of the pseudokinase domain. The purified recombinant N-terminal HeLo domain of *At*MLKL1 autonomously formed a higher-order oligomer with a 10 nm ring-like structure. Additionally, the purified recombinant phosphomimetic variant of *At*MLKL1

retained a tetrameric configuration similar as purified recombinant *At*MLKL1 wild-type, implying that *At*MLKL does not change it conformation via phosphorylation in the pseudokinase domain upon activation unlike animal MLKL.

Zusammenfassung

Pflanzen und Tiere ähneln sich in ihrem Immunsystem. Zuvor wurde herausgefunden, dass eine (neue) Proteinfamilie in Samenpflanzen konserviert ist, die strukturell tierischen MLKL (mixed lineage kinase domain-like) Proteinen ähnelt, welche nekroptotischen Zelltod vermitteln. Die MLKLs von *Arabidopsis* (*At*MLKLs) spielen eine Rolle bei der Krankheitsresistenz, die durch nukleotidbindende leucinreiche Wiederholungen (NLRs) vom TIR-Typ vermittelt wird. Im Gegensatz zur monomeren Struktur von tierischen MLKLs zeigen Cryo-EM-Strukturen von Arabidopsis-MLKLs (*At*MLKLs) eine tetramerische Konfiguration. Um die biologische Bedeutung des *At*MLKL-Tetramers zu verstehen, habe ich eine strukturgeleitete Studie durchgeführt. Zusammen mit einem neu etablierten Krankheitsresistenz-Assay in *N. benthamiana* deuten die Daten darauf hin, dass die *At*MLKL-Tetramere eine autorepressive Konformation der pflanzlichen MLKLs darstellen und die Freilegung der N-terminalen HeLo-Domäne des Tetramers ein wichtiger Aktivierungsschritt ist, der durch eine Phosphorylierung in der Aktivierungsschleife der Pseudokinase-Domäne vermittelt werden könnte. Um die genetische Beziehung zwischen Helfer-NLRs und Pflanzen-MLKLs aufzuklären, wurde die Krankheitsresistenzaktivität von *At*MLKL1-Varianten im Helfer-NLR-Null-Hintergrund und *eds1 pad4 sag101*-Null-Hintergrund untersucht. Die durch Pflanzen-MLKL vermittelte Immunität blieb im Hintergrund der helperless Mutante teilweise erhalten, aber nicht mehr in der *eds1 pad4 sag101* Mutante in *N. benthamiana*. Es wurde festgestellt, dass die *At*MLKL1 HeLo-Domäne in der menschlichen Zelllinie und in *N. benthamiana* einen Ca^{2+}-Einstrom auslöst. Diese Daten zeigen, dass sowohl planzliche als auch und tierische MLKLs die N-terminale HeLo-Domäne als Signaldomäne für die Immunantwort nutzen. Desweiteren, um den Aktivierungsschritt zu untersuchen, isolierte ich die N-terminale HeLo-Domäne von *At*MLKL1 sowie eine funktionsgewinnede variante von *At*MLKL1, welche

eine phosphomimetische Mutation in der Aktievierungsschleife der Pseudokinasedomain trägt. Die aufgereinigte, rekombinante N-terminale HeLo-Domäne von *At*MLKL1 alleine bildet ein höher geordnetes Oligomer mit einer 10 nm ringförmigen Struktur. Desweitern, behält die rekombinante, phoshomimetische Variante von *At*MLKL1, wie auch die aufgereingte, rekombinante Wildtyp-Variante von *At*MLKL1, eine tetramere Konfiguration. Dies impliziert, dass *At*MLKL im Gegensatz zu tierischem MLKL seine Konformation nicht über die Phosphorylierung der Pseudokinasedomäne nach Aktivierung ändert.

Preamble

Part of this thesis has been taken from manuscripts submitted or in preparation, as listed in the 'Manuscripts for publication' section. Figures that overlap with these papers have been noted in the figure legends to clarify my contribution to the two manuscripts referred to as the PVX manuscript and the MLKL manuscript. Some sections have been taken with some modifications from the papers listed above. Most of the experiments and analyses described in this paper were carried out by myself. Those carried out by others are listed in the "9. Contributions" section.

1. Introduction

1. Introduction

1.1. Plant immune system in multiple layers

Plants have immune system in multiple layers to combat against invading pathogens. Higher plants possess an enormous number of cell-surface and intracellular immune receptors to perceive a variety of immunogenic signals associated with pathogen infections[1,2]. First layer of the plant immunity is pattern-triggered immunity (PTI) initiated from the recognition of highly conserved molecules such as pathogen/microbe -associated molecular patterns (PAMPs/MAMPs) or host-derived damage-associated molecular patterns (DAMPs) by pattern recognition receptors (PRRs) located in the surface of the plant cell[3–5]. Pattern recognition receptors consists of receptor-like proteins (RLPs) and receptor kinases (RKs). And the second layer is effector-triggered immunity (ETI) induced by the recognition of pathogen effectors delivered into the plant cells by intracellular innate immune receptors called nucleotide-binding leucine-rich repeat receptors (NLRs)[6]. NLRs specifically sense the more variable pathogen effector proteins that are delivered into the plant cell. Based on the sequence of N-terminal domain, plant NLRs are classified into three groups: coiled-coil (CC) NLRs (CNLs), Toll/ interleukin-1 receptor (TIR) NLRs (TNLs), and the RPW8-like coiled-coil (CC_R) NLRs (RNLs)[7–9].

1.2. PAMP-triggered immunity (PTI)

Both plants and animals have evolved PAMP-triggered immunity (PTI) as the first layer of defence system against pathogens, suggesting the importance of this system in restriction of pathogen proliferation[10]. For example, flagellin, a representative PAMP molecule from bacterial pathogens, is recognized by both the plant receptor kinase (Flagellin Sensing 2 (FLS2) and animal Toll-like receptor 5 (TLR5)[5,11–13]. In plants, FLS2 binds to the N-terminal 22 amino acid residues of flagellin (flg22) in Gram-negative bacteria[14]. The recognition of flg22 induces the dimerization and rapid phosphorylation of FLS2 and BRASSINOSTEROID

INSENSITIVE 1-associated receptor kinase 1 (BAK1), accompanied by the phosphorylation of BIK1, a receptor-like cytoplasmic kinase (RLCK)[15–19]. This activated receptor complex initiates a rise in intracellular calcium levels, provokes the production of reactive oxygen species (ROS), fosters the phosphorylation of mitogen-activated protein kinases (MAPKs), stimulates callose deposition, and orchestrates a transcriptional reconfiguration within the cell. Consequently, this orchestrated sequence culminates in heightened resistance against pathogenic agents[20–23]. Furthermore, plants recognize damage-associated molecular patterns (DAMPs), which are released from the plant cell itself as the result of the degradation of plant organelles following the pathogen invasion[5,24]. For instance, pathogens damage the plant tissues through using their cell-wall-degrading enzymes and toxins, consequently releasing the fragments from the plant cell wall, extracellular ATP, and nicotinamide adenine dinucleotide (NAD)[25]. The molecules originating from the host plants function as damage-associated molecular patterns (DAMPs), thereby initiating immune responses. Nevertheless, pathogens also possess a mechanism to antagonize pattern-triggered immunity (PTI), enabling the deployment of their effectors upon infiltrating their host plants. The constituents within the PTI signaling cascade within the host plants become subjects of assault by diverse virulence effector proteins, which compromises plant immune system and enhances bacterial virulence[6]. For example, a type III effector originating from *Pseudomonas syringae*, namely AvrPtoB, degrades FLS2 via the 26S proteasome [26].

1.3. Effector-triggered immunity (ETI)

To counter the pathogen virulent activity, plants have evolved to recognize the effectors in cytoplasmic space. This recognition of effectors is performed by the resistance (R) proteins, which can either directly or indirectly detect the effectors when they enter into the host plant cell. This recognition of pathogen effectors initiates the second layer of plant immunity called effector-triggered immunity (ETI). ETI in plants is often accompanied with strong

programmed cell death (PCD) at the pathogen infection site, and the phenotype is called the hypersensitive response[27]. CNLs and TNLs sense the pathogen effectors to activate the effector-triggered immunity. Recent structural and electrophysiology study revealed that activated ZAR1, a type of CNLs in *Arabidopsis thaliana*, functions as calcium channels after dynamic conformational change from a monomeric state to the activated pentameric funnel-like structure, which is termed as a "resistosome"[28,29]. The ZAR1 resistosome revealed the very N-terminal domain as an executor domain for cell death[29]. This activation model proposed for CNLs is generally applicable to the activation of the other types of NLRs[30]. The bioinformatics analysis revealed that a part of NLRs possess a functionally conserved motif called MADA motif in α1 helix which is essential for cell death, suggesting that this activation model proposed for CNLs is generally applicable to the other NLRs[30]. Indeed, the cryo-electron microscope analysis of the wheat CNL Sr35 in complex with the effector AvrSr35 of the wheat stem rust pathogen revealed the conservation of resistosome pentameric structure in crops[31]. This conserved funnel-shaped resistosome directly inserts into the membranes forming a cation-selective channel with the inner diameter of approximately 1 nm that can pass cation channel such as calcium ion in a non-selective manner[31]. The calcium influx triggered by the resistosome is indispensable for cell death activity suggested by interference of calcium channel activity by the approaches using chemical inhibitors and structure-guided mutagenesis[28]. CNLs such as RPM1 (Resistance to *Pseudomonas syringae* pv. maculicola 1), RPS2 (Resistance to *Pseudomonas syringae* 2) and RPS5 (Resistance to *Pseudomonas syringae* 5) requires NDR1, which implies that calcium channel formed by activated CNLs might not the final executor of cell death[32–34].. TNL-triggered immunity is initiated from the recognition of cognate effectors by TNL receptors. Recent cryo-electron microscope analysis of RPP1 (Recognition of *Peronospora parasitica* 1) and ROQ1 (Recognition of XopQ 1) revealed that effector recognition activates TNLs to form a tetrameric resistosome structure[35,36].

This TNL resistosome function as NADase holoenzyme and the NADase activity is required for cell death activity[35,37,38]. In downstream of TNLs, it has been elucidated that the two branches of EDS1 (Enhanced disease susceptibility1)-SAG101 (Senescence-Associated Gene 101)-NRG1 (N requirement gene 1) and EDS1-PAD4 (Phytoalexin Deficient4)-ADR1 (Activated Disease Resistance 1) pathway function in a cooperative manner[39,40]. The recent two publications elucidated that effector induced-TNL resistosome degrades NAD to produce small molecules, and the small molecules act as a molecular glue between EDS1 and helper NLRs to activate the downstream components of TNL pathway: diADPR (ADP-ribosylated ADPR)//ADPr-ATP (ADP-ribosylated adenosine tri-phosphates) induces the direct interaction between EDS1-SAG101 and NRG1 while pRib-AMP/ADP (2′-(5′′-phosphoribosyl)-5′-adenosine mono-/di-phosphate) induces the direct interaction between EDS1-SAG101 and ADR1[41,42]. *Arabidopsis* has helper NLRs, ADR1, ADR1-L1, and ADR1-L2 induce SA biosynthesis[43,44]. In addition to the NADase activity of TNL resistosome, it was recently reported that TIR domains form filament structure to exhibit non-specific DNA/RNase activity, which produces 2',3'-cAMP (Adenosine-2',3'-cyclic monophosphate)/cGMP cGMP (Guanosine- 2', 3'- cyclic monophosphate) to induce cell death, however, the downstream signaling component remains unknown[45].

The concept of two-layered plant immune system, namely PTI and ETI, has advanced the understanding of plant innate immunity. However, the dichotomy between PTI and ETI as well as PAMPs and effectors is not clear in several cases suggested by the identification of different immunogenic ligand and receptor pairs[46]. Furthermore, the rice Xa21 protein, which is localized at the plasma membrane, elicits immune responses akin to effector-triggered immunity (ETI), suggesting that PTI and ETI responses are overlapping[47]. Indeed, recent studies indicate that PTI and ETI pathways function together for antimicrobial defences[48–50].

Additionally, the conceptual framework of PTI/ETI proves inadequate for comprehending the intricacies of cell non-autonomous signaling. This limitation of the PTI/ETI has provoked the concept that the plant immune system can sense pathogen by secretion and recognition of danger molecules for cell-cell communication[5,25,46,51].

1.5. Host cell death and pathogen growth restriction in plant innate immune system

Recognition of biotrophic or hemibiotrophic pathogens leads to inhibition of pathogen growth, which is often accompanied with the cell death called hypersensitive response (HR), a form of programmed cell death localized at the site of attempted pathogen invasion. Thus, HR is regarded as the hallmark of the plant innate immune responses to block pathogen colonization[52]. The HR cell death phenotypes typically associate with multiple morphological changes that includes similar phenotypes observed in animal cell death and the ones specific to plants such as cytoplasmic shrinkage, chromatin condensation, mitochondrial swelling, ROS production, vacuolization and chloroplast disruption[53]. For example, a type of *Arabidopsis* CNL, activated ZAR1 induces alterations of vacuolar structures and ROS generation before the cell death takes place[28]. However, it is worthwhile to note that pathogen growth inhibition is not accompanied with host cell death in many cases. For example, propagation of potato virus X is restricted without apparent cell death phenotype when the NLR Rx recognizes the coat protein of potato virus X [54].

1.6. Cell death and pathogen growth restriction assays to examine plant innate immunity

To assess disease resistance activity of NLRs, bacterial viability assays have been employed in combination with the transient *R* gene expression in *Nicotiana benthamiana*[55]. Bacterial viability assays however, require a series of multiple experimental procedures, including i) agroinfiltration, ii) pathogen infection, iii) bacteria count, hindering high-throughput examination of *R* gene functions. PVX (Potato virus X) is a single-stranded RNA virus[56] and

expression of full-length PVX cDNA via agroinfiltration-mediated gene expression allows PVX replication in *Nicotiana* species[57]. Insertion of a cDNA of fluorescent protein under a duplicated copy of the viral coat protein promoter enables the visualization of PVX replication in plants[58]. Contrasting to the bacterial viability assays, in which the step of pathogen infection takes place a few days after agroinfiltration, the steps of agroinfiltration and pathogen infection can be performed simultaneously in the PVX disease resistance assay[59], offering a minimal experimental procedure. Unlike bacterial pathogens, PVX proliferation in *N. benthamiana* is not restricted by the intrinsic activity of the EDS1 signaling pathway shown by a virus-induced *NbEDS1* gene silencing[58]. This feature increases the sensitivity to capture a milder disease resistance activity of *R* genes, as contribution of the basal immunity via the *Nb*EDS1 pathway to PVX is negligible. PVX proliferation in *N. benthamiana* has been examined by the quantifying the amount of viral RNA[58], viral coat protein[59], or an intensity quantification of fluorescent protein from images of leave epidermis[59]. However, some involve cumbersome procedures or do not assess the amount of virus inside the leaves.

1.7. MLKL proteins play a central role in necroptosis

1.7.1 Necroptosis

Necroptosis is the most well-studied regulated necrosis[60,61]. In certain types of cells, necroptosis-like cell death occurs compensatively when the TNFα-stimulated exogenous apoptotic pathway is inhibited, and in 2005, Junying Yuan and colleagues identified an inhibitor of necroptosis and named it Necrostatin (Nec)-1[62]. Furthermore, the identification of a serine threonine kinase called receptor interacting protein kinase-1 (RIPK1) as one of the target factors of Nec-1 led to a breakthrough in the elucidation of its molecular mechanism[60,61]. A kinase called RIPK3, which is homologous to RIPK1, and its substrate, mixed lineage kinase like (MLKL), are essential for the execution of necroptosis[63]. Recent analysis of tissue-specific RIPK1 gene-deficient mice revealed that RIPK1, which has been thought to be involved in

necroptosis, can either promote or inhibit necroptosis. During necroptosis, a protein complex called the Necrosome is formed that contains RIPK1, RIPK3, and MLKL. A model has been proposed in which RIPK3, multimerized and activated by phosphorylation, phosphorylates MLKL, which induces plasma membrane rupture via the formation of membrane pores on the plasma membrane or the orientation of ion channels to the plasma membrane[63]. In the nervous system, it has been suggested to be involved during ischemia-reperfusion injury and in pathological conditions such as ALS (amyotrophic lateral sclerosis)[62,64,65]. Necroptosis execution occurs via a variety of pathways, but is closely related to the regulation of apoptosis. Upon stimulation of extrinsic apoptotic pathway activation, apoptosis is executed if caspase-8 and FADD are present. Activated caspase-8 is considered to block necroptosis induction by cleaving and inactivating molecules involved in necroptosis induction, such as RIPK1, RIPK3. Conversely, when caspase-8 activity is lost due to compound- or virus-derived inhibitory proteins or genetic defects, necroptosis is executed. Given that caspase-8 serves as the pivotal suppressor of necroptosis, necroptosis has been posited as an emergent cellular backup mechanism, functioning as a contingency strategy when the apoptotic pathway activated by death receptors could not exterminate the infected cells. Similarly, RIPK3-MLKL-dependent necroptosis may also occur by the innate immune pathways Toll-like receptor (TLR) 4 and TLR3, suggesting cross-talk with pyroptosis. Thus, the execution of necroptosis is highly cell type- and situation-dependent[63].

1.7.2 Inflammatory roles of MLKL-induced necroptosis

MLKL (Mixed-lineage Kinase Domain-like) protein is conserved in animals and plays an essential role in execution of necroptosis, a type of programmed cell death. Necroptosis is important for the host defence against virus and intracellular bacteria[66]. For example, necroptosis plays a role in removal of simplex virus, cytomegalovirus, vaccinia virus, and influenza A virus[67–70]. Furthermore, MLKL inhibits growth of enteropathogenic bacteria,

Listeria monocytogenes in the gastrointestinal tract by direct interaction of MLKL with the bacteria in the cytosol without causing the host cell death[71]. Additionally, there are several reports on positive regulatory effects of MLKL in autoinflammatory diseases. For example, inhibition of necroptosis negatively affects psoriatic inflammation[72]. Particular homozygous mutations in the *Mlkl* gene leads to a lethal phenotype in mice[73]. These multiple evidences endow the essential role of MLKL-induced necroptosis for inflammation.

1.7.3 Activated MLKL forms a pore or a channel

Molecular mechanism of necroptosis has been studied for decades. In necroptosis, MLKL is activated by the upstream kinase, RIPK3, via phosphorylation of the activation loop of its pseudokinase domain to induce conformational change from a monomer to tetramer[74–77]. This oligomerized MLKL permeabilizes the plasma membrane via N-terminal HeLo domain, leading to cell death[78]. Many research groups have worked on how MLKL is activated at the plasma membrane, however, it still remains unclear whether MLKL protein forms a pore or a channel[79]. Multiple research groups report that MLKL permeabilizes the plasma membrane by forming a pore in a phosphatidylinositolphosphate-dependent manner[80,81]. A recent study suggested that MLKL forms different sizes of pores with inner diameters of around 4 nm in necroptotic cell death stimulated by polyethylene glycols (PEGs)[82]. However, in a contradictory manner, electrophysiological studies report that MLKL is a cation-selective channel that preferentially passes Mg^{2+}, Na^{+}, and K^{+}, over Ca^{2+} but does not pass Cl^{-} even though the pore should pass the ions in a non-selective manner[83,84]. Sodium influx was also observed in necroptosis but not in apoptosis[85]. Indeed, the importance of cation permiabilization is supported by several studies. Na^{+} influx was observed in necroptosis but not in apoptosis[85]. Also, calcium influx was reported to be necessary for necroptosis induced by TRPM7[86] although another study denied the requirement of calcium influx for necroptosis

by suggetsing that the smac mimetic treatment might induce observed calcium influx[82]. Although the function at the plasma membrane is unclear, the MLKL-mediated ion transport is considered to cause The unique explosion-like morphology[83,87].

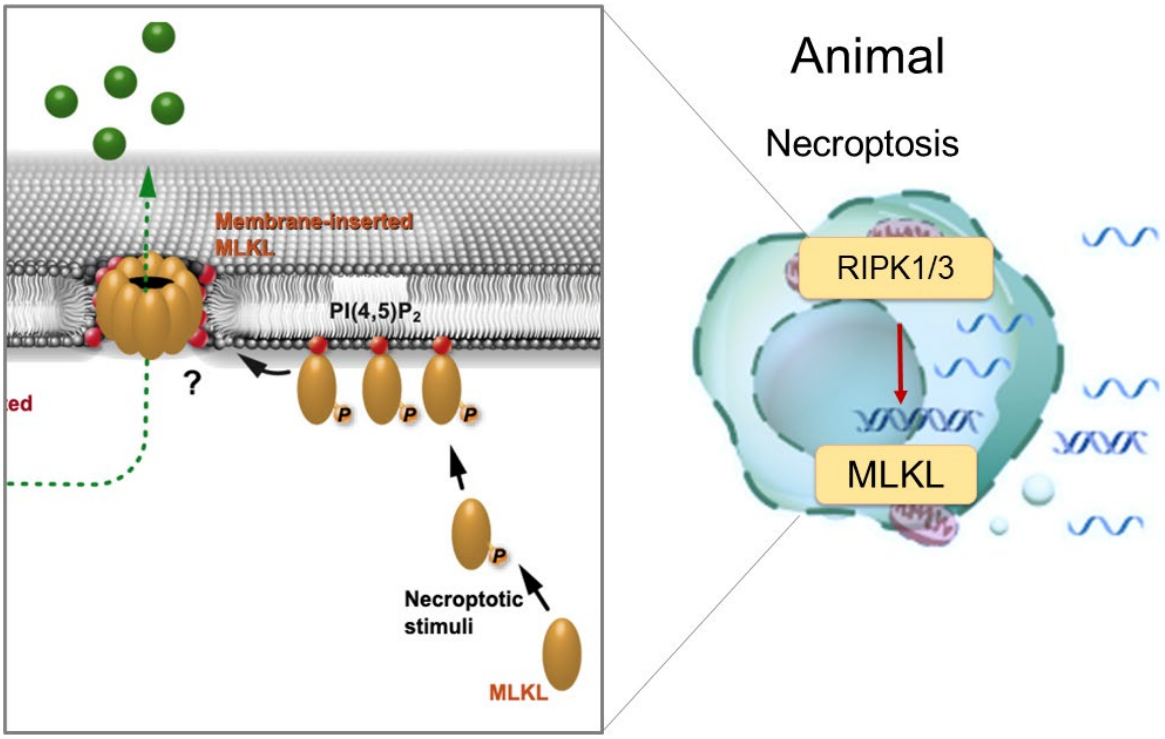

Figure 1. Proposed activation model of animal MLKL, a mediator of necroptosis in animals

1.7.4 The oligomeric state of activated MLKL

The oligomeric state of the activated MLKL during necroptosis has long been controversial. MLKL protein forms oligomers including trimers, tetramers, hexamers, and higher-order oligomers during necroptosis[77,78,85,86,88–90] while one study reveals disulfide-bond dependent amyloid polymer formation[89]. In line with this, necrosulfonamide (NSA), a pharmacological inhibitor of necroptosis, directly binds to human MLKL by forming covalent bond with its Cysteine 86 residue, supporting the significance of disulfide bond-mediated oligomer formation of MLKL in necroptosis[75]. To provide an integrative view of necroptotic cell death execution at the plasma membrane, high-resolution structure of the activated MLKLs in a membrane-bound state is warranted.

1.8. HeLo domain containing proteins in plants

The helper NLRs, N REQUIREMENT GENE1 (NRG1) and ACTIVATED DISEASE RESISTANCE1 (ADR1), are classified as the HeLo/RPW8-like coiled-coil (CC_R) NLRs (RNLs). This CC_R domain was discovered in *Arabidopsis* RESISTANCE TO POWDERY MILDEW 8[91]. The atypical disease resistance protein Resistance to Powdery Mildew 8.2 (RPW8.2) that does not have the canonical effector-sensing domain accumulates around the extrahaustorial membrane (EHM) to confer disease resistance[92]. Additionally, purified recombinant protein of a RPW8 homolog, $HR4^{Fei-0}$, forms an oligomer without auxillary proteins in size-exclusion analysis[93]. Furthermore, activated NRG1.1 oligomerizes in the plasma membrane as puncta, and conferred cytoplasmisc calcium ion flux in plant and human cells[94]. Thus, the pore-forming activity at the membrane might be the conserved mechanism of the HeLo/CC_R domain- containing protein. However, how the HeLo/CC_R domain- containing protein executes cell death in atomic details remains unclear as the no structure of the HeLo/CC_R domain- containing protein at the plasma membrane is available.

1.9. HeLo domain containing proteins in fungi

Proteins containing the HeLo domain can also be found in fungi. The most representative proteins containing the HeLo domain in fungi are the Het-S/Het-s proteins that is involved in self-incompatibility in a filamentous fungi, *P. anserina*[95]. The Het-S protein is composed of the two domains, the N-terminal HeLo domain and a C-terminal amyloid, Prion-Forming Domain (PFD). HET-s is a loss-of-function variant of Het-S with a mutation in the N-terminal helical HeLo domain of Het-S. These paired proteins determine the allelic specificity. When the Het-S and the HET-s interacts with each other, 21-amino acid repeat motifs in the C-terminal PFD provokes the fibrillar β-sheet amyloid formation. The amyloid formation of Het-S PFD serve as a structural template for the PFD of HET-S during the cell death reaction and causes the release of an N-terminal transmembrane a-helix, which attacks the plasma membrane[96–98]. *In-vitro* study revealed that the N-terminal domain of HET-S has an inhibitory effect on prion-formation in both cis on its own PFD and in trans on HET-s prion propagation[97]. Crystal structure of the N-terminal domains of Het-S and Het-s revealed that both HeLo domain of Het-S and Het-s self-dimerize, suggesting the conserved self-oligomerization activity of N-terminal HeLo domain across the organisms[97]. Also, the isolated N-terminal HeLo domain of Het-S without the presence of Het-s exhibits liposome leakage activity, suggesting the capability of Het-S self-activation in the absence of Het-s seed prion to some extent although the C-terminal PFD region of Het-s appear to facilitate the HET-S activation[98]. However, the activated form of Het-S at the plasma membrane remains unclear.

1.10. Discovery of plant MLKL proteins - Another player in TNL-triggered immunity

Recently, another HeLo domain-containing protein called plant MLKL (Mixed-lineage Kinase Domain-like) protein was reported to be involved in TNL-triggered immunity[99]. The N-terminal RPW8-like coiled-coil (CC_R) domain of RNLs is structurally and functionally similar to the HeLo domains of animal MLKLs[8,93,96,100,101]. Plants and animals have similarities in their

immune system. Recently, a new protein family conserved across seed plants that structurally resembles animal mixed lineage kinase domain-like (MLKL), a mediator of necroptotic cell death was reported. The *Arabidopsis* MLKLs (*At*MLKLs) play a role in disease resistance mediated by TIR-type nucleotide binding-leucine-rich repeats (NLRs) but not CNL-triggered immunity[99]. However, the genetic relationship between *At*MLKLs and helper NLRs in TNL-triggered immunity remains unclear. Cryo-EM structures of *Arabidopsis* MLKLs (*At*MLKLs) reveal a tetrameric configuration in contrast with the monomeric structure of animal MLKL. In tetrameric structure, N-terminal HeLo domain was sequestered inside, suggesting that plant MLKL tetramer is an auto-inhibited form. However, how plant MLKL is derepressed from auto-repressed form to activated form to induce immunity and the genetic relationship between the plant MLKL and helper NLRs in TNL-triggered immunity remains unclear[99].

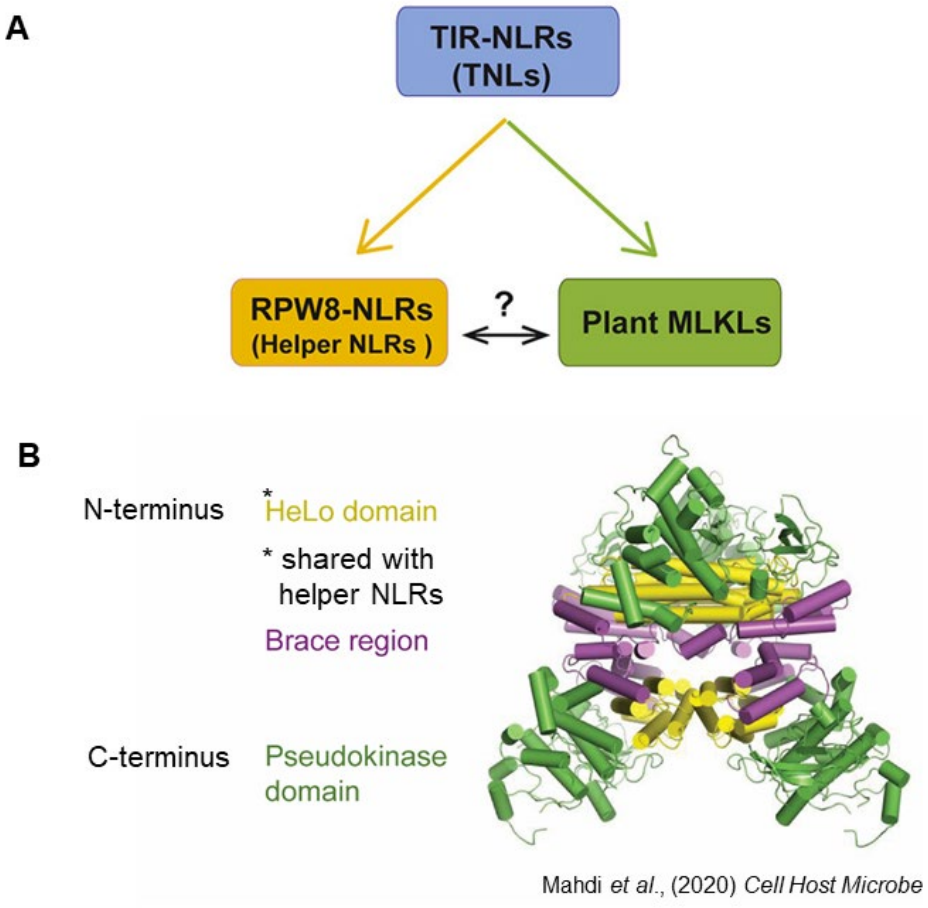

Figure 2. Key questions in plant MLKL-mediated immunity addressed in this study

(**A**) Plant MLKL and helper NLRs are downstream components of TNLs, however, the genetic relationship between plant MLKLs and helper NLRs remained unclear.

(**B**) The Cryo-EM structure of *At*MLKL tetramer may represent its auto-repressed conformation, however, the biological meaning of *At*MLKL tetramer remained unclear.

The figures were adapted from Mahdi et al[99].

1.11. Research aims

The four research objectives (A)-(D) below were addressed in my doctoral thesis.

(A). Establishment of the quantification system of the disease resistance activity

PVX disease resistance assay offers a high operational efficiency, however, the assay still involves laborious procedures or some do not assess the amount of virus inside the leaves. Thus, I aimed at developing a simple plate reader-based PVX assay without the use of western blotting.

(B). The biological meaning of plant MLKL tetramer

Cryo-EM structure of plant MLKL tetramer suggested that N-terminal domain plant MLKL tetramer is an auto-inhibited form. However, it remains unclear how plant MLKL is activated and whether plant and animal MLKL shares the common biochemical mechanism to execute cell death/immune responses. I performed structure-guided approaches to examine the biological meaning of plant MLKL tetrameric structure.

(C). Genetic analysis of plant MLKL proteins

The *Arabidopsis* MLKLs preferentially contribute to TNL- but not CNL-triggered immunity[99]. However, the genetic relationship between *At*MLKLs and helper NLRs in TNL-triggered immunity remains unclear. Thus, I aimed at the genetic dissection of *At*MLKLs in TNL-triggered immunity.

(D). What is the activated plant MLKL forms in the membrane?

The structural information of HeLo-domain containing protein including animal MLKL, fungal Het-S/Het-s, plant helper NLRs and RPW8 in lacking, which hampers our precise understanding of how HeLo domain-containing proteins confer immunity in atomic resolution across the species. Thus, I aimed at structural reconstitution of the plant MLKL HeLo domain oligomer to provide the structural insight into the HeLo domain-containing proteins at the plasma membrane and how cell death is executed.

2. Results

2. Results

2.1. Optimized PVX-based disease resistance assay reveals disease resistance activity of cell death deficient RBA1 C83A variant

To quantify *Potato virus X* (PVX)-produced YFP in *N. benthamiana* leaf extracts, we sought to optimize a fluorescence plate reader-based measurement (Figure 3A), which is simpler than quantification by Western blot. Briefly, in this method, agrobacteria carrying the PVX-YFP binary vector and agrobacteria carrying a resistance gene were co-infiltrated into *N. benthamiana* leaves. Four days after infiltration, leaf discs were collected from the infiltrated areas using a biopsy punch. The leaf protein extracts were used to measure YFP intensity. First, I determined the emission spectra of leaf extracts containing PVX-YFP or PVX without fluorescent protein (Figure 3B). The result showed that the PVX-produced YFP was in good agreement with the canonical emission spectrum of YFP in the leaf extract, and PVX replication in leaves did not produce fluorescence overlapping with the YFP spectrum (Figure 3B). The YFP intensity of a dilution series using a leaf protein extract from non-transformed leaves showed that this method has a high dynamic range with a linear correlation between fluorescence and dilution factor, and that a detergent, Triton X-100, can be omitted from the extraction buffer (Figure 3C). Furthermore, the quantified YFP fluorescence intensities in the plate reader-based measurement corresponded to some extent with the fluorescence images (Figure 3D). Consistent with the previous study (Peart et al., 2002), PVX-YFP proliferation was comparable in wild type and *eds1 pad4 sag101a sag101b* mutant of *N. benthamiana* (Figure 3E). Co-expression of a wheat NLR, Sr35 and its cognate effector, AvrSr35 (Förderer et al., 2022), caused host cell death in *N. benthamiana* in the presence of PVX-YFP (Figure 3F), suggesting that agrobacterium-mediated delivery of PVX-YFP T-DNA does not suppress NLR-induced host cell death. Furthermore, the very low YFP intensity (average intensity ± standard error = 1991 ± 402, n=4), which is nearly equivalent to the YFP intensity of leaf

protein extract from non-transformed leaves (Figure 3C) indicates that host cell death does not result in the production of metabolites that show autofluorescence in the YFP assay.

An *Arabidopsis* R protein, RBA1 (Response to HopBA1), which possesses a Toll/ interleukin-1 receptor like domain (TIR domain) induces host cell death upon transient overexpression in *N. benthamiana*[45]. The TIR domain of RBA1 contains NADase and nuclease activities, which are responsible for the generation of pRib-AMP/ADP (2′-(5′′-phosphoribosyl)-5′-adenosine mono-/di-phosphate) and diADPR (ADP-ribosylated ADPR)/ADPr-ATP (ADP-ribosylated adenosine tri-phosphates), and cyclic nucleotide monophosphates (cNMPs) such as 2′,3′-cAMP (Adenosine-2',3'-cyclic monophosphate)/cGMP (Guanosine- 2', 3'- cyclic monophosphate), respectively[38,45,102]. The two enzymatic activities of RBA1 require either of two catalytic residues, namely Cys83 and Glu86. The RBA1 Cys83, which is a highly conserved among TIR-containing proteins, is responsible for the nuclease activity but not for the NADase activity. In contrast, the RBA1 Glu86 is required for both catalytic activities of RBA1. The NADase activity of RBA1 alone is not sufficient for RBA1 cell death in *N. benthamiana*, because the RBA1(C83A) variant, which lacks the nuclease activity significantly loses cell death induction in *N. benthamiana* upon transient expression[45]. However, it remains unknown whether the C83A substitution in RBA1, which impairs cell death induction, also impairs disease resistance activity.

To address this question, I used the PVX-YFP-based assay to examine the disease resistance activity of the RBA1(C83A) variant and the RBA1 (E86A) variant as a control. Interestingly, we found that the RBA1 (C83A) variant retained disease resistance activity as wild-type RBA1, whereas the RBA1 (E86A) barley showed disease resistance activity to PVX (Figure 3G). These data suggest that the 2′,3′-cAMP/cGMP synthase activity (i.e., nuclease activity) of RBA1 is required for host cell death but the remaining NADase activity is sufficient to confer immunity to PVX. Furthermore, the disease resistance activity of the RBA1(C83A) variant was

significantly impaired in the *Nbepss* mutant background (Figure 3G), consistent with the model that the TIR NADase products confer immunity via the EDS1 pathway.

2. Results

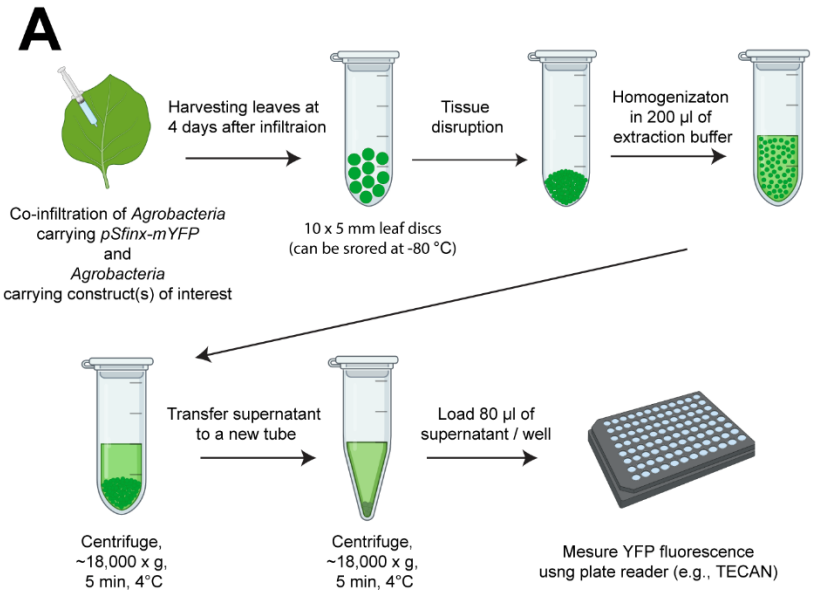
A
Harvesting leaves at
4 days after infiltraion
Tissue
disruption
Homogenizaton
in 200 µl of
extraction buffer
Co-infiltration of Agrobacteria
carrying pSfinx-mYFP
and
Agrobacteria
carrying construct(s) of interest
10 x 5 mm leaf discs
(can be srored at -80 °C)
Transfer supernatant
to a new tube
Load 80 µl of
supernatant / well
Centrifuge,
~18,000 x g,
5 min, 4°C
Centrifuge,
~18,000 x g,
5 min, 4°C
Mesure YFP fluorescence
usng plate reader (e.g., TECAN)

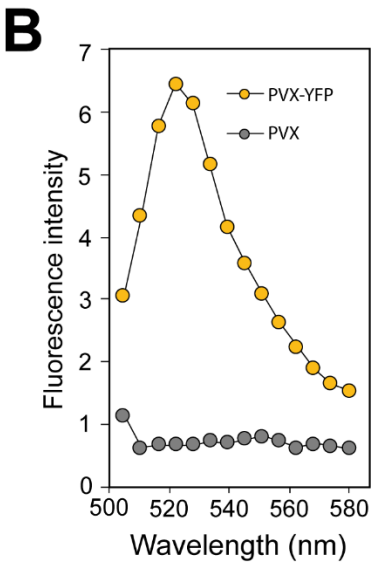
B
PVX-YFP
PVX
Fluorescence intensity
Wavelength (nm)

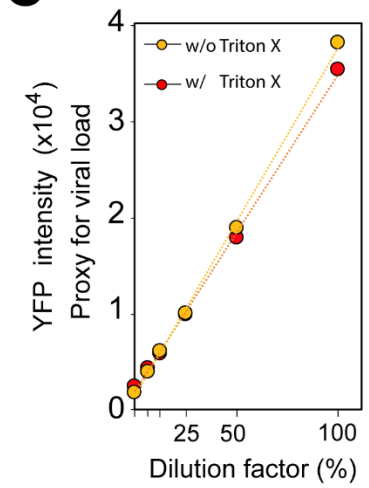
C
w/o Triton X
w/ Triton X
YFP intensity (x10⁴)
Proxy for viral load
Dilution factor (%)

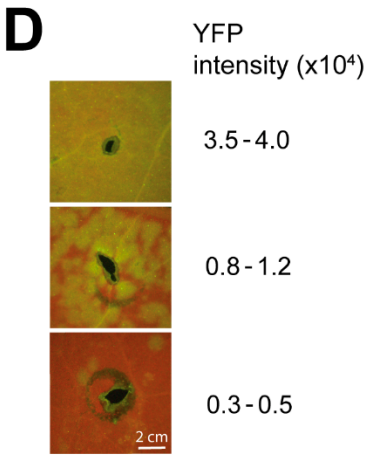
D
YFP
intensity (x10⁴)
3.5 - 4.0
0.8 - 1.2
0.3 - 0.5
2 cm

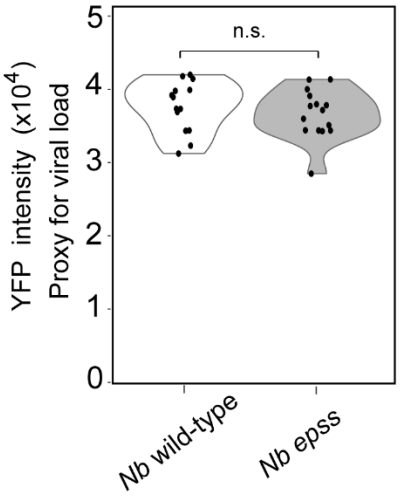
E
n.s.
YFP intensity (x10⁴)
Proxy for viral load
Nb wild-type
Nb epss

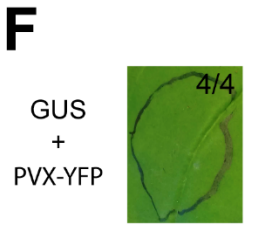
F
GUS
+
PVX-YFP
4/4

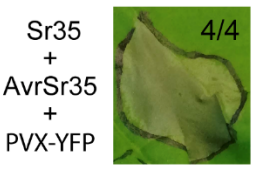
Sr35
+
AvrSr35
+
PVX-YFP
4/4

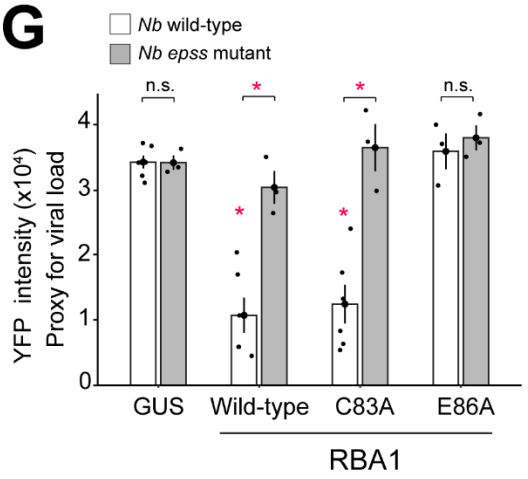
G
Nb wild-type
Nb epss mutant
n.s.
*
*
n.s.
YFP intensity (x10⁴)
Proxy for viral load
GUS
Wild-type
C83A
E86A
RBA1

Figure 3. Disease resistance assay using *Potato Virus X* expressing YFP in *N. benthamiana*

(**A**) Schematic representation of the disease resistance assay using Potato Virus X expressing YFP (PVX-YFP).

(**B**) The emission spectra for leaf extracts expressing PVX-YFP or PVX.

(**C**) A linear correlation between the fluorescence and the dilution factor in a leaf lysate in the presence and in the absence of 0.1% Triton X-100. Leaf lysate from non-transformed plants were used for dilution.

(**D**) Representative fluorescence stereomicroscopic images of *N. benthamiana* leaves infiltrated with PVX-YFP with corresponding YFP intensity measured with the TECAN plate reader. The leaves were examined at four days after agroinfiltration. YFP intensity measured with TECAN from two biologically independent samples are shown,

(**E**) Violin plots showing the degree of dispersion of the quantified YFP intensities from the leaf co-expressing GUS and PVX-YFP in *N. benthamiana*.

(**F**) Expression of Sr35 and with YFP-expressing potato virus X (PVX) caused host cell death in *N. benthamiana* (wild-type). β-glucuronidase (GUS), Sr35, and AvrSr35 (Förderer et al., 2022) were expressed under an independent 35S promoter. The images were taken at 4 days after infiltration of Agrobacteria. The numbers indicate the number of leaves that exhibits cell death out of the total numbers.

(**G**) A non-cell death inducing RBA (Response to HopBA1) variant (C38A), which lacks the 2',3'-cAMP/cGMP synthetase activity but retains the NADase activity (Yu et al., 2022), retains PVX resistance activity. Bar plots indicate the results of four independent replicates for wild-type and three independent replicates for wild-type and *epss* mutant of *N. benthamiana*. Asterisks depict significant differences between treatments as determined by analysis of variance (ANOVA) followed by Tukey's honestly significant difference (HSD) test ($p < 0.05$)

The figure is taken from the Figure 1 in the PVX manuscript.

2.2. The HeLo domain of *Arabidopsis* and human MLKL exhibit EDS1-dependent disease resistance activity

Plant MLKL is a multi-domain protein, comprising the N-terminal HeLo domain, followed by the brace, the pseudokinase, and the intrinsically disordered (ID) regions (Figure 1A, from Mahdi *et al.*[99]). To determine the domain(s) responsible disease resistance activity, I tested whether *At*MLKL was able suppress the PVX proliferation by co-expressing C-terminally HA-tagged *At*MLKL1 truncated variants with a PVX variant expressing YFP (Figure 4A). We measured the YFP intensity of the leaf lysate as a proxy of the disease resistance activity of *At*MLKL1 truncates. The HeLo domain alone and the HeLo plus brace domain variants significantly reduced the intensity of YFP comparted to the full-length *At*MLKL1 protein while neither the HeLo with brace and pseudokinase (H+B+P) variants, the variant lacking the HeLo domain (B+P+ID) exhibited the enhanced disease resistance activity (Figure 4B). Notably, expression of AtMLKL1 HeLo domain with the PVX did not cause the apparent cell death phenotype in *N. benthamiana* (Figure 4C). Next, to examine the genetic requirement of plant MLKL, the disease resistance activity of the HeLo domain was measured in the *eds1 pad4 sag101* mutant background. Intriguingly, the disease resistance activity of the HeLo domain was barely detected in the *eds1 pad4 sag101* mutant background (Figure 4D), suggesting that EDS1 circuit also contribute to the downstream signaling of the activated form of plant MLKLs. Taken together, these results suggested that plant MLKL use N-terminal domain as a signaling domain for immunity similar to animal MLKL[81]. Indeed, a previous study reported that the N-terminal HeLo domain (amino acids 1-125) and HeLo plus Brace domain (amino acids 1-180) of human MLKL (*Hs*MLKL) exhibits cell death activity and localizes at the plasma membrane in human cells. They exploited the human MLKL structure homology model that was built based on crystal structure of mouse MLKL[81,103]. The structural model predicted by AlphaFold2 confirmed that the previously defined truncated constructs of human MLKL (1-125) and (1-

180) does not disrupt the protein structure as the boundaries are located in the loop region between the domains (Figure 4E). By using these truncated constructs, I examined whether human MLKL has disease resistance activity in *N. benthamiana.* Strikingly, human MLKL N-terminal HeLo domain and HeLo plus Brace domain also suppressed PVX propagation (Figure 4F), suggesting that human and plant MLKL shares the HeLo domain as a common signaling domain for immunity.

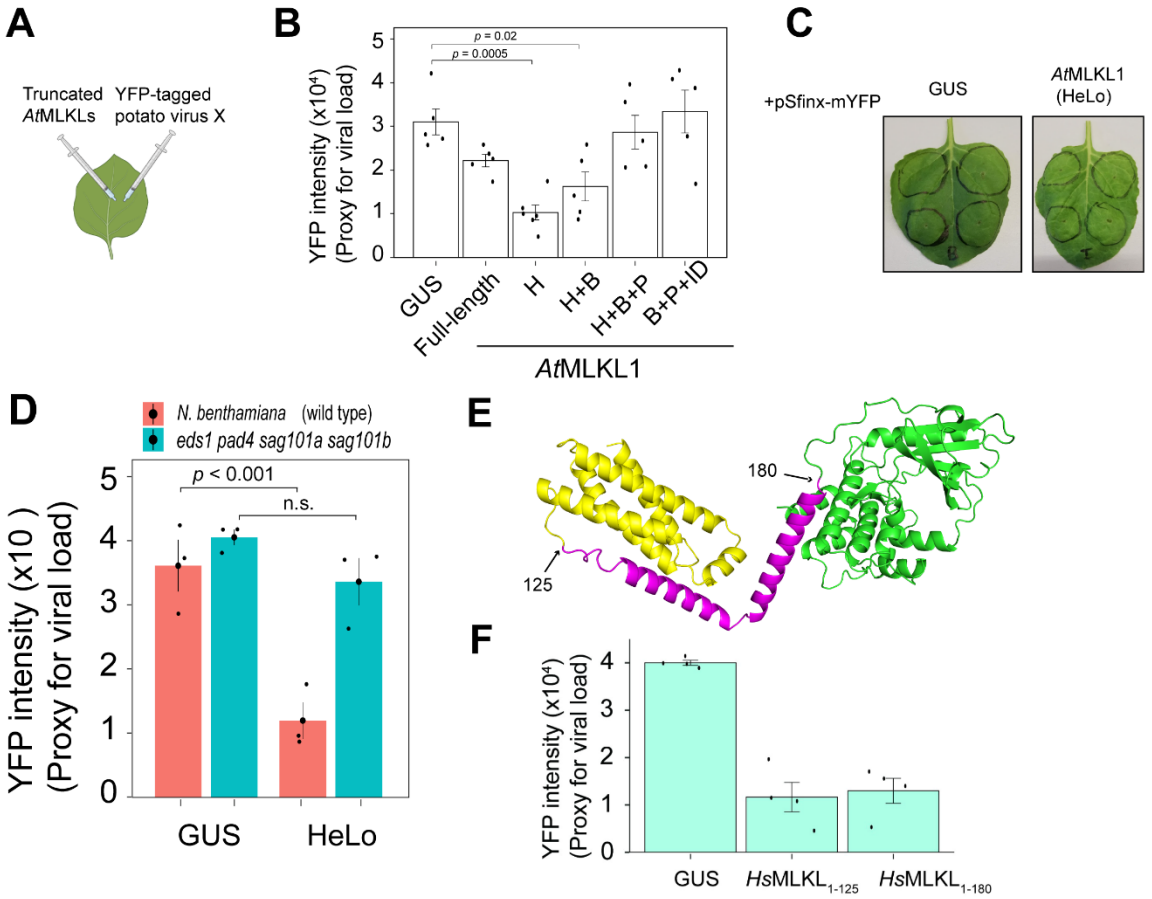

Figure 4. The HeLo domain of *Arabidopsis* and human MLKL exhibit disease resistance activity

(**A**) Schematic representation of agrobacterium-mediated truncated AtMLKL variants and YFP-tagged PVX. (**B**) Disease resistance activity of plant MLKL truncation constructs. (**C**) Expression of AtMLKL1 HeLo with the YFP expressing potato virus X (PVX) did not cause host cell death in N. benthamiana (wild type). GUS and *At*MLKL1 variants were expressed under the constitutive 35S promoter. The PVX was expressed using pSfinx vector. The images were taken at 4 days after infiltration of Agrobacteria. (**D**) Disease resistance activity against YFP expressing PVX by the C-terminally HA-tagged HeLo domain of *At*MLKL1was impaired in the *eds1 pad4 sag101a sag101b* mutant of *N. benthamiana*. The proteins were expressed under the constitutive 35S promoter. (**E**) A structure of full-length human MLKL predicted by AlphaFold2. (**F**) Expression of *Hs*MLKL variants under the constitutive 35S promoter confer resistance to the YFP expressing potato virus X (PVX). The figures are used in the Figure 1, Figure 3, and Figure S2 in the MLKL manuscript.

2.3. Structure-guided mutagenesis revealed the activation mechanism of plant MLKL tetramer

As the PVX-based disease resistance assay with the truncated *At*MLKL1 variants (Figure 5B) suggests that the HeLo domain functions as a signaling domain of plant MLKLs. To test whether the exposure of the HeLo domains from the tetramer is a pivotal activation step of plant MLKLs, we performed a structure-guided mutagenesis in an attempt to disrupt the autorepression by mutating the key residues responsible for the auto-repression. Each *At*MLKL1 protomers are packed by two intra-domains interfaces. The first interface is positioned between the HeLo domain and the pseudokinase domain (HP interface), and the 2nd interface is located between the HeLo domain and the brace domain (HB interface) (Figure 5A). In HP interface, 4 amino acid residues mediate the interaction between the subdomains (Figure 5B left). In HB interface, three hydrophobic residues (W93, I97, and F213) that form hydrophobic clusters mediate the interaction between the subdomains (Figure 5B right). In addition, the *At*MLKL tetramer is packed by two inter-domains interfaces between the protomers (Figure 5C). The first interface is positioned between the two HeLo domains (HH interface). HH interface is mediated by hydrophobic packing of two antiparallel α1 helices of the HeLo domains of the *At*MLKL3 homodimers (Figure 5D top). To disrupt these interfaces, the residues responsible for the interfaces were substituted with charged aspartate or glutamate or electrically neutral alanine. The combinatorial mutation in the HP + HH interfaces exhibited an increased disease resistance to YFP expressing PVX compared to the wild type *At*MLKL1 in *N. benthamiana* (Figure 5E). Similar to the above mutation, the mutation in the HP + HB interfaces also resulted in increased disease resistance. Phosphorylation in the activation loop of the pseudokinase domain is an initial step in MLKL-dependent necroptosis in animals. Furthermore, the previously identified gain-of-function variant carrying a phosphomimetic mutation (S393D) in the activation loop of the pseudokinase domain[99] exhibited increased

disease resistance activity in this assay (Figure 5E). We noticed that expression of AtMLKL1 variants with the PVX did not cause host cell death in *N. benthamiana* (Supplementary Figure 1). These data supported the structure-guided hypothesis that the tetrameric configuration of wild-type *At*MLKLs, in which the HeLo domains are buried represents an auto-repressed state of this protein family. Furthermore, both the intra- and inter-domain interfaces contribute to the auto-repression of *At*MLKL tetramer, and *At*MLKLs would undergo a conformational change that leads to the exposure of the HeLo domains during their activation.

2.4. The gain-of-function variants of *At*MLKL1 and the helper NLRs exhibits distinctive contributions to the EDS1 signaling

TNL-triggered immunity can recruit helper NLRs of the ADR1 (Activated Disease Resistance 1) and NRG1 (N-required Gene 1) families as well as plant MLKLs for downstream signaling[41,42,59,99]. However, the genetic and functional relationship between plant MLKL and helper NLR in TNL-triggered immunity has remained unclear[99]. To examine the genetic and functional relationship between plant MLKL and helper NLR, I examined the disease resistance activity of gain-of-function variants of *At*MLKL1 in the *adr1 nrg1* knockout mutant and in the *eds1 pad4 sag101* mutant of *N. benthamiana*. Intriguingly, the disease resistance activity of the gain-of function variants of *At*MLKL1 was largely retained in the *adr1 nrg1* mutant background, while the resistance activity was barely detected in the *eds1 pad4 sag101* mutant background (Figure 5E). These data suggest that helper NLRs and plant MLKLs can function at downstream signaling of the TNL-triggered immunity in a parallel manner while plant MLKLs are integrated in EDS1 signal amplification loop.

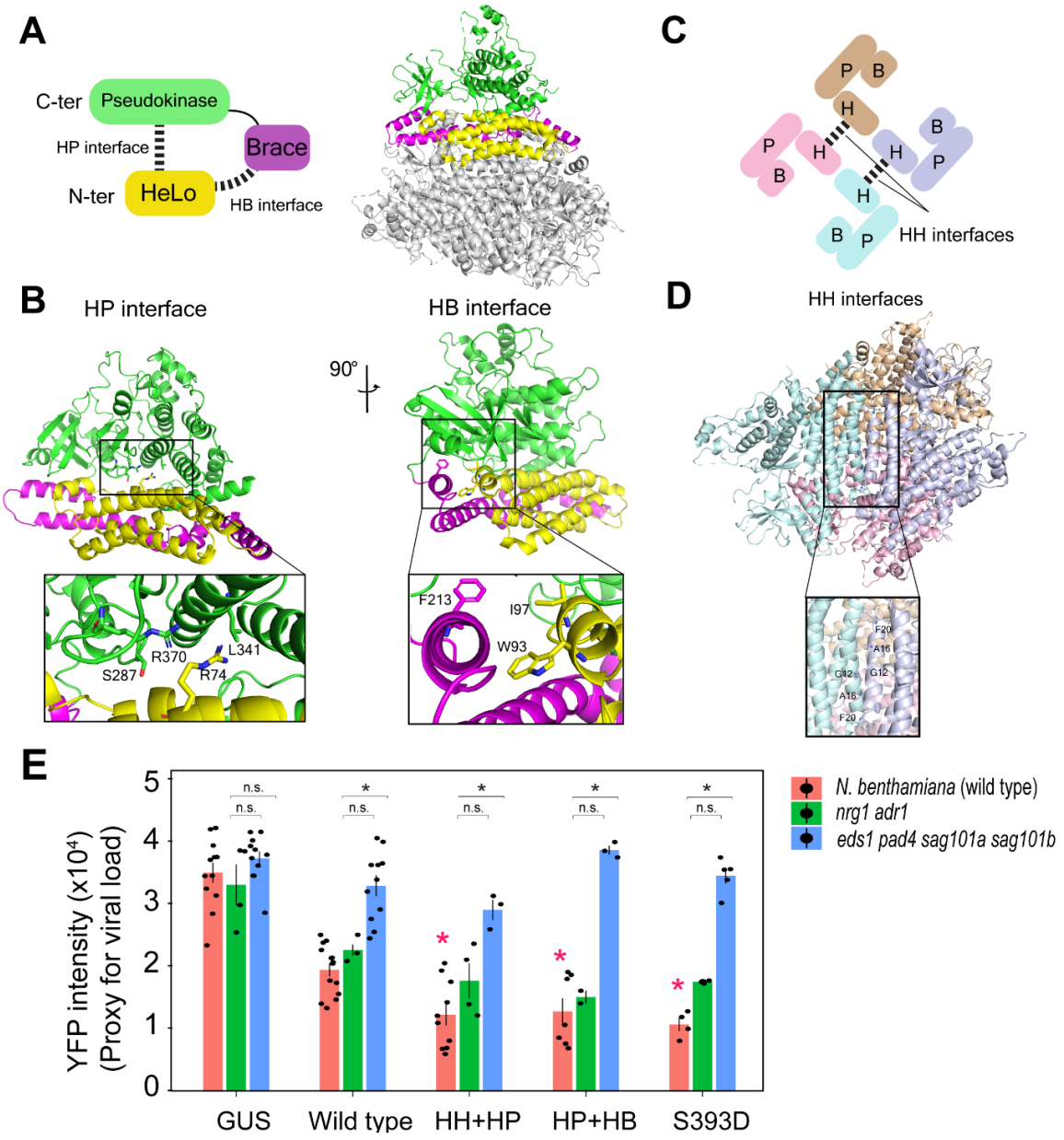

Figure 5. Structure-guided mutagenesis revealed distinctive contributions of the EDS1 family and the helper NLRs to the disease resistance activity mediated by the gain-of-function variants of *At*MLKL1

(A) Left: Schematic representation of the intra-domain interfaces indicated by blue dashed lines. Right: Tertiary structure of the *At*MLKL3 tetramer. As the cryo-EM structures of *At*MLKL2 and *At*MLKL3 are nearly identical and the protein sequences of *At*MLKL1, 2, and 3 are highly conserved, it is reasonable to predict that *At*MLKL1 also forms an *At*MLKL3 like tetramer. One of four protomers is shown in colors. The color code is identical to Fig. 1a. (**B**) The position of amino acid residues in the intra-domain interfaces. (**C**) Schematic representation of the inter-domain interfaces indicated by red dashed lines. (**D**) The position of amino acid residues in the inter-domain interfaces. (**E**) Disease resistance activity of *At*MLKL1 variants carrying mutations at either intra- or inter-domain interfaces to the YFP expressing PVX. All *At*MLKL1 variants were C-terminally tagged with HA epitope. The YFP intensity of the leaf lysate was measured as a proxy of the disease resistance activity. HH+HP and HP+HB indicate the mutant *At*MLKL1 variants harboring mutations at the HH+HP interfaces and HP+HB interfaces, respectively. The previously identified gain-of-function variant carrying a phosphomimetic mutation (S393D from Mahdi et al.[99] in the activation loop of the pseudokinase domain

was used as a control. The red asterisks indicate significant differences from the *At*MLKL1 wild type. The figure is used in the Figure 2 in the MLKL manuscript.

2.5. Plant MLKL mediates cytoplasmic calcium influx

Cytoplasmic calcium ion ($[Ca^{2+}]_{cyt}$) is a ubiquitous 2nd messenger involved in various signaling pathways including disease resistance and cell death[104,105]. With a newly established minimally invasive microscopic analysis, we monitored changes of $[Ca^{2+}]_{cyt}$ in leaves of wild type and *Atmlkl123* mutant plants expressing the GFP-based Ca^{2+} sensor, GCaMP3[106,107] during TNL and CNL-triggered immunity. I found that unlike the wild type plants, the *Atmlk123* mutant plants failed to mount the sustained $[Ca^{2+}]_{cyt}$ increase at 10-14 hours post infiltration with the Pf0-1 strain expressing AvrRps4 (Figure 6A), while the transient $[Ca^{2+}]_{cyt}$ increase at around 4 hours were detectable in both genotypes (Figure 6A). The transient and sustained $[Ca^{2+}]_{cyt}$ increases were a host response specific to the Pf0-1-AvrRps4 strain that activates the TNL pair RRS1/RPS4, as those $[Ca^{2+}]$cyt increases were undetectable upon infiltration of the Pf0-1 strain without effectors (Figure 4A). Strikingly, in agreement with the limited contribution of *At*MLKLs to CNL-triggered immunity[99], the $[Ca^{2+}]_{cyt}$ increase upon the Pf0-1 strain expressing AvrRpm1 that activates a CNL, RPM1 receptor[108] were similar between the wild type and the *Atmlk123* mutant backgrounds (Figure 6B). I noted that in wild type the patterns of $[Ca^{2+}]_{cyt}$ influx were markedly different in response to the two strains, implying the distinctive contributions of those TNL and CNL receptors to $[Ca^{2+}]_{cyt}$ influx. As the N-terminal HeLo domain of *At*MLKL1 confers disease resistance (Figure 4D), we subsequently tested whether the N-terminal HeLo domain of *At*MLKLs are able to elicit $[Ca^{2+}]_{cyt}$ influx in human HEK 293 cells. I took an advantage of an experimental system that enables a chemical (i.e., Rapamycin) induced de-repression of the HeLo domain activity in which, an inhibitory domain fused to the HeLo domain is removed by a rapamycin-induced split-ubiquitin dimerization (Figure 6E). Strikingly, upon rapamycin treatment, the N-terminal HeLo domain alone as wells as the HeLo domain plus the brace region of *At*MLKL1 induced $[Ca^{2+}]_{cyt}$ influx in human HEK293T cells (Figure 6C, D). Notably, the HeLo domain plus the brace region of human MLKL (*Hs*MLKL)

also elicited $[Ca^{2+}]_{cyt}$ influx in human HEK293T (Figure 6C, D). Furthermore, we detected an induced GCaMP3 signal in the stable transgenic *N. benthamiana* plants expressing GCaMP3[109] upon expression of the HeLo domain of *At*MLKL1 (Figure 6F). Taken together, it is plausible that plant MLKLs confer immunity through the HeLo-domain mediated $[Ca^{2+}]_{cyt}$ influx during TNL-triggered immunity.

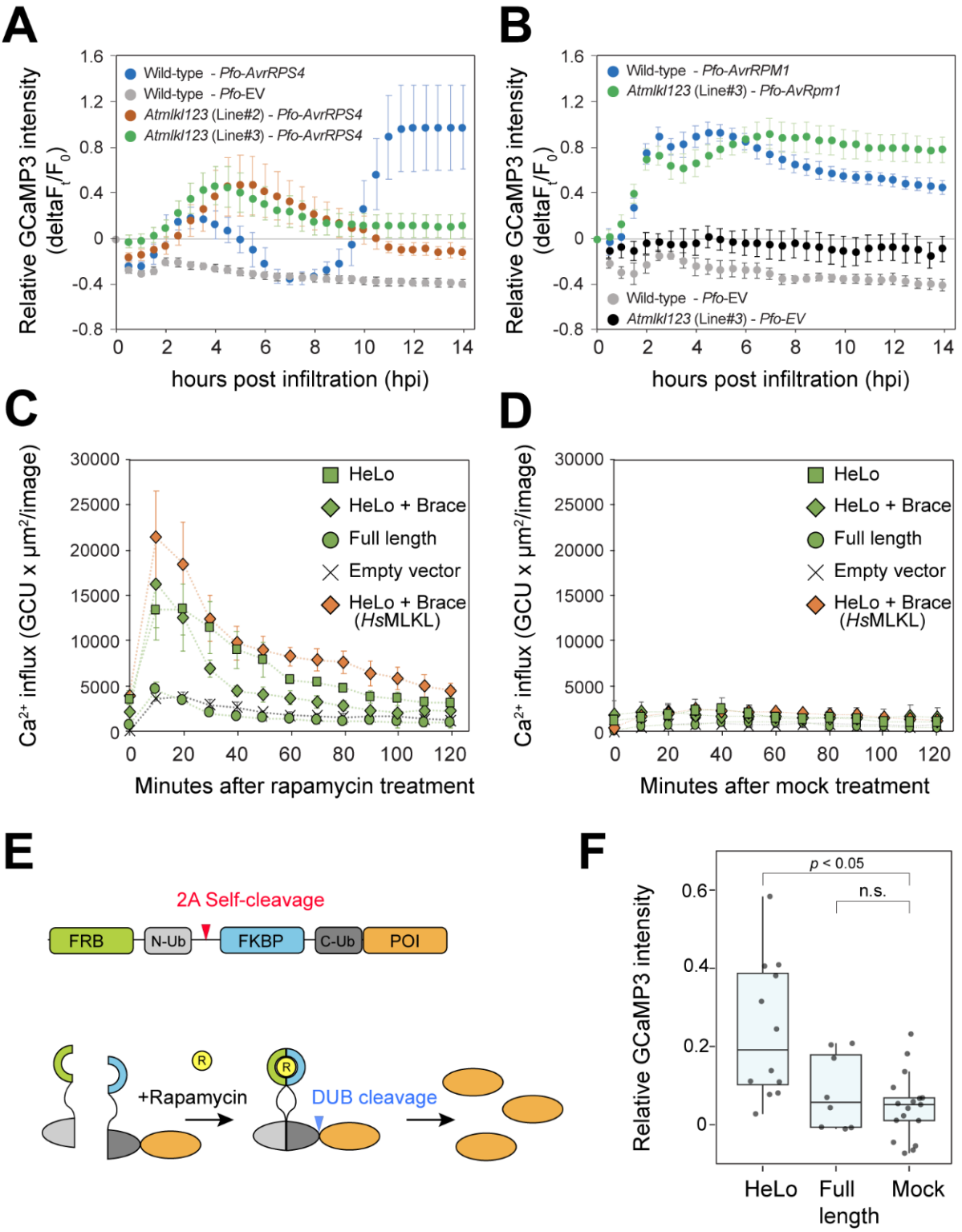

Figure 6. Plant MLKLs are mediator of cytoplasmic calcium ion influx

(A) and (B) A time course signal analysis of GCaMP3 in leaves of the Col-0 expressing GCaMP3 and two independent *Atmlkl123* transgenic lines expressing GCaMP3 generated in this study. Average and SE at each time points upon infiltration with (A), Pf0-1 expressing AvrRPS4 (Pf0-AvrRps4) or (b), Pf0-1 expressing AvrRpm1 (Pf0-AvrRpm1) are shown. Pf0-1 carrying empty vector (Pf0-EV) was used as a negative control. **(C)** and **(D)** the N-terminal HeLo domain alone and the HeLo domain plus the brace region of *At*MLKL1 induced

[Ca2+]cyt influx in human HEK293T cells. **(D)** mock control. A-c, the mean and the standard error of the replicates are shown. **(E)**. Schematic representation of the Rapamycin-induced release of N-terminal tag free protein of interest (POI) used in c and d. After transfection of the construct the N-terminal FRB-N-Ub and the C-terminal FKBP-C-Ub-POI are separated by the 2A self-cleavage. Rapamycin treatment leads to dimerization of FRB/FKBP, by which the formerly bisected ubiquitin can fuse together that allows deubiquitinases to cleave and release protein of interest (POI). **(F)** GCaMP3 signal in N. benthamiana upon expression of the HeLo domain and the full length *At*MLKL1 under the ß-estradiol inducible promoter. The average and ± SE are indicated ((HeLo (n=13), full length (n=8), Mock (n = 17)). For the mock control non-transformed agrobacteria was used. A one-way ANOVA followed by post-hoc Tukey HSD test ($p = 0.05$) was conducted. The figure is used in the Figure 4 in the MLKL manuscript.

2.6. Recombinant *At*MLKL1-HeLo domain forms a higher-order oligomer

Arabidopsis MLKL utilizes N-terminal HeLo domain as a signaling domain for immunity and calcium influx (Figure 4D and F, and Figure 6C). However, how plant MLKL triggers calcium influx and disease resistance activity was unclear. Thus, to understand the underlying mechanism, the characterization of recombinant HeLo domain of *Arabidopsis* MLKL1 was performed. To examine whether plant MLKL self-oligomerizes *in-vitro*, I performed gel-filtration analysis of purified recombinant protein HeLo domain of *Arabidopsis* MLKL1. Gel filtration analysis suggested that *At*MLKL1 HeLo domains form a higher-order oligomer, which composes c.a. 15 protomers (Figure 7A). The purified recombinant NHis6Sumo-*At*MLKL1(HeLo) domain appeared to be suitable for functional characterization with little contamination (Figure 7B). His6Sumo tag cleavage from His6Sumo-*At*MLKL1(HeLo) using GST-HRV3C enzyme produced the bands of cleaved *At*MLKL1(HeLo) and His6-Sumo tag at the position of correct molecular weight in SDS-PAGE gel (Figure 7C), suggesting that the purified His6Sumo-*At*MLKL1(HeLo) recombinant protein in Figure 5A is the target protein. Electron microscope analysis using negatives staining suggested that His6Sumo-HeLo domain of *At*MLKL1 domain might be assembled into a c.a.10 nm ring-like structure (Figure 7D and E). Next, to obtain high-resolution 3D structure of the oligomer, I performed cryo-EM analysis with two different types of grids for the protein. The Cryo-EM grids of the protein was prepared using the copper grids with and without 2 nm carbon support layer. The protein particles were observed on the copper grids with 2 nm carbon support layer (Figure 8A). and the ice thickness on grids was suitable for imaging and particle analysis (Figure 8B). However, the Cryo-EM particle analysis suggested that the particles of the purified His6Sumo-HeLo domain of *At*MLKL1 is heterogeneous, and that the protein needs to be stabilized (Figure 8A). One reason might be the lack of lipids that could stabilize the protein or lipid environment as membrane environment is critical for proper function of membrane proteins[110].

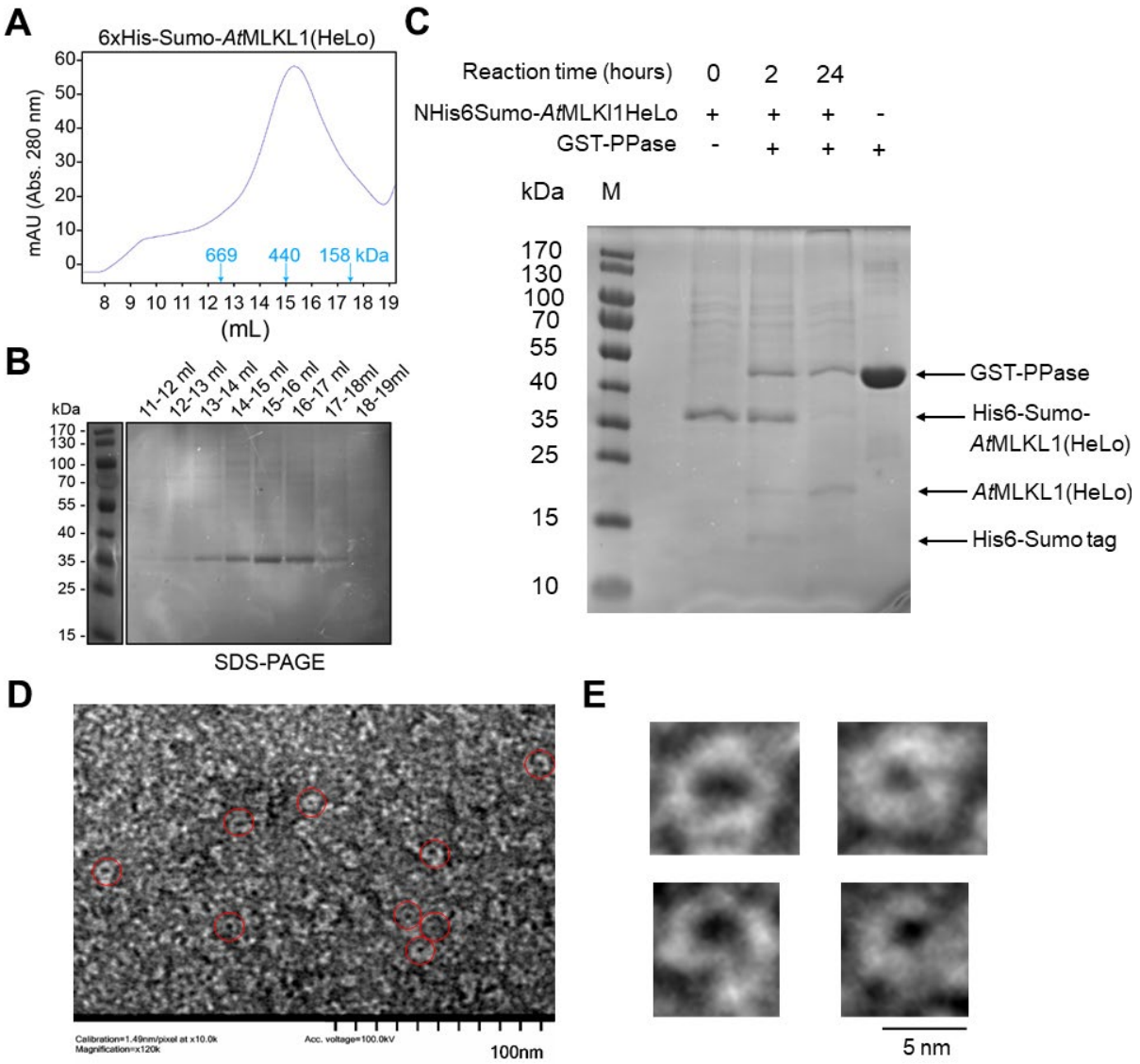

Figure 7. Purified recombinant *At*MLKL1 HeLo domains form a higher-order oligomer

(**A**) Size-exclusion chromatography profile of the 6xHis-Sumo-tagged HeLo domain of *At*MLKL1. Position of standard molecular weight is indicated. (**B**) The proteins in peak fractions in the size-exclusion chromatography were verified by SDS-PAGE. (**C**) Cleavage of N-terminal His6Sumo tag from NHis6Sumo-*At*MLKL1HeLo by GST-PPase at different time points of 0, 2, 24 hours. (**D**) A negative staining electron microscope image of the grids coated with the purified HeLo domain oligomer protein. The particles of the c.a. 10 nm ring-like structures are marked with red circles. (**E**) Enlarged individual particle images of the ring-like structures. The figure is used in the Figure 3 in the MLKL manuscript.

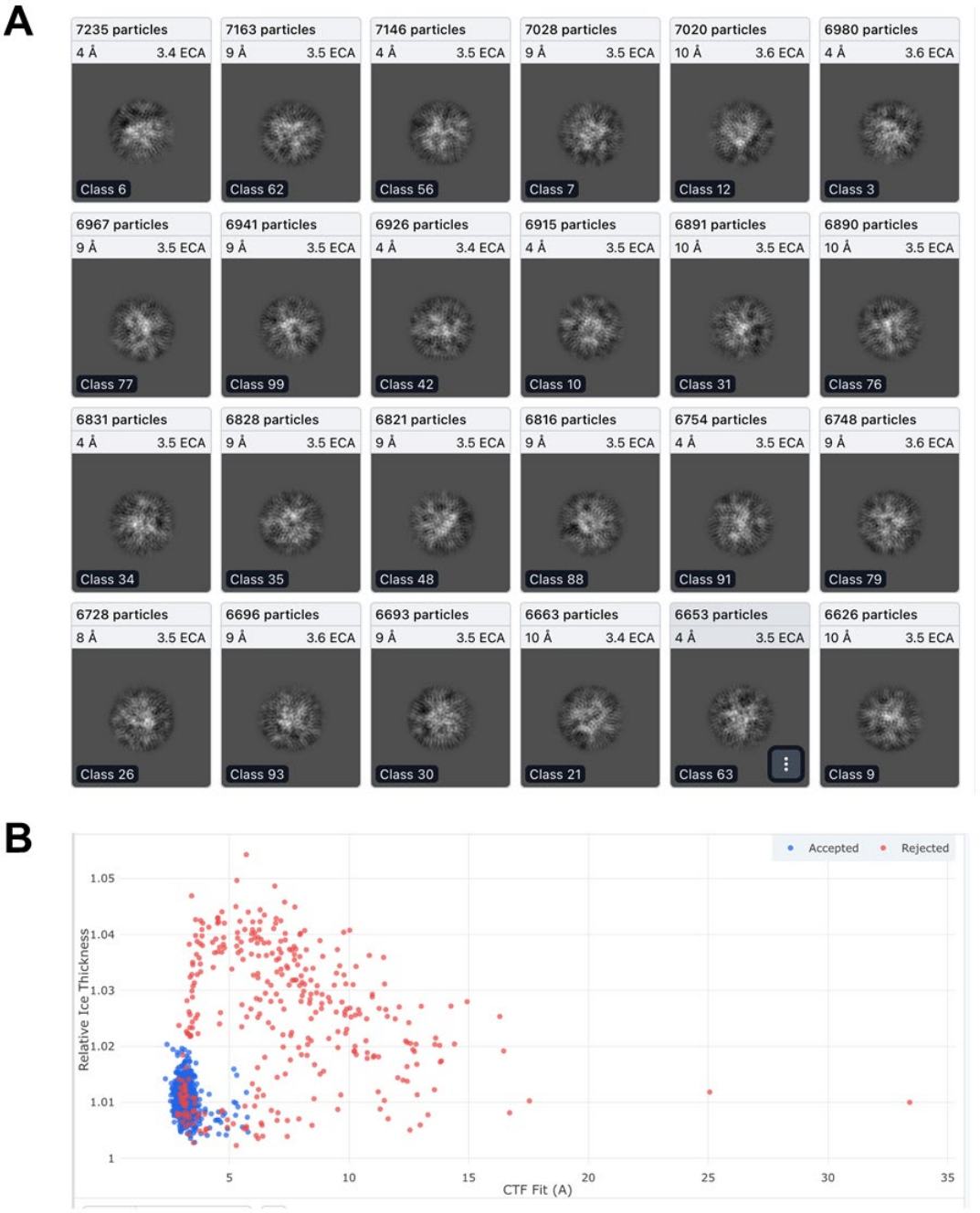

Figure 8. Cryo-EM analysis of purified recombinant *At*MLKL1-HeLo domain higher-order oligomer

(**A**) 2D Classification of cryo-EM of the 6xHis-Sumo-tagged HeLo domain *At*MLKL1 higher-order oligomer. (**B**) The relative ice thickness of the cryo-EM grids with HeLo domain oligomers.

2.7. HeLo domain and full-length plant MLKL protein bind to distinct phospholipid species

Phospholipids play a pivotal role in the plant membrane[111]. In plant immunity, the phospholipid signaling coordinates membrane trafficking and regulate the trafficking of the localization of at the plasma membrane in plant defence[112,113]. Phosphatidylinositol phosphates play essential roles in the membrane in animals as well. For instance, PI(4,5)P_2 plays a central role in maintaining the surface charge of the membrane, and PI4P and PI(3,4,5)P_3 redundantly contribute to the function as well[112]. Animal MLKL localizes at and permiablilizes the plasma membrane to induce cell death in a phosphatidyl inositol-dependent manner[74,77,78,81,85,114,115]. Plant MLKLs translocate to the plasma membrane when TNL pathway is activated. Therefore, it is tempting to hypothesize that plant MLKL use the phospholipids at the plasma membrane to induce resistance activity in a similar manner as animal MLKL. To examine this hypothesis, I investigated whether plant MLKL proteins have the phospholipid binding capacity using the fill-length and the truncated N-terminal HeLo domain of *At*MLKL3-His6 recombinant proteins *in vitro*. Lipid overlay assay suggested that full-length *At*MLKL3-His6 recombinant protein binds mainly to phosphatidylserine and the truncated HeLo-His6 of *At*MLKL3 domain binds to phosphatidylinositol phosphates (PIPs) (Figure 9A and B) in a mutually exclusive manner, supporting the cryo-EM structural observation that the HeLo domain is located inside the tetrameric structure. There are several chemical derivatives in phosphatidyl inositol phosphates, depending on the number and place of phosphates on the carbon ring attached with the acyl chain (Figure 9C). The increase in signal intensity of the spots on the membrane was dependent on the number of phosphates that compose PIPs with strongest binding capacity with PI(3,4,5)P_3 in the lipid overlay assay using the truncated N-terminal HeLo domain protein (Figure 9B), implying that the binding affinity of the N-terminal HeLo domain to the PIPs is determined through the electrostatic property of the PIPs. However, in plants, presence of

PtdIn(3,4)P_2 and PtdIn(3,4,5)P_3 has not yet been reported[116]. MAP-dOCRL(*Drosophila melanogaster orthologue of human oculocerebrorenal syndrome of Lowe 1) deprives PI(4,5)P_2 at the plasma membrane[117]. To examine whether plant MLKL HeLo domain requires phosphatidyl inositol phosphates in a similar manner as animal MLKL to exhibit immune responses[81], I investigated whether co-expression of MAP-mCherry-dOCRL that depletes PI(4,5)P_2 from the plasma membrane alters the resistance activity conferred by the *Arabidopsis* MLKL HeLo domain in *N. benthamiana* using PVX-based assay. Co-expression of MAP-mCherry-dOCRL with HeLo domain did not alter the HeLo-domain-mediated suppression of the proliferation of PVX in *N. benthamiana*, suggesting that plant MLKL HeLo domain does not require PI(4,5)P_2 for disease resistance activity unlike animal MLKL (Figure 9D).

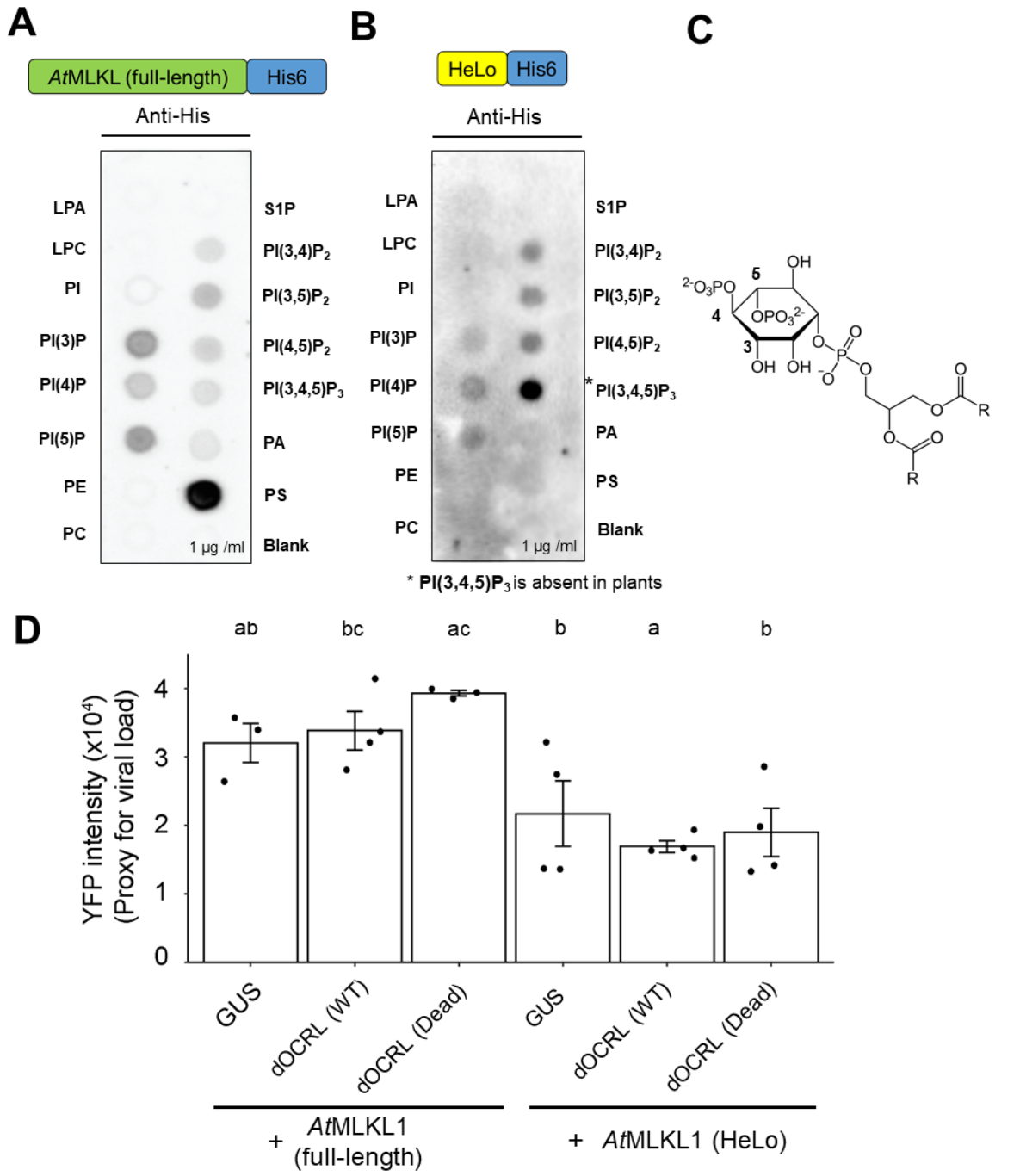

Figure 9. The HeLo domain associates with phosphatidylinositol phosphates (PIPs), while the full-length *At*MLKL associates with phosphatidylserine (PS)

(**A**)(**B**) Lipid overlay assays of recombinant *At*MLKL3 variants. Recombinant full-length *At*MLKL3-CHis6 (**A**) and truncated *At*MLKL3(HeLo)-CHis6 (**B**) were incubated with PIP strip. Immunodetection was performed with the anti-His tag antibody with exposure time of 30, and, 90 seconds, respectively. (**C**) Chemical structure of phosphatidylinositol 4,5-biphosphates. (**D**) Disease resistance activity of co-expression of *At*MLKL1 WT/HeLo domain alone and dOCRL, lipid depriving enzyme. Different letters indicate statistically significant difference at $p < 0.05$, which was determined with single-factor ANOVA followed by Tukey's test. Co-expression was induced under pBiFCt transient expression vectors under independent 35S promoter.

2.8. Phosphomimetic variant of *At*MLKL1(S393D) retains a tetrameric configuration

Phosphomimetic mutation in Serine 393 in the pseudokinase domain of *At*MLKL1 exhibited enhanced cell death in *Arabidopsis* protoplasts and resistance to powdery mildew pathogen[99]. Consistently, the phosphomimetic *At*MLKL1(S393D) variant showed increased disease resistance activity using PVX, supporting the previous observation (Figure 5E). Animal MLKL is reported to change its conformation from monomer to tetramer in a phosphorylation-dependent manner, during its activation in necroptosis[77]. Furthermore, structure-guided mutagenesis approach implied that the *At*MLKL tetramers represent an auto-repressed conformation of plant MLKLs and the exposure of the N-terminal HeLo-domain from the tetramer is an important activation step (Figure 4B and Figure 5E). The multiple lines of evidence provoked the hypothesis that the phosphorylation-induced conformational change in the activation loop is the conserved activation mechanism of plant and animal MLKL. Given that the activation loop is located far away from the HeLo domain in the tetrameric *At*MLKL2 and 3, this suggests that modifications of this portion of the pseudokinase domain may function to allosterically relieve the autoinhibition of *At*MLKLs, leading to exposure of the HeLo domain. To further study the activation step, I purified a gain-of-function variant of *At*MLKL1 carrying a phosphomimetic mutation in the activation loop of the pseudokinase domain for Cryo-EM. In contrary to this hypothesis, the phosphomimetic variant appeared to retain triangular shape in negative staining image and eluted in a fraction, corresponding with the molecular weight of a tetramer position, suggesting that the phosphomimetic variant retains a tetrameric configuration (Figure 10). The result suggests that phospholyration of plant MLKL protein does not lead to direct conformational changes of the protein such as the exposure of HeLo domain although animal MLKL is subject to dynamic conformational change upon phosphorylation. The data might suggest that plant MLKL protein might require different activation steps other than phosphorylsation for full-activation.

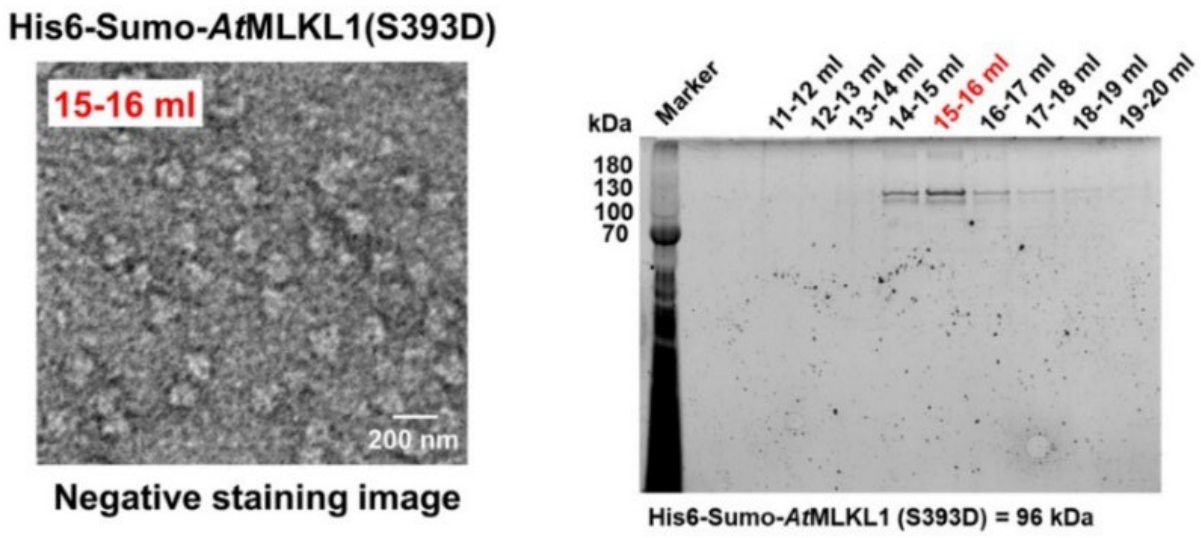

Figure 10. Recombinant phosphomimetic variant of His6Sumo-*At*MLKL1(S393D)

Negative staining image of purified recombinant phosphomimetic variant His6Sumo-*At*MLKL1 (S393D) (Left) Purified recombinant phosphomimetic variant of His6Sumo-*At*MLKL1(S393D) eluted in the tetramer position in gel filtration analysis using Superose 6 Increase column (Right)

2.9. Cell death activity of *At*MLKL1 does not correlate with immune response

Cryo-EM structures of *Arabidopsis* MLKLs (*At*MLKLs) reveal a tetrameric configuration in contrast with the monomeric structure of animal MLKL. In tetrameric structure, N-terminal HeLo domain was sequestered inside, suggesting that plant MLKL tetramer is an auto-inhibited form. The combinatorial mutation in the HP + HH and HP + HB interfaces exhibited an increased disease resistance to YFP expressing PVX compared to the wild-type *At*MLKL1 in *N. benthamiana* (Figure 5E). In parallel, I examined whether the cell death activity of the *At*MLKL1 variants using luciferase-based viability assay of the *Arabidopsis* mesophyll protoplasts isolated from the triple mutant *Atmlkl123*. The mutation in either HB or HP interface that disrupt the intra-domain interaction resulted in enhanced cell death compared with wild-type *At*MLKL1. The mutation in HH interface, one of the inter-domain interfaces, resulted in enhanced cell death compared with wild-type but the mutation in BB interface did not result in enhanced cell death. Next, I examined whether the variants that harbour the mutations in multiple interfaces exhibit increase in the cell death activity compared with the variants that possess the mutations in one of the interfaces. The variants, HB+HH and HP*+HB showed enhanced cell death compared with wild-type *At*MLKL1 but did not show significantly different cell death activity compared with the variants that harbour mutation in one of the interfaces. This result suggested that disruption of one of the interfaces responsible for intra-domain interaction or inter-domain interaction is sufficient to de-repress the *At*MLKL tetramer to exhibit the cell death activity. In western-blotting, protein expression was detectable (Figure 11F). However, the identified gain-of-function variant of HP+HH and HP+HB for the disease resistance activity in *N. benthamiana* (Figure 5E) did not exhibit enhanced cell death activity in protoplasts.

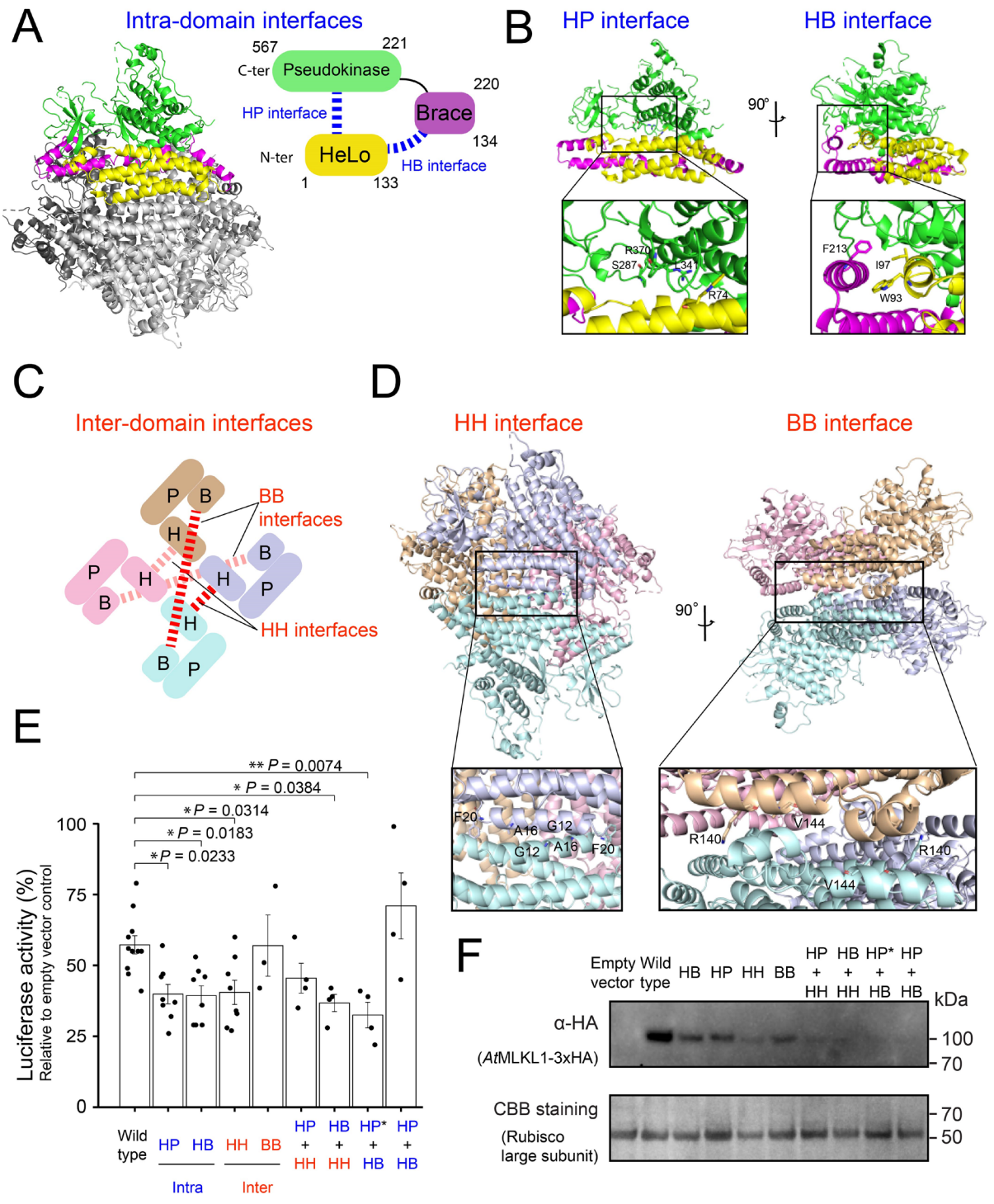

Figure 11. Cell death activity of *At*MLKL1 variants designed by structure-guided mutagenesis

(**A**) Tertiary structure of *At*MLKL1 tetramer (left) and schematic representation of the intra-domain interfaces in *At*MLKL1 protomer (right). One of four protomers is shown in colors. Blue dashed lines indicate two intra-domain interfaces in *At*MLKL1 protomer. The interfaces exist between HeLo and Pseudokinase domains (HP interface) and between HeLo and Brace domains (HB interface), respectively (**B**) The location of amino acid residues at the HP and HB interfaces (**C**) Schematic representation of the inter-domain interfaces in *At*MLKL1 tetramer. Red dashed lines indicate the two-

inter-domain interfaces in *At*MLKL1 tetramer The interfaces exist between HeLo domains (HH interface) and between Brace domains (BB interface), respectively (**D**) The location of amino acid residues at the HH and BB interfaces. (**E**) Cell death activity of *At*MLKL1 variants in mesophyll protoplasts of *Atmlkl123.* Luciferase and *At*MLKL1 expression constructs were co-transfected into protoplasts of *Atmlkl123* and luciferase activity relative to empty vector control was measured as a proxy of cell viability at 13-16 hours post transfection. The C-terminally HA tagged variants were expressed under the control of the constitutive cauliflower mosaic virus 35S promoter. (E) The positions of the mutated residues, which were substituted to glutamic acid (E) are indicated in Figure 11B and. HP* is a HP interface variant (S287E, L341E, and R370E) that harbors mutations only in the Pseudokinase domain, Data represent mean +-s.e.m. Significant differences between the samples were analyzed using Kruskal-Wallis (KW) analysis followed by the Dunnett test. Calculated KW *P*-value = 0.001776 (**P*<0.05, ***P*<0.01 in Dunette test). (F) Western blot analysis of the C-terminally HA-tagged *At*MLKL1 variants. Total protein extracts were collected from mesophyll protoplasts of *Atmlkl123* at seven hours post transfection.

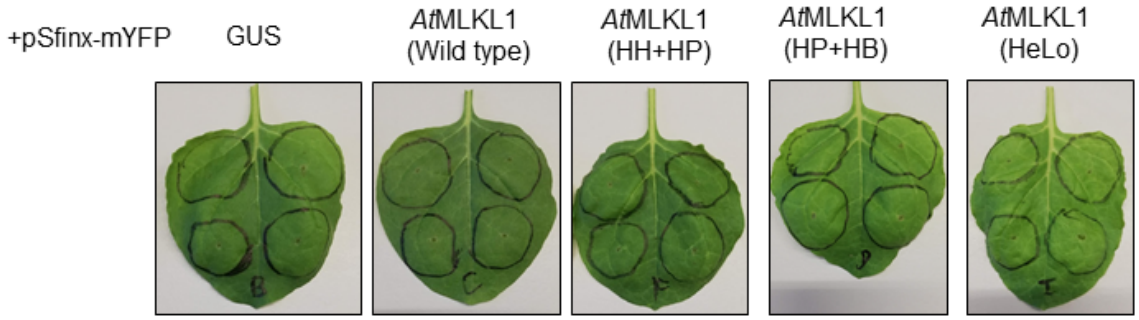

Supplementary Figure 1: Expression of *At*MLKL1 variants in *N. benthamiana* with PVX

Expression of *At*MLKL1 variants with the YFP expressing potato virus X (PVX) did not cause host cell death in *N. benthamiana* (wild type). GUS and *At*MLKl1 variants were expressed under the constitutive 35S promoter. the PVX was expressed using pSfinx vector. The images were taken at 4 days after infiltration of *Agrobacteria*. The figure is used in the Figure S2 in the MLKL manuscript.

3. Manuscripts for publication

3. Manuscripts for publication

3.1. A simplified disease resistance assay using YFP expressing *Potato Virus X* in *N. benthamiana* revealed a cell death independent immunity of RBA1

Keiichi Hasegawa, Ton Timmers, Jijie Chai, and Takaki Maekawa

Under submission to *Plant Physiology*

Author contributions: K.H., J.C., and T.M. conceived the project. K.H. and T.T. performed the investigations. K.H., T.T., J.C., and T.M. validated the data, J.C. and T.M. supervised the work, K.H., and T.M. wrote the paper with co-author contributions.

Specific contributions:
In this study, I developed a plate reader-based disease resistance assay using PVX-YFP by introducing a modification into the previously documented PVX assay in *N. benthamiana*[59]. By using this assay, I revealed the cell death-deficient activity of RBA1 C83A variant. I wrote the manuscript with co-author contributions.

Page numbers in the attached paper are not counted in the pagination of the thesis.

3.2. Cytoplasmic Calcium influx mediated by plant MLKLs confers TNL-triggered immunity

Authors
Qiaochu Shen*, Keiichi Hasegawa*, Nicole Oelerich, Anna Prakken, Lea Weiler Tersch, Frowin Reichhardt, Alexandra Tersch, Ton Timmers, Kay Hofmann, Jijie Chai and Takaki Maekawa
*Equal contribution

Under review in Cell host microbe

Author contributions: J.C. and T.M. conceptualized the project; Q.S., K.H., N.O., A.P., L.W.T., F.R., and A.T. performed the investigations. Q.S., K.H., N.O., A.P. L.W.T. F.R., A.T., K.H., J.C., and T.M. validated the data, T.T., K.H., J.C., T.M. supervised the work, Q.S., K.H., and T.M. wrote the paper with co-author contributions. The first two authors should be regarded as joint first authors. Co-first authors can prioritize their names when adding this paper's references to their resumes.

Specific contributions:
In this study, I showed plant MLKL tetramer is an auto-inhibited form by structure-guided mutagenesis approach, showing that HeLo domain is the executer domain for immunity. Furthermore, I showed that plant MLKL exhibits disease resistance activity in an EDS1-dependent but a helper NLR-independent manner in a genetic analysis using *N. benthamiana* PVX assay. I showed that human MLKL N-terminal domain suppress the propagation of PVX. Additionally, I purified and analyzed the recombinant *At*MLKL1 HeLo domain, showing that *At*MLKL1 HeLo domain has a self-clustering activity. I wrote the manuscript with co-author contributions.

Page numbers in the attached paper are not counted in the pagination of the thesis.

4. Discussion

4. Discussion

4.1. Inhibition and activation of plant and animal MLKL proteins

In this study, structure-guided mutagenesis approach approach has validated the hypothesis that the full-length MLKL tetrameic form represents an inactive form, and showed that intra-domain or inter-domain interactions within the *At*MLKL tetramer is responsible for the auto-repression of *At*MLKL tetramer function. Furthermore, the result indicated that exposure of HeLo domain is a key activation step of plant MLKLs (Figure 5E). In animals, MLKL is activated through phosphorylation by RIPK3 in the activation loop of the pseudokinase domain. The phosphorylated MLKL undergoes conformational change from a monomer to a tetramer[75,77]. However, the size-exclusion analysis and the electron microscope analysis of the recombinant phosphomimetic variant of *At*MLKL1 (Figure 10) revealed that the phosphomimetic *At*MLKL1 variant retains a tetrameric configuration, suggesting that phosphorylation of plant MLKL does not induce dynamic conformational change of plant MLKL proteins from the tetrameric state unlike animal MLKL. This result implies that phosphorylation of MLKL might be a priming step for its activation and plant MLKL protein requires multiple activation steps for full-activation. Alternatively, the phosphorylation of plant MLKL might alter the binding affinity with the EDS1 receptor complex that might comprise the activation of plant MLKL protein given that plant MLKLs are preferentially engaged by TNL- but not CNL-triggered immunity[99].

4.2. Oligomerization and membrane damage mediated by HeLo domain

The oligomerized animal MLKL permeabilizes the PM via incompletely characterized mechanisms[79,80] although it is in a general consensus in the field that the N-terminal HeLo domain is indispensable for immunity and cell death[74,79]. The HeLo-domain helices of mouse, human, and plant MLKLs can be classified as an amphipathic helix, carrying both but segregated hydrophilic and hydrophobic surfaces[80,104]. This amphipathic nature of helical

proteins often leads to their oligomerization with their membrane lytic activities[104,118,119]. Indeed, the plant MLKL N-terminal HeLo domain protein drives the self-oligomerization of the protein *in vitro* (Figure 7B). In ferroptosis, other type of programmed cell death in animals, partial PM damage results in formation of a transient pore at PM that causes cytosolic Ca^{2+} fluxes[120]. Therefore, a partial PM damage by the oligomerized HeLo domains of plant MLKL could be the underlying mechanism for the plant MLKL-mediated cytosolic Ca^{2+} influx. In animals, this membrane lytic activity of animal MLKL is dependent on binding capacity to phosphatidylinositol phosphates mediated by HeLo domain[81]. Similarly, plant MLKL N-terminal HeLo domain preferentially binds to the phosphatidyl inositol phosphates (Figure 9B). Thus, it is tempting to hypothesize that plant MLKL HeLo domain permeabilizes the phosphatidylinositol 4,5-bisphosphates. However, the enzymatic deprivation of phosphatidylinositol 4,5-bisphosphates at the plasma membrane did not affect the immune upregulation mediated by HeLo domain (Figure 9D), denying the involvement of phosphatidylinositol 4,5-bisphosphates at the plasma membrane in HeLo domain-mediated immune upregulation. This might suggest that the plant MLKL HeLo domain uses different phosphatidyl inositol species other than phosphatidylinositol 4,5-bisphosphates to induce the immune upregulation. Alternatively, the enzymatic deprivation of phosphatidylinositol 4,5-bisphosphates at the plasma membrane by dOCRL was not efficiently executed in the tested experiment condition. It would be informative to test whether plant MLKL N-terminal HeLo domain exhibits lytic activity in vitro by liposome permeabilization assay in a manner depending on phosphatidylinositol phosphates similar as the animal MLKL HeLo domain[81].

4.3. Activated MLKL pore might release DAMPs

The HeLo domain of *At*MLKL1 possess a self-clustering activity to form a higher-order oligomer with an approx.15 protomers (Figure 7A). Furthermore, negative staining analysis suggested that the particles of the HeLo domain can form a higher-order oligomer with a pore-

like structure with the diameter of c.a. 10 nm (Figure 7D), which is large enough for small molecules such as DAMPs to pass through although the requires structure determination in atomic resolution. The major types of plant DAMPs include extracellular ATP, oligomeric plant cell-wall-derived pectin termed oligogalacturonides (OGs), and fragments of chitin[121–123]. Furthermore, HeLo domain forms a punctate structure that is similar to the punctate structure of full-length *At*MLKL1 upon activation of TNL pathway, indicating that self-clustering activity of HeLo domain is a signature of plant MLKL activation. In pyroptosis, gasdermin pores release immunogenic peptides, IL1-β (Interleukin-1 beta) and IL-18 (Interleukin-18)[124,125]. The cryo-EM structure of Gasdemin D revealed that the pore has the inner diameter of 22 nm and the electrostatic property of the membrane pore allows preferential passage of IL1-β and IL-18 over the precursors[124]. Plants release the immunogenic peptides called phytocytokines that correspond to the cytokines in animals. Plant Elicitor Peptides (Peps), which were originally identified from endogenous peptides in *Arabidopsis thaliana*, induce amplification of defence signaling like PTI when recognized by its cognate receptors, *At*Pep-Receptors (*At*PepRs)[126,127]. Plant elicitor peptides (Peps) are prominent phytocytokines that trigger plant defences when recognized by the leucine-rich repeat RKs (LRR-RKs) PEPR1 and PEPR2[128]. *At*PROPEP genes show tissue-specific expression patterns[129]. *At*PEPR1 and *At*PEPR2 are present in all tissues, suggesting functionality of the system throughout the plant[130]. *At*PROPEP genes do not encode N-terminal signal peptides for secretion[126,127,130]. This has led to the assumption that the peptides are only released upon tissue damage. However, *At*PROPEP3 is likely to be released upon treatment with *At*Pep1 or *At*Pep2, or upon bacterial infection[131], suggesting that *At*PROPEP3 may be released as a leaderless peptide in a tissue non-destructive manner[25] similar to the secretion of IL1-β through the gasdermin pore. In consistent with this, plant MLKL-mediated immunity is engaged by EDS1 signaling. PROPEP3 is a peptide with 96 amino acid residues with flexibility that can be smaller than 10

nm in one length, suggested by a predicted structure in AlphaFold2 (Figure 12A and B). It is a reasonable hypothesis that the PROPEP3 molecules might pass through the pore mediated by HeLo-domain of plant MLKL, implying the potential link between DAMP signaling and plant MLKL-mediated immunity. In this scenario, plant MLKL function as a connecting point of PTI and ETI in plant immunity mediated via pore formation. Consistently, recent studies suggest the link between PEP1 and NLR triggered immunity[48,49]. Thus, to determine the precise size and architecture of the plant MLKL HeLo domain oligomer on the membrane and the electrostatic property of the pore surface is crucial for precise understanding of how plant MLKL contributes to the immune signaling.

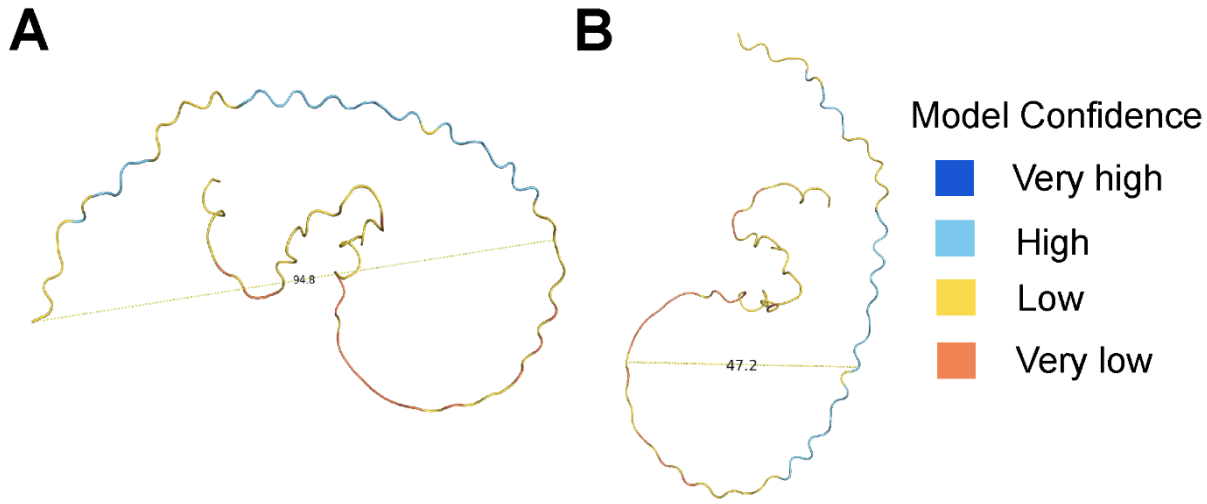

Figure 12. Predicted PROPEP3 structures by AlphaFold2 with different orientations

In the panel (A) and (B), the longest distances between the two regions in the PROPEP3 peptide are described (A: 94.8 Å, B: 47.2 Å). The color in the structure represents the model confidence.

4.4. Plant MLKL mediates sustained calcium influx

MLKLs and RNLs appear to confer cytoplasmic Ca^{2+} influx in either phase of TNL-mediated immunity. It might be reasoned that the MLKL-dependent sustained $[Ca^{2+}]_{cyt}$ increase (Figure 6A) is that structural variations of the TIR-produced metabolites may influence the selection of client proteins for the EDS1-receptors. The plant TIR-produced metabolites pRib-AMP and ADPr-ATP promote association of EDS1-receptors with the downstream RNLs, NRG1 and ADR1[41,42] while plant TIR-only proteins like BdTIR generate ~100-fold more v-cADPR (2′cADPR) in planta relative to TIR-domains from TNL proteins[38]. Furthermore, plant TIR-only proteins also generate 2′,3′-cNMPs linked with abiotic stress response[45,132]. Therefore, it is tempting to speculate that the considerable variations in composition and structure of TIR-products in the course of pathogen challenge allows distinctive EDS1-receptor complexes to preferentially activate MLKLs over RNLs.

4.5. Plant MLKL pathway as a backup mechanism in TNL-triggered immunity

Animal MLKL-mediated necroptosis has evolved as a backup pathway in case apoptosis is not activated. Plant MLKL pathway in TNL-triggered immunity might have evolved to function as a backup pathway to counteract the effector-mediated suppression of the immune signaling pathway by the invading pathogens similar to animal necroptosis. In *Arabidopsis*, the helper NLRs, ADR1 and its 2 paralogs ADR1-LIKE 1 (ADR1-L1) and ADR1-LIKE 2 (ADR1-L2) function downstream of TNLs in a redundant manner[39,43,133,134]. Recently, it was found that the *Pseudomonas syringae AvrPtoB* effector suppresses cell death mediated by helper NLRs, ADR1-L1- and ADR1-L2[135] while RNLs and plant MLKLs can function in signaling downstream of TNL in a parallel fashion (Figure 5E). However, even when the function of helper NLRs is restricted, plant MLKLs still retains their function as downstream components in effector-triggered immunity as a backup mechanism, which might contribute to the robustness of ETI.

4.6. Bifurcation of TIR-mediated cell death and immune response

Host cell death is associated with the plant immune responses in many cases. However, cell death and pathogen growth restriction have been uncoupled in several cases[59,134]. I found that the RBA1 (C83A) cell death deficient variant retained disease resistance activity like wild-type RBA1, whereas the RBA1 (E86A) barely showed disease resistance activity (Figure 3G). RBA1 TIR domain exhibits NADase to generate 2'-(5"-phosphoribosyl)-5'-adenosine monophosphate (pRib-AMP),and nuclease activity to produce diphosphate (pRib-ADP) and cyclic nucleotide monophosphates (cNMPs) such as 2′,3′-cAMP/cGMP, respectively, to induce cell death[38,45,102]. The data suggest that the 2′,3′-cAMP/cGMP synthase activity (i.e., nuclease activity) of RBA1 is required for host cell death and the remaining NADase activity is sufficient to confer immunity to PVX. Furthermore, the disease resistance activity of the RBA1(C83A) variant was significantly compromised in the *Nb*epss mutant background (Figure 3G), supporting the previous finding that the TIR NADase products activate the EDS1 signaling pathway. In summary, my study based on the modified method of PVX assay has uncoupled cell death and immune responses mediated by RBA1 C83A cell death deficient variant. Consistently, *Arabidopsis* TNL SNC1 (Suppressor of npr1-1, constitutive 1) does not require the 2′,3′-cAMP/cGMP synthetase activity for immune signaling[136]. Therefore, it is tempting to speculate that 2′,3′-cAMP/cGMP produced by TIR nuclease activity may target different downstream components than EDS1 and that the signaling molecules produced by TIR nuclease and NADase activity promote cell death and the immune response pathway, respectively, to bifurcate the cell death and immune response pathways. Non-mutually exclusive explanation is that both the TIR NADase and TIR 2′,3′-cAMP/cGMP synthase activitities might be required for TIR-mediated cell death response to cross the threshold between cell death and immune response while the TIR NADase activity comprises the primary immune signaling.

4.7. Advantages of PVX-based disease resistance assay to assess the plant immune response

PVX disease resistance assay offers a high operational efficiency, however, the assay still involves laborious procedures or some do not assess the amount of virus inside the leaves. In the modified method of plate reader-based PVX assay described enabled rapid measurement of the disease resistance activity. The modified assay can ignore the effect of endogenous EDS1 signaling pathway as suggested by a virus-induced *NbEDS1* gene silencing[58] and the comparable vial load in wild type and *eds1 pad4 sag101 saga 101* in *N. benthamiana* (Figure 3E). This characteristic allows the assessment of milder moderate resistance activity. Furthermore, the samples can be stored in a freezer until its use, which allows measurement of disease resistance activity of multiple R genes. I emphasize that disease resistance assays are not exclusive to the widely used cell death assay in the *N. benthamiana* transient gene expression system, but rather complementary to understanding cell death-independent immunity of R proteins.

5. Materials

5. Materials

5.1. Enzymes

All enzymes used are listed in Table 2.1. These were stored at -20 °C and freshly thawed before use.

Table 2.1 | Enzymes for protoplast isolation.

Name	Supplier
Macerozyme R-10	Yakurt Pharmaceutical
Cellulase R-10	Duchefa Biochemie

5.2. Antibodies

Table 2.2 lists the primary and secondary antibodies used for immunoblot detection. Stock solutions of antibodies were stored at -20 °C in aliquots and freshly thawed before use.

Table 2.2 | Antibodies

Name	Supplier	Indetifier
Rat monoclonal α-HA	Sigma-Aldrich, MO, USA	AB_390918
Mouse monoclonal α-6X His	Abcam	AB_18184
Goat α-rat IgG-HRP	Sigma-Aldrich, MO, USA	AB_91300
Goat α-mouse IgG-HRP	Santa Cruz Biotechnology, TX, USA	AB_2687626

5.3. Oligonucleotides

Oligonucleotides were purchased from Sigma-Aldrich. Lyophilise d primers were resuspended in Mili Q water to a final concentration of 10 µM.

5.4. Buffers and Solutions

Buffers and solutions frequently used in this thesis are listed in Table 2.3.

Table 2.3 | Buffers and solutions for DNA and protein separation in electrophoresis

Buffer	Components	Purpose
50× TAE buffer	Tris base (2 M), acetic acid (1 M), EDTA (50 mM)	Agarose gel electrophoresis
1× TBS-T buffer	Tris-HCl pH 7.4 (20 mM), NaCl (150 mM), Tween 20 (0.1% (w/v))	Western blotting
10× TGS buffer	Tris base (0.25 M), Glycine (1.9 M), SDS (35 mM)	SDS-PAGE

Table 2.4. Solutions for cell death assay in *Arabidopsis* mesophyll protoplast

Buffer	Composition
Enzyme solution	10mM MES, 0.6M mannitol, 20mM KCl, 1,5% Cellulase R-10, 0,5% Macerozyme R-10, 10 mM CaCl2, 0.1% BSA
Wash solution	2 mM MES, 154 mM NaCl, 125 mM CaCl2, 5 mM KCl
T1 solution	4 mM MES, 0.4M mannitol , 15 mM MgCl2
T2 solution	40% PEG4000, 0.2M mannitol, 100 mM CaCl2
Regeneration solution	4mM MES, 0.6M mannitol, 20 mM KCl

5.5. Materials for recombinant protein expression

Table 2.5 | Untransformed *E.coli* strains.

Bacterial strains	Supplier	Genotype
E. coli Rosetta (DE3)	Koncz	F- *ompT hsdS*B(rB- mB-) *gal dcm* (DE3) pRARE (Cam^R)
E. coli DH5α	Thermo	F– φ80*lac*ZΔM15 Δ(*lac*ZYA-*arg*F)U169 *rec*A1 *end*A1 *hsd*R17(rK–, mK+) *pho*A *sup*E44 λ–*thi*-1 *gyr*A96 *rel*A1
BL21 (DE3)	NEB	F–ompT hsdSB (rB–, mB–) gal dcm (DE3)
E. coli DH10Bac	Thermo	F-mcrA Δ(mrr-hsdRMS-mcrBC) Φ80lacZΔM15 ΔlacX74 recA1 endA1 araD139 Δ(ara, leu)7697 galU galK λ-rpsL nupG/pMON14272/pMON7124

Table 2.6 | Empty plasmids vector for protein expression in *E.coli* and insect cell

Gene	Vector	Tag	Sequence origin
*At*MLKL1(HeLo)	pFastBac1	N-terminal His6Sumo tag	Coding sequence
*At*MLKL1(WT)	pFastBac1	N-terminal His6Sumo tag	Coding sequence
*At*MLKL3(HeLo)	pGEX6p-1	N-terminal GST tag and C-teriminal His6 tag	Coding sequence
*At*MLKL3(WT)	pGEX6p-1	N-terminal GST tag and C-teriminal His6 tag	Coding sequence

Table 2.7 | Media for *E. coli* and *A. tumefaciens* culture.

Name	Supplier
LB Broth with agar (Lennox)	Sigma
LB media (Lennox)	Roth

Table 2.8 | Media for *Arabidopsis thaliana* culture.

Name	Supplier
Murashige and Skoog Basal Medium	Sigma

Table 2.9 | Empty plasmids for *A. tumefaciens* transformation.

Constructs	Resistance
pAMPAT-35s-GW-3HA	Carbenicillin
pAMPAT-35S-*At*MLKL1(wild-type)-3HA	Carbenicillin

Table 2.10 | Media and chemicals for insect cell culture.

Name	Supplier
Sf-900 II SFM	Gibco /Thermo fisher Scientific
X-treme Gene HP DNA transfection reagent	Sigma
Antibiotic Antimycotic Solution, stabilized	Sigma
Fetal Bovine Serum, qualified, heat-inactivated	Thermo

Table 2.11 Resins and columns for recombinant protein purification

Name	Supplier
Glutathione Sepharose 4B	Cytiva/Sigma
HisPur Cobalt Resin	Thermo Fisher Scientific
Superdex 200 Increase 10/300 GL	Cytiva/GE healthcare
Superose 6 Increase 10/300 GL	Cytiva/GE healthcare

6. Methods

6. Methods

6.1 Molecular Cloning

6.1.1 PCR (Polymerase Chain Reaction)

All the PCR for molecular cloning were performed using KOD one PCR Master Mix (sigma) according to manufacturers' instructions. A typical reaction mixture and the thermocycling conditions are described as follows.

Table 2.12 PCR reaction mixture using KOD one PCR Master Mix in 50 µl

Component	Volume
KOD one PCR Master Mix	25 µl
10 µM Forward primers	1.5 µl
10 µM Reverse primers	1.5 µl
10 ng/µl Template	1 µl
Mili Q	21 µl

Table 2.13 Thermocycling setting for PCR using KOD one PCR Master Mix

Stage	Temperature	Time	Number of cycles
Initial denaturation	98 °C	30 seconds	1
Denaturation	98 °C	10 seconds	
Annealing	60 °C	5 seconds	30
Extension	68 °C	5 seconds/kb	
final extension	68 °C	1 minute	1

6.1.2 Site-directed mutagenesis

Point mutations were introduced using Q5 Site-Directed Mutagenesis Kit (NEB) according to manufacturer's instructions. Mutagenesis PCR was performed with wild-type gene sequence as template and mutagenic primers. After mutagenesis PCR, KLD enzyme reaction mixture was added into DH5α competent cells for transformation and plated on LB plates with appropriate antibiotics for colony isolation.

Table 2.14 Site-directed mutagenesis PCR reaction mixture in 50 µl

Component	Volume
Q5 Hot Start High-Fidelity 2X Master Mix	12.5 µl
10 µM Forward primers	1.25 µl
10 µM Reverse primers	1.25 µl
10 ng/µl Template	1 µl
Mili Q	9 µl

Table 2.15 Thermocycling setting for PCR using Q5 Site-Directed Mutagenesis Kit (NEB)

Stage	Temperature	Time	Number of cycles
Initial denaturation	98 °C	30 seconds	1
Denaturation	98 °C	10 seconds	
Annealing	55 °C	30 seconds	30
Extension	72 °C	30 seconds/kb	
final extension	72 °C	2 minutes	1

6.1.3. Purification of PCR products

PCR products were purified using the NucleoSpin Gel and PCR Clean-up (Macherey Nagel) following the manufacturer's instructions.

6.1.4 Agarose gel electrophoresis

To separate the DNA fragments after PCR, agarose gel electrophoresis was performed. First, gels were prepared at a concentration of 1% (w/v) agarose in 1×TAE buffer, supplemented with 10 µl SYBR Green for a total volume of 100 ml. Samples were mixed with 6 × loading dye before loading them onto the gel. Agarose gel electrophoresis was performed with running condition at 180 V for 20 minutes and visualized by Gel Doc XR+Imager (Bio-Rad). GeneRuler 1kb Plus (Thermo Fisher Scientific) was used as a gene marker.

6.1.5 DNA extraction from agarose gels

The PCR amplified DNA fragments separated by electrophoresis were cut out from the agarose gel and purified with the PCR clean-up and gel extraction kit (Macherey Nagel) according to manufacturer's instructions.

6.1.6 Plasmid DNA isolation from bacteria

For all the plasmid DNA preparation, NucleoSpin Plasmid Kit (Macherey-Nagel) was used according to manufacturer's instructions.

6.1.7 Seamless cloning

The primers were designed to have 15-20 bases overlapping regions in vector and insert. Linear insert and linear vector were prepared individually by PCR amplification and subject to agarose

electrophoresis. In-Fusion reaction was performed using In-Fusion Snap Assembly master mixes (Takara Bio) following the manufacturer's instructions.

6.1.8 Plasmid construction for full-length and HeLo domain of *At*MLKL1 in insect cells

The N-terminal domain of *At*MLKL1 (residues 1-133) with N-terminal His6-Sumo tag in the pFastBac1 vector (Invitrogen) was generated by PCR using pFastBac1 vector (Invitrogen) encoding full-length *At*MLKL1 coding sequence as a template.

6.1.9 Plasmid construction for full-length and HeLo domain of *At*MLKL3 in *E.coli*

The N-terminal domain of *At*MLKL3 (residues 1-133) with N-terminal GST tag in the pGEX-6p-1 vector (Invitrogen) was generated by PCR using pGEX-6p-1 vector (Invitrogen) encoding full-length *At*MLKL1 coding sequence as a template.

6.1.10 Plasmid construction for cell death assay in protoplasts and *Nicotiana Benthamiana*

The coding sequences of GUS (Thermo Fisher Scientific), the HH+HP (G12D, A16D, L20D, R74E, S287E, L341E, R370E) variant of *At*MLKL1, the HP+HB (R74E, W93A, I97E, F213E, S287E, L341E, R370E) variant of *At*MLKL1 and the S393D variants of AtMLKL1 were cloned into pXCSG-3HA[137] using LR Clonase II or (Thermo Fisher Scientific) or In-Fusion cloning (Takara Clontech). Coding sequences of A thalina without stop codons were initially cloned into pENTR/D-TOPO (Thermo Fisher Scientific).

6.1.11 DNA sequencing analysis

The sequences of plasmid sequences were verified by sequencing service offered by Eurofins Genomics using its Mix2Seq Kit.s

6.2 Disease resistance assay using potato virus X

The monomeric YFP coding region was amplified from pXCSG-YFP[138] by PCR using the primers containing the SfiI recognition sites (SfiIA-mYFPf: TTGGCCATTATGGCCATGGTGAGCAAGGGCGAGGA, SfiIB-mYFPr: TTGGCCGAGGCGGCCTTACTTGTACAGCTCGTCCA) and the PCR product was digested with SfiI (NEB) and ligated into the SfiIA and SfiIB sites of the binary PVX-based expression

vector. The resulting plasmid designated as pSfinx-mYFP was transformed into A. tumefaciens strain GV3101 pSoup[139]. The coding regions of GUS (Thermo Fisher Scientific), the HH+HP (G12D, A16D, L20D, R74E, S287E, L341E, R370E) variant of AtMLKL1, the HP+HB (R74E, W93A, I97E, F213E, S287E, L341E, R370E) variant of *At*MLKL1 and the S393D variants of AtMLKL1 were cloned into pXCSG-3HA[137] using LR Clonase II or (Thermo Fisher Scientific) or In-Fusion cloning (Takara Clontech). The resulting plasmids were transformed into A. tumefaciens strain GV3101 pMP90RK[140]. The *A. tumefaciens* strain carrying pSfinx-mYFP (OD600 = 0.001) and the *A. tumefaciens* strain carrysing either of GUS or AtMLKL1 variants (OD600 = 0.6) were co-infiltrated into leaves of wild type, *adr1 nrg1* mutant[141], or *eds1 pad4 sag101a sag101b* mutant[142] of *N. benthamiana* (*Nbepss*). At 4 days after infiltration, ten 5 mm leaf-discs per condition were collected using a biopsy punch from the infiltrated areas. The collected leaf-discs were snap frozen using liquid nitrogen and kept in -80°C freezer until use. The leaf-discs were ground using a pestle or Retsch mill, and 200 µl of the extraction buffer (50 mM Tris-HCl pH 8.40 150 mM NaCl, proteinase inhibitor (Roche: cOmplet, EDTA-free Protease Inhibitor Cocktail)) was added. The resulting lysate was centrifuged for 5 min at 30,000 x g and 80 µl of the supernatant was loaded into black 96 well plate (Corning: CLS3915-100EA). The fluorescence microplate reader (TECAN: tecan infinite 200 pro) was used to measure YFP intensity (Excitation: 516 nm and Emission: 560 nm). YFP intensity was used as a proxy for PVX viral load.

6.3. Recombinant protein expression and purification and its characterization

6.3.1 Protein expression of full-length and HeLo domain of *At*MLKL1 in insect cells

Insect cell protein expression system was employed to express the recombinant protein of the full-length His6Sumo-*At*MLKL1 protein and the truncated His6Sumo-*At*MLKL1(HeLo) protein. The genes were cloned into pFastBac.1 Bacmid isolation was performed with isopropanol precipitation method instead of using commercial kit to obtain the plasmid with high purity for efficient insect cell transformation. YFP fluorescence was used as a proxy for viral infection in insect cells. To increase the titer, P0 P1, P2 virus were generated and P2 virus was generally used for protein expression. Protein expression was induced by the P2 baculovirus at a ratio of 1:40 (virus:cells, v:v) in Sf-900 II SFM media (Gibco/Thermo fisher scientific) supplemented with 10% FBS to increase protein expression amount.

6.3.2 Protein expression of full-length and HeLo domain of *At*MLKL3 in *E.coli*

E. coli protein expression system was employed to express the recombinant protein of full-length GST-*At*MLKL3-His6 and truncated GST-*At*MLKL3(HeLo)-His6 proteins. Rosetta (DE3) was transformed with the expression vectors, pGEX-6p-1-*At*MLKL3-His6 and pGEX-6p-1-*At*MLKL3HeLo-His6 for full-length and truncated HeLo domain protein expression, respectively. Transformant selection was performed on LB agar supplemented with 50 µg/ml ampicillin and chloramphenicol and grown at 37°C for overnight. An isolated single colony was picked up to prepare a pre-culture in LB containing 50 ug/ml ampicillin and chloramphenicol. The pre-culture was inoculated with new LB media containing 50 ug/ml ampicillin and chloramphenicol and grown at 37°C until OD600 reaches 0.8, and then, the protein expression was induced by 1 mM IPTG (Isopropyl β-D-1-thiogalactopyranoside) and grown at 18°C for overnight. The cell pellet was stored at -80°C until use.

6.3.3 Protein purification

6.3.3.1 Protein purification of *At*MLKL1variants

Full-length wild-type, phosphomimetic S393D variant, and N-terminal HeLo domain of *At*MLKL1 with N-terminal His6Sumo tag was generated by standard PCR-based cloning strategy and its identity was confirmed by sequencing. The protein was expressed in Sf21 insect cells using the vector pFastBac1 (Invitrogen). One litre of cells was infected with 20 ml baculovirus at 28°C. After growth at 28°C for 48 hours, the cells were harvested, re-suspended in a buffer containing 50 mM Tris-HCl pH 8.0 and 300 mM NaCl and lysed by French Press press at 2,000 bar by passing the filter 2 times. After centrifuging for 1 hour at 15,000g, 4°C the *At*MLKL1 variants with N-terminal His6Sumo tag were purified from the supernatant using His tag affinity chromatography with HisPur Cobalt Resin (Thermofisher Scientific). The protein was further purified by gel filtration (Superose 6, 10/30; GE Healthcare). For cryo-EM investigations, the purified protein was concentrated to 0.3 mg/mL in buffer containing 50 mM HEPES pH 8.0 and 150 mM NaCl.

6.3.3.2 Protein purification of full-length and HeLo domain of *At*MLKL3

E.coli cells expressing full-length and truncated GST-*At*MLKL3-His6 were disrupted by French press at 1,400 bar by passing the filter 2 times. After centrifuging for 1 hour at 15,000g, 4°C, the proteins were purified from the supernatant using GST affinity chromatography with Glutathione Sepharose 4B (Cytiva/Sigma). N-terminal GST tag was cleaved by GST-tagged HRV3C, and C-terminally His-tagged full-length and truncated N-terminal HeLo domain of *At*MLKL3 on-column.

6.3.4 SDS-PAGE (SDS-Polyacrylamide Gel Electrophoresis)

Protein quality was examined by SDS-PAGE analysis. The protein samples were mixed with 4×SDS-PAGE loading buffer (Bio-Rad), then loaded on 12% TGX Stain-Free polyacrylamide gels (Bio-Rad) without boing step to avoid aggregation. and run in SDS running buffer at 280 V for 30 minutes. PageRuler Prestained Protein Ladder (Thermo Fisher Scientific) was used as a protein marker.

6.3.5 Western blotting

Proteins were separated by SDS-PAGE based on their electrophoretic mobility. The samples were mixed with 4×SDS-PAGE loading buffer (Bio-Rad), then loaded on 10% polyacrylamide gels without boing step to avoid aggregation. and run in SDS running buffer at 100 V for 60-90 minutes and the gel was transferred to nitrocellulose membrane. The membrane was blocked with TBS-T buffer containing 3% non- fat dry milk at room temperature for 2 hours, probed with peroxidase-conjugated anti-HA antibody overnight at 4°C. Detection was performed with SuperSignal West Femto Maximum Sensitivity Substrate (Thermo Fisher Scientific).

6.3.6 Lipid overlay assay

Lipid overlay assay was performed with full-length and truncated N-terminal HeLo domain from *At*MLKL3 with C-terminal His6 tag using commercially available PIP strip (Echelon Biosciences, Cat. no: P-6001) according to manufacturer instructions. In short, the PIP strip membranes were blocked using fatty acid-free 3% bovine serum albumin (BSA) in TBS-T for 1 h followed by incubation with c.a. 100 ng of full-length *At*MLKL3 and truncated N-terminal HeLo domain from *At*MLKL3 diluted in 3% BSA in TBS-T for 1 h. Next, the membranes were washed in TBS-T for 40 min and the bound proteins were visualized with anti-His antibodies (abcam, Cat. no: ab18184) in a ratio of 1:10000 in TBS-T for 1h. All steps were performed at room temperature other than recombinant protein preparation steps.

6.3.7 Electron microscope analysis

6.3.7.1 Protein particle observation on transmission electron microscope

For preliminary electron microscopic analysis to examine the protein particles, negative staining method was used for grid preparation. 6 µl of protein at a concentration of about mg/ml, was applied to glow-discharged carbon film coated ECF400-Cu-50 grids (ScienceServices) for 45 seconds followed by staining procedure with 2 % uranyl acetate solution. Grids were washed with 6 µl of MiliQ twice and dried until microscope observation. Protein particle observation on the grids were performed using a Hitachi H-7650 120 kV transmission electron microscope (TEM) and AMT XR-41 camera.

Table 2.16 Thermocycling setting for PCR using Q5 Site-Directed Mutagenesis Kit (NEB)

Grids	**Supplier**	**Article Number**	**Purpose**
Quantifoil R1.2/1.3 on Cu 300 mesh grid	Quantifoil	N1-C14nCu30-01	Cryo-EM
Quantifoil R 1.2/1.3 plus C2 on 300 copper mesh	Quantifoil	X-101-Cu300C2	Cryo-EM
TEM Grids, Carbon Film coated, 400 Mesh, Cu	ScienceServices	ECF400-Cu-50	Negative Staining

6.3.7.2 Cryo-EM sample preparation and data collection

Cryo-EM sample was prepared with purified NHis6Sumo-*At*MLKL1 oligomer at a concentration of about 0.5 mg/ml, 3 µl of protein was applied to holey carbon grids (Quantifoil Cu 1.2/1.3, 300 mesh) after glow-discharge for 30 seconds. Grids were then blotted on filter paper (TED PELLA, INC.) for 2.5 seconds in 8 °C with 100% humidity and flash-frozen in liquid ethane using FEI Vitrobot Marked IV. Titan Krios microscope was operated with accelerating voltage at 300 kV, equipped with FalconIII camera to collect micrographs. A nominal magnification of 96,000× was used to obtain the images with a pixel size of 0.862 [Å/px]. Defocus range values started from -0.5 µm to -2.5 µm. Exposure rate of data collection was 23 electron per pixel per second. The exposure time was 43.24 seconds dose-fractionated into 42 sub-frames with total electron exposure of 35.47 electrons/Å^2.

6.4. Protoplast based cell death assay

The procedure of *Arabidopsis* protoplast isolation, transient gene expression and luciferase activity measurement were performed as described previously[143]. The preparation of the expression gene is described in Protoplasts were isolated from the leaves of four-week-old *Arabidopsis* plants grown in liquid 1 x Murashige and Skoog medium.

7. References

7. References

1. Kourelis, J. & van der Hoorn, R. A. L. Defended to the Nines: 25 Years of Resistance Gene Cloning Identifies Nine Mechanisms for R Protein Function. *Plant Cell* **30**, 285–299 (2018).
2. Van de Weyer, A.-L. *et al.* A Species-Wide Inventory of NLR Genes and Alleles in Arabidopsis thaliana. *Cell* **178**, 1260-1272.e14 (2019).
3. Yu, X., Feng, B., He, P. & Shan, L. From Chaos to Harmony: Responses and Signaling upon Microbial Pattern Recognition. *Annu. Rev. Phytopathol.* **55**, 109–137 (2017).
4. DeFalco, T. A. & Zipfel, C. Molecular mechanisms of early plant pattern-triggered immune signaling. *Mol. Cell* **81**, 3449–3467 (2021).
5. Boller, T. & Felix, G. A renaissance of elicitors: perception of microbe-associated molecular patterns and danger signals by pattern-recognition receptors. *Annu. Rev. Plant Biol.* **60**, 379–406 (2009).
6. Jones, J. D. G. & Dangl, J. L. The plant immune system. *Nature* **444**, 323–329 (2006).
7. Jacob, F., Vernaldi, S. & Maekawa, T. Evolution and Conservation of Plant NLR Functions. *Front. Immunol.* **4**, 297 (2013).
8. Jubic, L. M., Saile, S., Furzer, O. J., El Kasmi, F. & Dangl, J. L. Help wanted: helper NLRs and plant immune responses. *Curr. Opin. Plant Biol.* **50**, 82–94 (2019).
9. Maekawa, T., Kufer, T. A. & Schulze-Lefert, P. NLR functions in plant and animal immune systems: so far and yet so close. *Nat. Immunol.* **12**, 817–826 (2011).
10. Ausubel, F. M. Are innate immune signaling pathways in plants and animals conserved? *Nat. Immunol.* **6**, 973–979 (2005).
11. Gómez-Gómez, L. & Boller, T. FLS2: an LRR receptor-like kinase involved in the perception of the bacterial elicitor flagellin in Arabidopsis. *Mol. Cell* **5**, 1003–1011 (2000).
12. Hayashi, F. *et al.* The innate immune response to bacterial flagellin is mediated by Toll-like receptor 5. *Nature* **410**, 1099–1103 (2001).

13. Yoon, S.-I. *et al.* Structural basis of TLR5-flagellin recognition and signaling. *Science* **335**, 859–864 (2012).

14. Dunning, F. M., Sun, W., Jansen, K. L., Helft, L. & Bent, A. F. Identification and mutational analysis of Arabidopsis FLS2 leucine-rich repeat domain residues that contribute to flagellin perception. *Plant Cell* **19**, 3297–3313 (2007).

15. Chinchilla, D. *et al.* A flagellin-induced complex of the receptor FLS2 and BAK1 initiates plant defence. *Nature* **448**, 497–500 (2007).

16. Heese, A. *et al.* The receptor-like kinase SERK3/BAK1 is a central regulator of innate immunity in plants. *Proc. Natl. Acad. Sci. U. S. A.* **104**, 12217–12222 (2007).

17. Lu, D. *et al.* A receptor-like cytoplasmic kinase, BIK1, associates with a flagellin receptor complex to initiate plant innate immunity. *Proceedings of the National Academy of Sciences* **107**, 496–501 (2010).

18. Zhang, J. *et al.* Receptor-like cytoplasmic kinases integrate signaling from multiple plant immune receptors and are targeted by a Pseudomonas syringae effector. *Cell Host Microbe* **7**, 290–301 (2010).

19. Sun, Y. *et al.* Structural Basis for flg22-Induced Activation of the *Arabidopsis* FLS2-BAK1 Immune Complex. *Science* **342**, 624–628 (2013).

20. Segonzac, C. & Zipfel, C. Activation of plant pattern-recognition receptors by bacteria. *Curr. Opin. Microbiol.* **14**, 54–61 (2011).

21. Dubiella, U. *et al.* Calcium-dependent protein kinase/NADPH oxidase activation circuit is required for rapid defense signal propagation. *Proc. Natl. Acad. Sci. U. S. A.* **110**, 8744–8749 (2013).

22. Boudsocq, M. *et al.* Differential innate immune signalling via Ca2+ sensor protein kinases. *Nature* **464**, 418–422 (2010).

23. Asai, T. *et al.* MAP kinase signalling cascade in Arabidopsis innate immunity. *Nature* **415**, 977–983 (2002).

24. Saijo, Y., Loo, E. P.-I. & Yasuda, S. Pattern recognition receptors and signaling in plant-microbe interactions. *Plant J.* **93**, 592–613 (2018).

25. Gust, A. A., Pruitt, R. & Nürnberger, T. Sensing danger: Key to activating plant immunity. *Trends Plant Sci.* **22**, 779–791 (2017).

26. Göhre, V. *et al.* Plant pattern-recognition receptor FLS2 is directed for degradation by the bacterial ubiquitin ligase AvrPtoB. *Curr. Biol.* **18**, 1824–1832 (2008).

27. Caplan, J., Padmanabhan, M. & Dinesh-Kumar, S. P. Plant NB-LRR immune receptors: from recognition to transcriptional reprogramming. *Cell Host Microbe* **3**, 126–135 (2008).

28. Bi, G. *et al.* The ZAR1 resistosome is a calcium-permeable channel triggering plant immune signaling. *Cell* **184**, 3528-3541.e12 (2021).

29. Wang, J. *et al.* Reconstitution and structure of a plant NLR resistosome conferring immunity. *Science* **364**, (2019).

30. Adachi, H. *et al.* An N-terminal motif in NLR immune receptors is functionally conserved across distantly related plant species. *Elife* **8**, (2019).

31. Förderer, A. *et al.* A wheat resistosome defines common principles of immune receptor channels. *Nature* **610**, 532–539 (2022).

32. Aarts, N. *et al.* Different requirements for EDS1 and NDR1 by disease resistance genes define at least two R gene-mediated signaling pathways in Arabidopsis. *Proc. Natl. Acad. Sci. U. S. A.* **95**, 10306–10311 (1998).

33. Century, K. S., Holub, E. B. & Staskawicz, B. J. NDR1, a locus of Arabidopsis thaliana that is required for disease resistance to both a bacterial and a fungal pathogen. *Proc. Natl. Acad. Sci. U. S. A.* **92**, 6597–6601 (1995).

34. Knepper, C., Savory, E. A. & Day, B. The role of NDR1 in pathogen perception and plant defense signaling. *Plant Signal. Behav.* **6**, 1114–1116 (2011).

35. Ma, S. *et al.* Direct pathogen-induced assembly of an NLR immune receptor complex to form a holoenzyme. *Science* **370**, eabe3069 (2020).

36. Martin, R. *et al.* Structure of the activated ROQ1 resistosome directly recognizing the pathogen effector XopQ. *Science* **370**, (2020).

37. Horsefield, S. *et al.* NAD^+ cleavage activity by animal and plant TIR domains in cell death pathways. *Science* **365**, 793–799 (2019).

38. Wan, L. *et al.* TIR domains of plant immune receptors are NAD+-cleaving enzymes that promote cell death. *Science* **365**, 799–803 (2019).

39. Wu, Z. *et al.* Differential regulation of TNL-mediated immune signaling by redundant helper CNLs. *New Phytol.* **222**, 938–953 (2019).

40. Qi, T. *et al.* NRG1 functions downstream of EDS1 to regulate TIR-NLR-mediated plant immunity in Nicotiana benthamiana. *Proc. Natl. Acad. Sci. U. S. A.* **115**, E10979–E10987 (2018).

41. Jia, A. *et al.* TIR-catalyzed ADP-ribosylation reactions produce signaling molecules for plant immunity. *Science* **377**, eabq8180 (2022).

42. Huang, S. *et al.* Identification and receptor mechanism of TIR-catalyzed small molecules in plant immunity. *Science* **377**, eabq3297 (2022).

43. Bonardi, V. *et al.* Expanded functions for a family of plant intracellular immune receptors beyond specific recognition of pathogen effectors. *Proceedings of the National Academy of Sciences* **108**, 16463–16468 (2011).

44. Dong, O. X. *et al.* TNL-mediated immunity in Arabidopsis requires complex regulation of the redundant ADR1 gene family. *New Phytol.* **210**, 960–973 (2016).

45. Yu, D. *et al.* TIR domains of plant immune receptors are 2′,3′-cAMP/cGMP synthetases mediating cell death. *Cell* **185**, 2370-2386.e18 (2022).

46. Thomma, B. P. H. J., Nürnberger, T. & Joosten, M. H. A. J. Of PAMPs and effectors: the blurred PTI-ETI dichotomy. *Plant Cell* **23**, 4–15 (2011).

47. Lee, S.-W. *et al.* A Type I–Secreted, Sulfated Peptide Triggers XA21-Mediated Innate Immunity. *Science* **326**, 850–853 (2009).

48. Ngou, B. P. M., Ahn, H.-K., Ding, P. & Jones, J. D. G. Mutual potentiation of plant immunity by cell-surface and intracellular receptors. *Nature* **592**, 110–115 (2021).

49. Yuan, M. *et al.* Pattern-recognition receptors are required for NLR-mediated plant immunity. *Nature* **592**, 105–109 (2021).

50. Tian, H. *et al.* Activation of TIR signalling boosts pattern-triggered immunity. *Nature* **598**, 500–503 (2021).

51. Cook, D. E., Mesarich, C. H. & Thomma, B. P. H. J. Understanding Plant Immunity as a Surveillance System to Detect Invasion. *Annu. Rev. Phytopathol.* **53**, 541–563 (2015).

52. Morel, J. B. & Dangl, J. L. The hypersensitive response and the induction of cell death in plants. *Cell Death Differ.* **4**, 671–683 (1997).

53. Mur, L. A. J., Kenton, P., Lloyd, A. J., Ougham, H. & Prats, E. The hypersensitive response; the centenary is upon us but how much do we know? *J. Exp. Bot.* **59**, 501–520 (2008).

54. Bendahmane, A., Kanyuka, K. & Baulcombe, D. C. The Rx gene from potato controls separate virus resistance and cell death responses. *Plant Cell* **11**, 781–792 (1999).

55. Sun, X. *et al.* Pathogen effector recognition-dependent association of NRG1 with EDS1 and SAG101 in TNL receptor immunity. *Nat. Commun.* **12**, 3335 (2021).

56. He, M., He, C.-Q. & Ding, N.-Z. Evolution of Potato virus X. *Mol. Phylogenet. Evol.* **167**, 107336 (2022).

57. Larsen, J. S. & Curtis, W. R. RNA viral vectors for improved Agrobacterium-mediated transient expression of heterologous proteins in Nicotiana benthamiana cell suspensions and hairy roots. *BMC Biotechnol.* **12**, 21 (2012).

58. Peart, J. R., Cook, G., Feys, B. J., Parker, J. E. & Baulcombe, D. C. An EDS1 orthologue is required for N-mediated resistance against tobacco mosaic virus. *Plant J.* **29**, 569–579 (2002).

59. Collier, S. M., Hamel, L.-P. & Moffett, P. Cell death mediated by the N-terminal domains of a unique and highly conserved class of NB-LRR protein. *Mol. Plant. Microbe. Interact.* **24**, 918–931 (2011).

60. Degterev, A. *et al.* Identification of RIP1 kinase as a specific cellular target of necrostatins. *Nat. Chem. Biol.* **4**, 313–321 (2008).

61. Hitomi, J. *et al.* Identification of a molecular signaling network that regulates a cellular necrotic cell death pathway. *Cell* **135**, 1311–1323 (2008).

62. Degterev, A. *et al.* Chemical inhibitor of nonapoptotic cell death with therapeutic potential for ischemic brain injury. *Nat. Chem. Biol.* **1**, 112–119 (2005).

63. Pasparakis, M. & Vandenabeele, P. Necroptosis and its role in inflammation. *Nature* **517**, 311–320 (2015).

64. Re, D. B. *et al.* Necroptosis drives motor neuron death in models of both sporadic and familial ALS. *Neuron* **81**, 1001–1008 (2014).

65. Jouan-Lanhouet, S. *et al.* Necroptosis, in vivo detection in experimental disease models. *Semin. Cell Dev. Biol.* **35**, 2–13 (2014).

66. Kolbrink, B., Riebeling, T., Kunzendorf, U. & Krautwald, S. Plasma Membrane Pores Drive Inflammatory Cell Death. *Front Cell Dev Biol* **8**, 817 (2020).

67. Cho, Y. *et al.* Phosphorylation-Driven Assembly of the RIP1-RIP3 Complex Regulates Programmed Necrosis and Virus-Induced Inflammation. *Cell* **137**, 1112–1123 (2009).

68. Upton, J. W., Kaiser, W. J. & Mocarski, E. S. DAI/ZBP1/DLM-1 complexes with RIP3 to mediate virus-induced programmed necrosis that is targeted by murine cytomegalovirus vIRA. *Cell Host Microbe* **11**, 290–297 (2012).

69. Wang, X. *et al.* Direct activation of RIP3/MLKL-dependent necrosis by herpes simplex virus 1 (HSV-1) protein ICP6 triggers host antiviral defense. *Proc. Natl. Acad. Sci. U. S. A.* **111**, 15438–15443 (2014).

70. Nogusa, S. *et al.* RIPK3 Activates Parallel Pathways of MLKL-Driven Necroptosis and FADD-Mediated Apoptosis to Protect against Influenza A Virus. *Cell Host Microbe* **20**, 13–24 (2016).

71. Sai, K., Parsons, C., House, J. S., Kathariou, S. & Ninomiya-Tsuji, J. Necroptosis mediators RIPK3 and MLKL suppress intracellular Listeria replication independently of host cell killing. *J. Cell Biol.* **218**, 1994–2005 (2019).

72. Duan, X. *et al.* Inhibition of keratinocyte necroptosis mediated by RIPK1/RIPK3/MLKL provides a protective effect against psoriatic inflammation. *Cell Death Dis.* **11**, 1–14 (2020).

73. Hildebrand, J. M. *et al.* A missense mutation in the MLKL brace region promotes lethal neonatal inflammation and hematopoietic dysfunction. *Nat. Commun.* **11**, 3150 (2020).

74. Wang, H. *et al.* Mixed lineage kinase domain-like protein MLKL causes necrotic membrane disruption upon phosphorylation by RIP3. *Mol. Cell* **54**, 133–146 (2014).

75. Sun, L. *et al.* Mixed lineage kinase domain-like protein mediates necrosis signaling downstream of RIP3 kinase. *Cell* **148**, 213–227 (2012).

76. Garnish, S. E. *et al.* Conformational interconversion of MLKL and disengagement from RIPK3 precede cell death by necroptosis. *Nat. Commun.* **12**, 2211 (2021).

77. Petrie, E. J. *et al.* Conformational switching of the pseudokinase domain promotes human MLKL tetramerization and cell death by necroptosis. *Nat. Commun.* **9**, 2422 (2018).

78. Hildebrand, J. M. *et al.* Activation of the pseudokinase MLKL unleashes the four-helix bundle domain to induce membrane localization and necroptotic cell death. *Proceedings of the National Academy of Sciences* **111**, 15072–15077 (2014).

79. Flores-Romero, H., Ros, U. & Garcia-Saez, A. J. Pore formation in regulated cell death. *EMBO J.* **39**, e105753 (2020).

80. Su, L. *et al.* A plug release mechanism for membrane permeation by MLKL. *Structure* **22**, 1489–1500 (2014).

81. Dondelinger, Y. *et al.* MLKL Compromises Plasma Membrane Integrity by Binding to Phosphatidylinositol Phosphates. *Cell Rep.* **7**, 971–981 (2014).

82. Ros, U. *et al.* Necroptosis Execution Is Mediated by Plasma Membrane Nanopores Independent of Calcium. *Cell Rep.* **19**, 175–187 (2017).

83. Xia, B. *et al.* MLKL forms cation channels. *Cell Res.* **26**, 517–528 (2016).

84. Xia, B., Qie, J., Shen, X., Wang, S. & Gao, Z. Enhanced channel activity by PI(4,5)P2 ignites MLKL-related pathogenic processes. *Cell Discov* **8**, 111 (2022).

85. Chen, X. *et al.* Translocation of mixed lineage kinase domain-like protein to plasma membrane leads to necrotic cell death. *Cell Res.* **24**, 105–121 (2014).

86. Cai, Z. *et al.* Plasma membrane translocation of trimerized MLKL protein is required for TNF-induced necroptosis. *Nat. Cell Biol.* **16**, 55–65 (2014).

87. Chen, X. *et al.* Pyroptosis is driven by non-selective gasdermin-D pore and its morphology is different from MLKL channel-mediated necroptosis. *Cell Res.* **26**, 1007–1020 (2016).

88. Huang, D. *et al.* The MLKL Channel in Necroptosis Is an Octamer Formed by Tetramers in a Dyadic Process. *Mol. Cell. Biol.* **37**, (2017).

89. Liu, S. *et al.* MLKL forms disulfide bond-dependent amyloid-like polymers to induce necroptosis. *Proc. Natl. Acad. Sci. U. S. A.* **114**, E7450–E7459 (2017).

90. Davies, K. A. *et al.* The brace helices of MLKL mediate interdomain communication and oligomerisation to regulate cell death by necroptosis. *Cell Death Differ.* **25**, 1567–1580 (2018).

91. Lapin, D., Johanndrees, O., Wu, Z., Li, X. & Parker, J. E. Molecular innovations in plant TIR-based immunity signaling. *Plant Cell* **34**, 1479–1496 (2022).

92. Wang, W., Wen, Y., Berkey, R. & Xiao, S. Specific targeting of the Arabidopsis resistance protein RPW8.2 to the interfacial membrane encasing the fungal Haustorium renders broad-spectrum resistance to powdery mildew. *Plant Cell* **21**, 2898–2913 (2009).

93. Li, L., Habring, A., Wang, K. & Weigel, D. Atypical Resistance Protein RPW8/HR Triggers Oligomerization of the NLR Immune Receptor RPP7 and Autoimmunity. *Cell Host Microbe* **27**, 405-417.e6 (2020).

94. Jacob, P. *et al.* Plant "helper" immune receptors are Ca2+-permeable nonselective cation channels. *Science* **373**, 420–425 (2021).

95. Saupe, S. J. The [Het-s] prion of Podospora anserina and its role in heterokaryon incompatibility. *Semin. Cell Dev. Biol.* **22**, 460–468 (2011).

96. Daskalov, A. *et al.* Identification of a novel cell death-inducing domain reveals that fungal amyloid-controlled programmed cell death is related to necroptosis. *Proc. Natl. Acad. Sci. U. S. A.* **113**, 2720–2725 (2016).

97. Greenwald, J. *et al.* The mechanism of prion inhibition by HET-S. *Mol. Cell* **38**, 889–899 (2010).

98. Seuring, C. *et al.* The mechanism of toxicity in HET-S/HET-s prion incompatibility. *PLoS Biol.* **10**, e1001451 (2012).

99. Mahdi, L. K. *et al.* Discovery of a Family of Mixed Lineage Kinase Domain-like Proteins in Plants and Their Role in Innate Immune Signaling. *Cell Host Microbe* **28**, 813-824.e6 (2020).

100. Barragan, C. A. *et al.* RPW8/HR repeats control NLR activation in Arabidopsis thaliana. *PLoS Genet.* **15**, e1008313 (2019).

101. Bentham, A. R., Zdrzalek, R., De la Concepcion, J. C. & Banfield, M. J. Uncoiling CNLs: Structure/Function Approaches to Understanding CC Domain Function in Plant NLRs. *Plant Cell Physiol.* **59**, 2398–2408 (2018).

102. Tian, L. & Li, X. TIR domains as two-tiered enzymes to activate plant immunity. *Cell* **185**, 2208–2209 (2022).

103. Murphy, J. M. *et al.* The pseudokinase MLKL mediates necroptosis via a molecular switch mechanism. *Immunity* **39**, 443–453 (2013).

104. Maekawa, T., Kashkar, H. & Coll, N. S. Dying in self-defence: a comparative overview of immunogenic cell death signalling in animals and plants. *Cell Death Differ.* (2022) doi:10.1038/s41418-022-01060-6.

105. Grant, M. *et al.* The RPM1 plant disease resistance gene facilitates a rapid and sustained increase in cytosolic calcium that is necessary for the oxidative burst and hypersensitive cell death. *Plant J.* **23**, 441–450 (2000).

106. Tian, L. *et al.* Imaging neural activity in worms, flies and mice with improved GCaMP calcium indicators. *Nat. Methods* **6**, 875–881 (2009).

107. Vincent, T. R. *et al.* Interplay of Plasma Membrane and Vacuolar Ion Channels, Together with BAK1, Elicits Rapid Cytosolic Calcium Elevations in Arabidopsis during Aphid Feeding. *Plant Cell* **29**, 1460–1479 (2017).

108. Grant, M. R. *et al.* Structure of the *Arabidopsis RPM1* Gene Enabling Dual Specificity Disease Resistance. *Science* **269**, 843–846 (1995).

109. DeFalco, T. A. *et al.* Using GCaMP3 to Study Ca2+ Signaling in Nicotiana Species. *Plant Cell Physiol.* **58**, 1173–1184 (2017).

110. Palsdottir, H. & Hunte, C. Lipids in membrane protein structures. *Biochim. Biophys. Acta* **1666**, 2–18 (2004).

111. Nakamura, Y. Plant Phospholipid Diversity: Emerging Functions in Metabolism and Protein–Lipid Interactions. *Trends Plant Sci.* **22**, 1027–1040.

112. Marković, V. & Jaillais, Y. Phosphatidylinositol 4-phosphate: a key determinant of plasma membrane identity and function in plants. *New Phytol.* **235**, 867–874 (2022).

113. Xing, J., Zhang, L., Duan, Z. & Lin, J. Coordination of Phospholipid-Based Signaling and Membrane Trafficking in Plant Immunity. *Trends Plant Sci.* **26**, 407–420 (2021).

114. Quarato, G. *et al.* Sequential Engagement of Distinct MLKL Phosphatidylinositol-Binding Sites Executes Necroptosis. *Mol. Cell* **61**, 589–601 (2016).

115. Samson, A. L. *et al.* MLKL trafficking and accumulation at the plasma membrane control the kinetics and threshold for necroptosis. *Nat. Commun.* **11**, 1–17 (2020).

116. Zarreen, F., Kumar, K. & Chakraborty, S. Phosphoinositides in plant-pathogen interaction: trends and perspectives. *Stress Biology* **3**, 4 (2023).

117. Doumane, M. *et al.* Inducible depletion of PI(4,5)P2 by the synthetic iDePP system in Arabidopsis. *Nat Plants* **7**, 587–597 (2021).

118. Adachi, H., Kamoun, S. & Maqbool, A. A resistosome-activated “death switch.” *Nature plants* vol. 5 457–458 (2019).

119. Kayagaki, N. *et al.* NINJ1 mediates plasma membrane rupture during lytic cell death. *Nature* **591**, 131–136 (2021).

120. Pedrera, L. *et al.* Ferroptotic pores induce Ca2+ fluxes and ESCRT-III activation to modulate cell death kinetics. *Cell Death Differ.* **28**, 1644–1657 (2020).

121. Ferrari, S. *et al.* Oligogalacturonides: plant damage-associated molecular patterns and regulators of growth and development. *Front. Plant Sci.* **4**, 49 (2013).

122. De Lorenzo, G., D'Ovidio, R. & Cervone, F. The role of polygalacturonase-inhibiting proteins (PGIPs) in defense against pathogenic fungi. *Annu. Rev. Phytopathol.* **39**, 313–335 (2001).

123. Choi, J. *et al.* Identification of a plant receptor for extracellular ATP. *Science* **343**, 290–294 (2014).

124. Xia, S. *et al.* Gasdermin D pore structure reveals preferential release of mature interleukin-1. *Nature* **593**, 607–611 (2021).

125. Heilig, R. *et al.* The Gasdermin-D pore acts as a conduit for IL-1β secretion in mice. *Eur. J. Immunol.* **48**, 584–592 (2018).

126. Yamaguchi, Y. & Huffaker, A. Endogenous peptide elicitors in higher plants. *Curr. Opin. Plant Biol.* **14**, 351–357 (2011).

127. Huffaker, A., Pearce, G. & Ryan, C. A. An endogenous peptide signal in *Arabidopsis* activates components of the innate immune response. *Proceedings of the National Academy of Sciences* **103**, 10098–10103 (2006).

128. Yamaguchi, Y., Huffaker, A., Bryan, A. C., Tax, F. E. & Ryan, C. A. PEPR2 is a second receptor for the Pep1 and Pep2 peptides and contributes to defense responses in Arabidopsis. *Plant Cell* **22**, 508–522 (2010).

129. Bartels, S. *et al.* The family of Peps and their precursors in Arabidopsis: differential expression and localization but similar induction of pattern-triggered immune responses. *J. Exp. Bot.* **64**, 5309–5321 (2013).

130. Bartels, S. & Boller, T. Quo vadis, Pep? Plant elicitor peptides at the crossroads of immunity, stress, and development. *J. Exp. Bot.* **66**, 5183–5193 (2015).

131. Yamada, K. *et al.* Danger peptide receptor signaling in plants ensures basal immunity upon pathogen-induced depletion of BAK1. *EMBO J.* **35**, 46–61 (2016).

132. Kosmacz, M. *et al.* Interaction of 2',3'-cAMP with Rbp47b Plays a Role in Stress Granule Formation. *Plant Physiol.* **177**, 411–421 (2018).

133. Saile, S. C. *et al.* Two unequally redundant "helper" immune receptor families mediate Arabidopsis thaliana intracellular "sensor" immune receptor functions. *PLoS Biol.* **18**, e3000783 (2020).

134. Lapin, D. *et al.* A Coevolved EDS1-SAG101-NRG1 Module Mediates Cell Death Signaling by TIR-Domain Immune Receptors. *Plant Cell* **31**, 2430–2455 (2019).

135. Wang, M.-Y. *et al.* The immune receptor SNC1 monitors helper NLRs targeted by a bacterial effector. *bioRxiv* 2023.03.23.533910 (2023) doi:10.1101/2023.03.23.533910.

136. Tian, L., Lu, J. & Li, X. Differential requirement of TIR enzymatic activities in TIR-type immune receptor SNC1-mediated immunity. *Plant Physiol.* **190**, 2094–2098 (2022).

137. Maekawa, T. *et al.* Coiled-Coil Domain-Dependent Homodimerization of Intracellular Barley Immune Receptors Defines a Minimal Functional Module for Triggering Cell Death. *Cell Host Microbe* **9**, 187–199 (2011).

138. Feys, B. J. *et al.* Arabidopsis SENESCENCE-ASSOCIATED GENE101 Stabilizes and Signals within an ENHANCED DISEASE SUSCEPTIBILITY1 Complex in Plant Innate Immunity. *Plant Cell* **17**, 2601–2613 (2005).

139. Takken, F. L. *et al.* A functional cloning strategy, based on a binary PVX-expression vector, to isolate HR-inducing cDNAs of plant pathogens. *Plant J.* **24**, 275–283 (2000).

140. Koncz, C. & Schell, J. The promoter of TL-DNA gene 5 controls the tissue-specific expression of chimaeric genes carried by a novel type of Agrobacterium binary vector. *Mol. Gen. Genet.* **204**, 383–396 (1986).

141. Prautsch, J. *et al.* Effector XopQ-induced stromule formation in Nicotiana benthamiana depends on ETI signaling components ADR1 and NRG1. *Plant Physiol.* **191**, 161–176 (2022).

142. Gantner, J., Ordon, J., Kretschmer, C., Guerois, R. & Stuttmann, J. An EDS1-SAG101 Complex Is Essential for TNL-Mediated Immunity in Nicotiana benthamiana. *Plant Cell* **31**, 2456–2474 (2019).

143. Saur, I. M. L., Bauer, S., Lu, X. & Schulze-Lefert, P. A cell death assay in barley and wheat protoplasts for identification and validation of matching pathogen AVR effector and plant NLR immune receptors. *Plant Methods* **15**, 118 (2019).

8. Curriculum Vitae

8. Curriculum Vitae

Keiichi Hasegawa

1. PERSONAL INFORMATION

Mailing Address: Melatengürtel 113, 203, 50825 Köln, Germany

Nationality: Japan

Phone: +49-(0)15110287019

E-mail: khasegawa@mpipz.mpg.de

2. EDUCATION

August 2020-Present

University of Cologne, Cologne, Germany

Faculty of Mathematics and Natural Sciences

PhD student, Research Group Jijie Chai and Takaki Maekawa

April 2018–March 2020

The University of Tokyo, Tokyo, Japan (GPA: 3.9/4.0)

M.S. Department of Applied Biological Chemistry

April 2014–March 2018

Tokyo Institute of Technology (GPA: 3.6/4.0)

B.S. Department of Life Science and Technology

3. RESEARCH FIELDS

Plant Immunity, Plant Receptor Biology, Structural Biology, Protein Engineering, Signal Transduction, Membrane Proteins

4. RESEARCH SKILLS

Molecular Cloning, Protein Expression, Protein Purification, Protein Crystallization, Cryo-EM, Molecular Interaction Analysis, Western Blotting, Cell Culture, HPLC, Mass Spectrometry, Plant Cell Death Assays

5. RESEARCH EXPERIENCE

1. PhD Thesis Project

"Structural insight into activation mechanism of plant MLKL"

Supervisor: Prof. Dr. Jijie Chai and Dr. Takaki Maekawa

Co-Supervisor: Prof. Dr. Jane Parker

Faculty of Mathematics and Natural Sciences, University of Cologne

2. Master's Thesis Project

"Analysis of ligand recognition mechanism by ethylene receptor, ETR1"

Supervisor: Assoc. Prof. Dr. Koji Nagata

Co-Supervisor: Assoc. Prof. Dr. Michio Suzuki

Collaborator: Prof. Dr. Tadao Asami

Laboratory of Food Biotechnology and Structural Biology

Department of Applied Biological Chemistry, Graduate School of Agricultural and Life Sciences, The University of Tokyo, April 2018–March 2020

3. Bachelor's Thesis Project

"Development of cell recovery method using thermo–responsive protein hydrogel"

Supervisor: Prof. Dr. Eiry Kobatake and Assoc. Prof. Dr. Masayasu Mie

Department of Life Science and Technology, Tokyo Institute of Technology,

April 2017 – March 2018

6. CONFERENCE PRESENTATION

1. ○**Keiichi Hasegawa**, Qiaochu Shen, Anna Prakken, Nicole Oelerich, Menghang Huang, Frowin Reichhardt, Alexandra Tersch, Alexander Foerderer, Kay Hofman, Jijie Chai, Takaki Maekawa, "Activation mechanism of plant mixed lineage kinase domain-like (MLKL) proteins, conferring TIR-NLR-mediated immunity", Providence, Rhode Island, United States, 2023 International Society for Molecular Plant-Microbe Interactions Congress, July 2023.

(Poster Presentation)

2. ○**Keiichi Hasegawa**, Qiaochu Shen, Anna Prakken, Nicole Oelerich, Menghang Huang, Frowin Reichhardt, Alexandra Tersch, Alexander Foerderer, Kay Hofman, Jijie Chai, Takaki Maekawa, "Activation mechanism of plant mixed lineage kinase domain-like (MLKL) proteins, conferring TIR-NLR-mediated immunity", Cologne, Germany, Cologne cell death spring meeting, March 2023.

(Poster Presentation)

3. ○**Keiichi Hasegawa**, Qiaochu Shen, Anna Prakken, Nicole Oelerich, Menghang Huang, Frowin Reichhardt, Alexandra Tersch, Alexander Foerderer, Kay Hofman, Jijie Chai, Takaki Maekawa, "Activation mechanism of plant mixed lineage kinase domain-like (MLKL) proteins, conferring TIR-NLR-mediated immunity", Hennef, Germany, The 64th Annual Meeting of the Japanese Society of Plant Physiologists, March 2023.

(Poster Presentation)

4. ○**Keiichi Hasegawa**, Qiaochu Shen, Anna Prakken, Nicole Oelerich, Menghang Huang, Frowin Reichhardt, Alexandra Tersch, Alexander Foerderer, Kay Hofman, Jijie Chai, Takaki Maekawa, "Activation mechanism of plant mixed lineage kinase domain-like (MLKL) proteins,

conferring TIR-NLR-mediated immunity", Sendai, Japan, The 64th Annual Meeting of the Japanese Society of Plant Physiologists, March 2023.

(Oral Presentation)

5. ○**K. Hasegawa**, P. Lu, I. Takahashi, Y. Katayama, Yi Lu, K. Okamoto, M. Suzuki, H. Nakamura, M. Nakajima, T. Asami, K. Nagata, "Expression of recombinant protein of full-length and ligand-binding domain of the ethylene receptor", 1E6p10, Tokyo University of Agriculture, The Japan Society for Bioscience, Biotechnology, and Agrochemistry, March 2019

(Oral Presentation)

6. ○**K. Hasegawa**, P. Lu, I. Takahashi, Y. Katayama, Yi Lu, K. Okamoto, M. Suzuki, H. Nakamura, M. Nakajima, T. Asami, K. Nagata, "Expression and purification of the ethylene receptor AtETR1", The University of Tokyo Life Science Symposium, The University of Tokyo, April 2019

(Poster Presentation)

7. ○**K. Hasegawa**, M. Zhang, P. Lu, K. Hayakawa, Y. Katayama, H. Katayama, J. Nakayama, K. Sonomoto, M. Tanokura, K. Nagata, "Expression, Purification, Crystallization and Preliminary X-ray Crystallographic Studies of FsrC, the Cell Surface Receptor of the Cyclic Peptide Quormone GBAP", The 10th International Peptide Symposium, PA-071, ROHM Theatre Kyoto and Miyako Messe, December 2018

(Poster Presentation)

(Proceedings: PEPTIDE SCIENCE 2018, The Japanese Peptide Society, ISBN: 978-4-931541-191, ISSN: 1344-7661, p.35, March 2019)

7. TEACHING EXPERIENCE

1. Visualization of protein structure by PyMOL in a lecture series
   "Signaling molecules and communication in plants (elective module I)"
   University of Cologne, November 2020
2. Mentoring three master-internship students with hands-on teaching of basic molecular biology techniques and scientific thinking. In parallel, I gave a project derived from my part of doctoral project for a master student internship.
   Max Planck Institute for Plant Breeding Research
   January 2021-June 2021and January 2022-June 2022
3. "Enzyme production by microorganisms and functional analysis", October 2018

   Bachelor Student Experiment, Department of Agriculture, The University of Tokyo,

4. Bachelor Student Experiment, Department of Life Science and Technology, Tokyo Institute of Technology, 2017

5. "Bioengineering Contest", Tokyo Institute of Technology, 2017

8. SEMINAR ATTENDANCE

1. Department seminar at Max Planck Institute for Plant Breeding Research held every Tuesday and **gave talks three times in the department up to now.**

2. NLR biology meeting held on Wednesday every 2 weeks and **gave three talks** up to now once a certain amount of my research progress.
3. Department seminar for plant-microbe interactions section at university of Cologne every month attended
4. Journal Club at AG Maekawa held every two-week and **I performed five presentations about peer-reviewed journals**
5. Progress report at AG Maekawa held every two-week and **I performed twenty presentations about research progress up-to-date.**
6. SFB basic cell death seminar held once or twice a month
7. "1st Meeting of Japanese plant biology researchers in Europe", 26 January 2021 **I performed a presentation about my research progress up-to-date.**
8. "2nd Meeting of Japanese plant biology researchers in Europe", 9 September 2022

9. WORKSHOP ATTENDANCE

1. Online Lectures on basics of Cryo-EM and Structural biology, October 1st Provided by AMED-BINDS, University of Tokyo
2. Lectures on how to perform image analysis after Cryo-EM data collection by Dr. XiaoXiao Zhang, May 6 2021
3. Workshop for biases in science by Prof. Dr. Niels Gehring, University of Cologne, 5 October 2021
4. "Data analysis with R workshop" by Rick Scavetta, 28 October 2021- 6 November 2022
5. An Ex-Cell Press Editor presents: "Telling your Story in a Scientific Paper" by Dr. Spyros Goulas, June 24 2022, organized by The Institute of Advanced Study of Human Biology, Kyoto University

10. THESIS ADVISORY COMMITTEE (TAC) MEETING

1. 1st TAC meeting, 7th January 2021
2. 2nd TAC meeting, 29th October 2021
3. 3rd TAC meeting, planned on August 2023

11. EXTRA-CURRICULAR SCIENTIFIC ACTIVITY

1. **Seminar**

Tokyo University, April 15 2022

Food Biotechnol & Struct Biol Lab

I gave a presentation on my doctoral project and doctoral life in Germany and discussed with my former advisors and colleagues in the previous lab where I conducted my master's thesis.

12. REVIEWING ACTIVITY OF SCIENTIFIC MANUSCRIPT

1. Plant Biotechnology Journal, June 2021
2. Nature Communications Journal, July 2021

13. RETREAT ATTENDANCE

1. SFB 1403 retreat cell death, in immunity, inflammation and disease, 04.11.2021-05.11.2021 Bonn.
2. PhD retreat **Presentation**: "Structural and functional study of plant MLKL proteins" Cologne, Germany; 29.10.2020
3. Departmental retreat from Max Planck Institute for Plant Breeding Research Berlin 18-21, 05, 2022, **flash talk**, "Structural and functional study of plant MLKL proteins

14. SCHOLARSHIPS

1. JASSO (Japan Student Services Organization) April 2018 -March 2020.

9. Contributions

9. Contributions

Most of the experiments and analyses described in this thesis were conducted by myself. Those that were conducted by and in corporation with other people are indicated below.

• Figure 3B The emission spectra for leaf extracts taken by Dr. Ton Timmers at MPIPZ.

• Figure 6 A, B and F: These data were generated by Lea Weiler Tersch, and Frowin Reichhardt at University of Cologne.

• Figure 6 C and D: These experiments were generated by Nicole Oelerich at University of Cologne.

10. Acknowledgements

10. Acknowledgements

I would like to show thanks to prof. Dr. Jijie Chai and Dr. Takaki Maekawa for their supervision during my stay in Germany, teaching me the spirits of scientists. I would like to show my thanks to all the members of Chai lab and Maekawa lab. Furthermore, I would like to show thanks to Prof. Dr. Jane parker for giving suggestions and supporting me as a TAC member. I would like to show thanks to Alexander Förderer and Nitika Mukhi for assisting my insect cell culture and protein expression. I would like to show thanks to Ulla Neumann and Jan Jirschitzka for routinely assisting my protein sample quality check in electron microscope. I would like to show thanks to Elmar behrmann for performing Cryo-EM data analysis using Cryo-Sparc and Monika Gunkel for helping Cryo-grid preparation. Lastly, I would like to express my gratitude to Jane E. Parker's lab for kindly sharing their *Nbeds1 sag101a sag101b pad4 mutant* mutant; Johannes Stuttmann for their *Nbadr1nrg1* mutant. Finally, I would like to show my great gratitude to Noah Kürtös for proofreading of my Phd thesis and cheering me up during the writing time.

11. Erklärung

A simplified disease resistance assay using YFP-expressing *Potato Virus X* in *N. benthamiana* reveals a cell death-independent immune function of RBA1

Keiichi Hasegawa[1], Ton Timmers[2], Jijie Chai[1,3,5], and Takaki Maekawa[3,4*]

1 Institute for Biochemistry, University of Cologne, 50674 Cologne, Germany

2 Max Planck Institute for Plant Breeding Research, 50829 Cologne, Germany

3 Cluster of Excellence on Plant Sciences (CEPLAS), Cologne, Germany

4 Institute for Plant Sciences, University of Cologne, Cologne, 50674, Germany.

5 Current address: School of Life Sciences, Westlake University, Zhejiang China

*Author for correspondence: tmaekawa@uni-koeln.de (T.M.)

Dear Editor,

R (resistance) proteins, such as intracellular NLRs (nucleotide-binding leucine-rich repeat receptors), are integral components of the plant innate immune system (van Wersch et al., 2020). Host responses following R protein activation include the generation of reactive oxygen species, sustained increases in cytosolic Ca^{2+}, transcriptional reprogramming and, typically, rapid host cell death at sites of pathogen infection, which together ultimately lead to pathogen growth restriction (Wang et al., 2023). To assess the activity of R proteins, agroinfiltration-mediated transient gene expression assays have been widely used in *Nicotiana* species (e.g., *N. benthamiana*). In these transient assays, host cell death is often chosen as an indicator of R protein activity from the host responses mentioned above, in part because of the ease of experimentation. However, the extent to which host cell death is a proxy for disease resistance signaling has long been debated, as host cell death and pathogen growth restriction can be uncoupled in several cases (Bendahmane et al., 1999; Coll et al., 2010; Heidrich et al., 2011, Maekawa et al., 2023). To assess the disease resistance activity of R proteins, bacterial growth assays have been

employed in combination with transient *R* gene expression in *N. benthamiana* (Sun et al., 2021). Bacterial growth assays, however, require multiple experimental procedures, including agroinfiltration, pathogen infection and bacterial counts, which hinders high-throughput studies of *R* gene-mediated disease resistance. Here, we report a simple plate reader-based assay to assess *R* gene-mediated disease resistance activity against PVX (Potato virus X) that expresses YFP (PVX-YFP). Unlike bacterial pathogens, PVX proliferation in *N. benthamiana* is not restricted by the intrinsic activity of the EDS1 signaling pathway as previously shown by virus-induced *NbEDS1* gene silencing (Peart et al., 2002) and as we consistently show in this study using a *Nbeds1* gene knockout mutant. This feature would increase the sensitivity of the assay, allowing it to capture a weak-to-moderate disease resistance activity of R proteins, as the contribution of basal immunity to PVX via the *Nb*EDS1 pathway is negligible. Using this assay, we show that a non-cell death-inducing mutant of the R protein of RBA1 (Response to HopBA1), which lacks 2′,3′-cAMP/cGMP synthetase activity but retains NADase activity, confers PVX resistance in an EDS1 signaling pathway-dependent manner.

PVX is a single-stranded RNA virus and expression of full-length PVX cDNA via agroinfiltration-mediated gene expression allows PVX replication in *Nicotiana* species (Larsen and Curtis, 2012). Insertion of a cDNA of fluorescent protein under a duplicated copy of the viral coat protein promoter allows tracking of PVX replication in plants (Peart et al., 2002). Unlike bacterial growth assays in *Nicotiana* species, in which pathogen infection takes place a few days after agroinfiltration, in the PVX disease resistance assay agroinfiltration and pathogen infection can be performed simultaneously (Collier et al., 2011), with minimal experimental efforts. In this study, we generated a binary vector that allows for PVX replication along with monomeric YFP expression and used YFP intensity as a proxy for PVX viral load. To quantify PVX-produced YFP in *N. benthamiana* leaf extracts, we optimized a fluorescence plate reader-based measurement (Fig. 1A), which is simpler than quantification by western blot. Briefly, in this method agrobacteria carrying the PVX-YFP binary vector and agrobacteria carrying a *R* gene were co-infiltrated into *N. benthamiana* leaves. Four days after infiltration, leaf discs were collected from the infiltrated areas using a biopsy punch. The leaf

protein extracts were used to measure YFP intensity (detailed method is described in the Supplemental Methods). First, we determined the emission spectra of leaf extracts containing PVX-YFP or PVX without fluorescent protein (Fig. 1B). The emission spectrum of PVX-produced YFP was in good agreement with the canonical spectrum of YFP in the leaf extract, and PVX replication in leaves did not produce fluorescence that overlapped with the YFP spectrum (Fig. 1B). The YFP intensity of a dilution series using a leaf protein extract from non-transformed leaves showed that this method has a high dynamic range with a linear correlation between fluorescence and dilution factor and that a detergent, Triton X-100, can be omitted from the extraction buffer (Fig. 1C). Furthermore, the quantified YFP fluorescence intensities in the plate reader-based measurement corresponded to some extent with the fluorescence images (Fig. 1D). Consistent with a previous study (Peart et al., 2002), PVX-YFP proliferation was comparable in wild type and the *eds1 pad4 sag101a sag101b* mutant of *N. benthamiana* (Fig. 1E). Co-expression of a wheat NLR, Sr35 and its cognate effector, AvrSr35 (Förderer et al., 2022), caused host cell death in *N. benthamiana* in the presence of PVX-YFP (Fig. 1F), suggesting that agrobacterium-mediated delivery of PVX-YFP T-DNA does not suppress NLR-induced host cell death. Furthermore, the very low YFP intensity (average intensity ± standard error = 1991 ± 402, n=4), which is nearly equivalent to the YFP intensity of leaf protein extract from non-transformed leaves (Fig. 1C), indicates that host cell death does not result in the production of metabolites that show autofluorescence in the YFP assay.

An *Arabidopsis* R protein, RBA1 (Response to HopBA1), which possesses a Toll/ interleukin-1 receptor like domain (TIR domain) induces host cell death upon transient overexpression in *N. benthamiana* (Nishimura et al., 2017, Yu et al., 2022). The TIR domain of RBA1 harbors NADase and nuclease activities, which are responsible for the generation of pRib-AMP/ADP and diADPR/ADPr-ATP and cyclic nucleotide monophosphates (cNMPs) such as 2′,3′-cAMP/cGMP, respectively (Wan et al., 2019; Tian and Li, 2022; Yu et al., 2022). The two enzymatic activities of RBA1 require one of two catalytic residues, namely, Cys83 or Glu86. The RBA1 Cys83, which is a highly conserved among TIR-containing proteins, is responsible for nuclease activity but not for NADase activity. In

contrast, RBA1 Glu86 is required for both catalytic activities of RBA1. The NADase activity of RBA1 alone is not sufficient for RBA1 cell death in *N. benthamiana*, because the RBA1(C83A) variant, which lacks nuclease activity, is significantly impaired in cell death induction in *N. benthamiana* upon transient expression (Yu et al., 2022). However, it remains unknown whether the C83A substitution in RBA1, which impairs cell death induction, also impairs disease resistance activity.

To address this question, we used the PVX-YFP-based assay to examine the disease resistance activity of the RBA1(C83A) variant and the RBA1 (E86A) variant as a control. Interestingly, we found that the RBA1 (C83A) variant retained the same disease resistance activity as wild-type RBA1, whereas the RBA1 (E86A) barley showed disease resistance activity to PVX (Fig. 1G). These data suggest that the 2′,3′-cAMP/cGMP synthase activity (i.e., nuclease activity) of RBA1 is required for host cell death but that the remaining NADase activity is sufficient to confer immunity to PVX. Furthermore, the disease resistance activity of the RBA1(C83A) variant was significantly impaired in the *Nbepss* mutant background (Fig. 1G), consistent with the model that TIR NADase products confer immunity via the EDS1 pathway (Huang et al., 2023). In summary, our results have uncoupled the disease resistance activity of RBA1 from the host cell death that is induced by the 2′,3′-cAMP/cGMP synthetase activity. Similar to RBA1, the *Arabidopsis* TIR-containing NLR SNC1 (Suppressor of *npr1-1* constitutive 1) does not seem to require 2′,3′-cAMP/cGMP synthetase activity (i.e., nuclease activity) for disease resistance (Tian et al., 2022). Therefore, it is possible that 2′,3′-cAMP/cGMP produced by TIR enzymes may be sensed by cell death-inducing receptor(s) other than the EDS1 receptor complexes that sense the TIR NADase products. Another possibility is that there may be a threshold for cell death. In this scenario, both TIR NADase and 2′,3′-cAMP/cGMP synthase activities are required to reach the threshold for cell death induction. Finally, we would like to emphasize that disease resistance assays are not intended as a replacement for the widely used cell death assay in the *N. benthamiana* and *N. benthamiana* transient gene expression system; rather, these two assays should be seen as playing complementary roles in illuminating the cell death-independent immunity of R proteins.

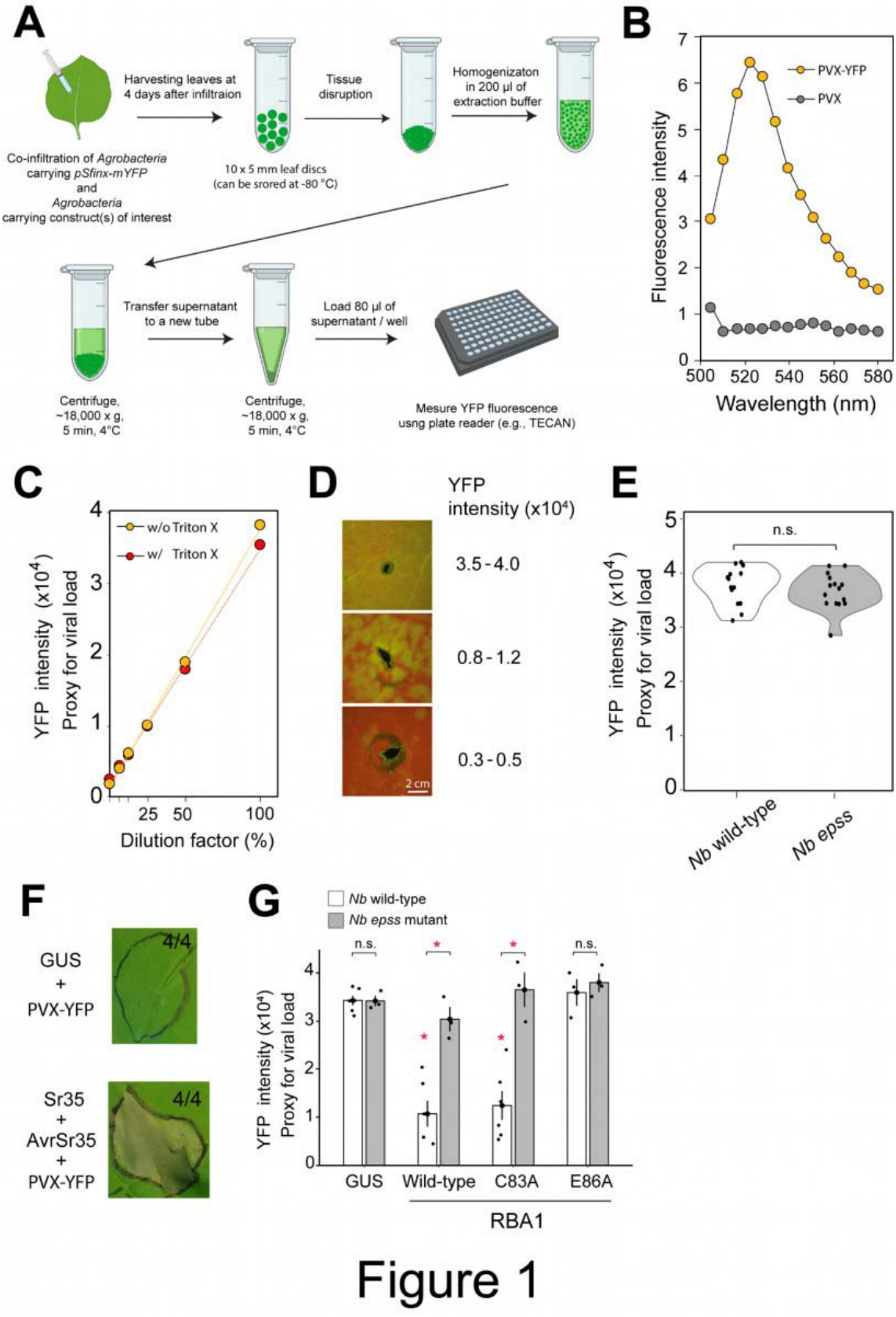
A
Harvesting leaves at 4 days after infiltraion
Tissue disruption
Homogenizaton in 200 µl of extraction buffer
Co-infiltration of Agrobacteria carrying pSfinx-mYFP and Agrobacteria carrying construct(s) of interest
10 x 5 mm leaf discs (can be srored at -80 °C)
Transfer supernatant to a new tube
Load 80 µl of supernatant / well
Centrifuge, ~18,000 x g, 5 min, 4°C
Centrifuge, ~18,000 x g, 5 min, 4°C
Mesure YFP fluorescence usng plate reader (e.g., TECAN)
B
PVX-YFP
PVX
Fluorescence intensity
Wavelength (nm)
C
w/o Triton X
w/ Triton X
YFP intensity (x10⁴) Proxy for viral load
Dilution factor (%)
D
YFP intensity (x10⁴)
3.5 - 4.0
0.8 - 1.2
0.3 - 0.5
2 cm
E
n.s.
YFP intensity (x10⁴) Proxy for viral load
Nb wild-type
Nb epss
F
GUS + PVX-YFP
4/4
Sr35 + AvrSr35 + PVX-YFP
4/4
G
Nb wild-type
Nb epss mutant
n.s.
YFP intensity (x10⁴) Proxy for viral load
GUS
Wild-type
C83A
E86A
RBA1

Figure 1

108

Figure 1. Disease resistance assay using *Potato Virus X* expressing YFP in *N. benthamiana*.

A) Schematic representation of the disease resistance assay using Potato Virus X expressing YFP (PVX-YFP).

B) The emission spectra for leaf extracts expressing PVX-YFP or PVX.

C) A linear correlation between fluorescence and dilution factor in a leaf lysate in the presence and in the absence of 0.1% Triton X-100. Leaf lysates from non-transformed plants were used for dilution.

D) Representative fluorescence stereomicroscopic images of *N. benthamiana* leaves infiltrated with PVX-YFP with corresponding YFP intensity measured with the TECAN plate reader. The leaves were examined at four days after agroinfiltration. YFP intensity measured with the plate reader from two biologically independent samples is shown.

E) Violin plots showing the degree of dispersion of the quantified YFP intensities from leaves co-expressing GUS and PVX-YFP in *N. benthamiana*.

F) Expression of Sr35 and YFP-expressing potato virus X (PVX) caused host cell death *in N. benthamiana* (wild-type). β-glucuronidase (GUS), Sr35, and AvrSr35 (Förderer et al., 2022) were expressed under an independent 35S promoter. The images were taken at four days after infiltration of Agrobacteria. The numbers indicate the numbers of leaves that exhibited cell death out of the total numbers.

G) A non-cell death-inducing RBA (Response to HopBA1) variant (C38A), which lacks 2',3'-cAMP/cGMP synthetase activity but retains NADase activity (Yu et al., 2022) and PVX resistance activity. Bar plots describe the results of four independent replicates for wild type and three independent replicates for wild type and the *epss* mutant of *N. benthamiana*. Asterisks depict significant differences between treatments as determined by analysis of variance (ANOVA) followed by Tukey's honest significant difference (HSD) test ($p < 0.05$).

References

Bendahmane A, Kanyuka K, Baulcombe DC (1999) The Rx gene from potato controls separate virus resistance and cell death responses. Plant Cell **11**: 781–792

Coll NS, Vercammen D, Smidler A, Clover C, Van Breusegem F, Dangl JL, Epple P (2010) Arabidopsis type I metacaspases control cell death. Science **330**: 1393–1397

Collier SM, Hamel L-P, Moffett P (2011) Cell death mediated by the N-terminal domains of a unique and highly conserved class of NB-LRR protein. Mol Plant Microbe Interact **24**: 918–931

Feys BJ, Wiermer M, Bhat RA, Moisan LJ, Medina-Escobar N, Neu C, Cabral A, Parker JE (2005) Arabidopsis SENESCENCE-ASSOCIATED GENE101 Stabilizes and Signals within an ENHANCED DISEASE SUSCEPTIBILITY1 Complex in Plant Innate Immunity. Plant Cell **17**: 2601–2613

Förderer A, Li E, Lawson AW, Deng Y-N, Sun Y, Logemann E, Zhang X, Wen J, Han Z, Chang J, et al (2022) A wheat resistosome defines common principles of immune receptor channels. Nature **610**: 532–539

Gantner J, Ordon J, Kretschmer C, Guerois R, Stuttmann J (2019) An EDS1-SAG101 Complex Is Essential for TNL-Mediated Immunity in Nicotiana benthamiana. Plant Cell **31**: 2456–2474

Huang S, Jia A, Ma S, Sun Y, Chang X, Han Z, Chai J (2023) NLR signaling in plants: from resistosomes to second messengers. Trends Biochem Sci **48**: 776-787

Heidrich K, Wirthmueller L, Tasset C, Pouzet C, Deslandes L, Parker JE (2011) Arabidopsis EDS1 connects pathogen effector recognition to cell compartment-specific immune responses. Science **334**: 1401–1404

Larsen JS, Curtis WR (2012) RNA viral vectors for improved Agrobacterium-mediated transient expression of heterologous proteins in Nicotiana benthamiana cell suspensions and hairy roots. BMC Biotechnol **12**: 21

Maekawa T, Kashkar H, Coll NS (2023) Dying in self-defence: a comparative overview of immunogenic cell death signalling in animals and plants. Cell Death Differ **30**: 258-268

Nishimura MT, Anderson RG, Cherkis KA, Law TF, Liu QL, Machius M, Nimchuk ZL, Yang L, Chung EH, El Kasmi F, et al. (2017) TIR-only protein RBA1 recognizes a pathogen effector to regulate cell death in Arabidopsis. Proc Natl Acad Sci USA **114**: E2053-E2062.

Peart JR, Cook G, Feys BJ, Parker JE, Baulcombe DC (2002) An EDS1 orthologue is required for N-mediated resistance against tobacco mosaic virus. Plant J **29**: 569–579

Sun X, Lapin D, Feehan JM, Stolze SC, Kramer K, Dongus JA, Rzemieniewski J, Blanvillain-Baufumé S, Harzen A, Bautor J, et al (2021) Pathogen effector recognition-dependent association of NRG1 with EDS1 and SAG101 in TNL receptor immunity. Nat Commun **12**: 3335

Tian L, Lu J, Li X (2022) Differential requirement of TIR enzymatic activities in TIR-type immune receptor SNC1-mediated immunity. Plant Physiol **190**: 2094–2098

Wang J, Song W, Chai J (2023) Structure, biochemical function, and signaling mechanism of plant NLRs. Mol Plant **16**: 75–95

van Wersch S, Tian L, Hoy R, Li X (2020) Plant NLRs: The Whistleblowers of Plant Immunity. Plant Commun **1**: 100016

Acknowledgments: We thank Frank Takken, Johannes Stuttmann, Martin Hartmut Schattat, Li Liu, and Alexander Förderer for the pSfinx plasmid and the *Nbeds1 sag101a sag101b pad4* mutant, *RBA1* variant plasmids, and *AvrSr35*/*Sr35* plasmids, respectively. We also thank Neysan Donnelly for editing the manuscript. This work was supported by the Deutsche Forschungsgemeinschaft (DFG, German Research Foundation, SFB-1403–414786233 to J.C., and T.M.). A part of Figure 1 was prepared with BioRender.com.

Author contributions: K.H., J.C., and T.M. conceived the project. K.H. and T.T. performed the investigations. K.H., T.T., J.C., and T.M. validated the data, J.C. and T.M. supervised the work, K.H., and T.M. wrote the paper with co-author contributions.

Supplemental Methods

The monomeric YFP coding region was amplified from pXCSG-YFP (Feys et al., 2005) by PCR using primers containing the SfiI recognition sites (SfiIA-mYFPf: TTGGCCATTATGGCCATGGTGAGCAAGGGCGAGGA, SfiIB-mYFPr: TTGGCCGAGGCGGCCTTACTTGTACAGCTCGTCCA), and the PCR product was digested with SfiI (NEB) and ligated into the SfiIA and SfiIB sites of the binary PVX-based expression vector (Takken et al., 2000). The *Agrobacterium tumefaciens* strain GV3101 pMP90RK (Koncz and Schell, 1986) carrying pSfinx-mYFP (OD_{600} = 0.001) and the *A. tumefaciens* strain GV3101 pMP90RK (Koncz and Schell, 1986) carrying resistance genes (OD_{600} = 0.6) were co-infiltrated into leaves of *Nicotiana benthamiana*. At four days after infiltration, ten 5-mm leaf-discs per condition were collected using a biopsy punch from the infiltrated areas. The collected leaf-discs were snap-frozen using liquid nitrogen and kept in a -80 °C freezer until use. The leaf-discs were ground using a pestle or Retsch mill, and 200 µl of the extraction buffer (50 mM Tris-HCl pH 8.0, 150 mM NaCl, proteinase inhibitor (Roche: cOmplet, EDTA-free Protease Inhibitor Cocktail)) were added. The resulting lysate was centrifuged for 5 min at 18,000 x g at 4 °C. The supernatant was transferred into a new tube and centrifuged for 5 min at 18,000 x g at 4 °C. Then, 80 µl of the supernatant were loaded into a black 96 well plate (Corning: CLS3915-100EA). A fluorescence microplate reader (TECAN: Tecan infinite 200 pro) was used to measure YFP intensity. We configured excitation/emission spectra of 516/560 nm

199 with the Tecan infinite 200 pro. While we note that excitation/emission spectra of 500/540 nm can be
200 similarly used in place of 516/560 nm, the excitation/emission spectra of 516/530 nm, which are
201 theoretically optimal for YFP, did not detect the YFP intensity. This may be due to the small Stokes
202 shifts of YFPs. The emission spectra of leaf extracts with expression of PVX-YFP or PVX shown in
203 Fig. 1C were determined by a confocal microscope using the lambda scan function (Leica,
204 STELLARIS 5). The fluorescence stereomicroscopic images of the abaxial leaf surface of *N.*
205 *benthamiana* shown in Fig. 1D were obtained using a fluorescence stereomicroscope (Leica, MZ16
206 FA) with a GFP filter equipped with a CCD color sensor. In this assay, we infiltrated the *Agrobacteria*
207 carrying pSfinx-mYFP with OD_{600} = 0.01, 0.001 or 0.0001 and the samples were examined at four
208 days after infiltration. For the Sr35 assay in Fig. 1F, *A. tumefaciens* strain GV3101 pMP90RK
209 carrying Sr35 (OD_{600} = 0.5) and AvrSr35(OD_{600} = 0.075) (Förderer et al., 2022) were co-infiltrated
210 with *A. tumefaciens* carrying pSfinx-mYFP (OD_{600} = 0.001). The images and leaf samples were taken
211 at four days after infiltration of Agrobacteria. For the RBA assay in Fig. 1F, *A. tumefaciens* strain
212 carrying pSfinx-mYFP (OD_{600} = 0.001) and the *A. tumefaciens* strain carrying either of GUS or RBA1
213 wild-type, C83A, and E86A (OD_{600} = 0.6) were co-infiltrated into leaves of wild type or the *eds1 pad4*
214 *sag101a sag101b* mutant (Gantner et al., 2019) of *N. benthamiana* (*Nbepss*).
215

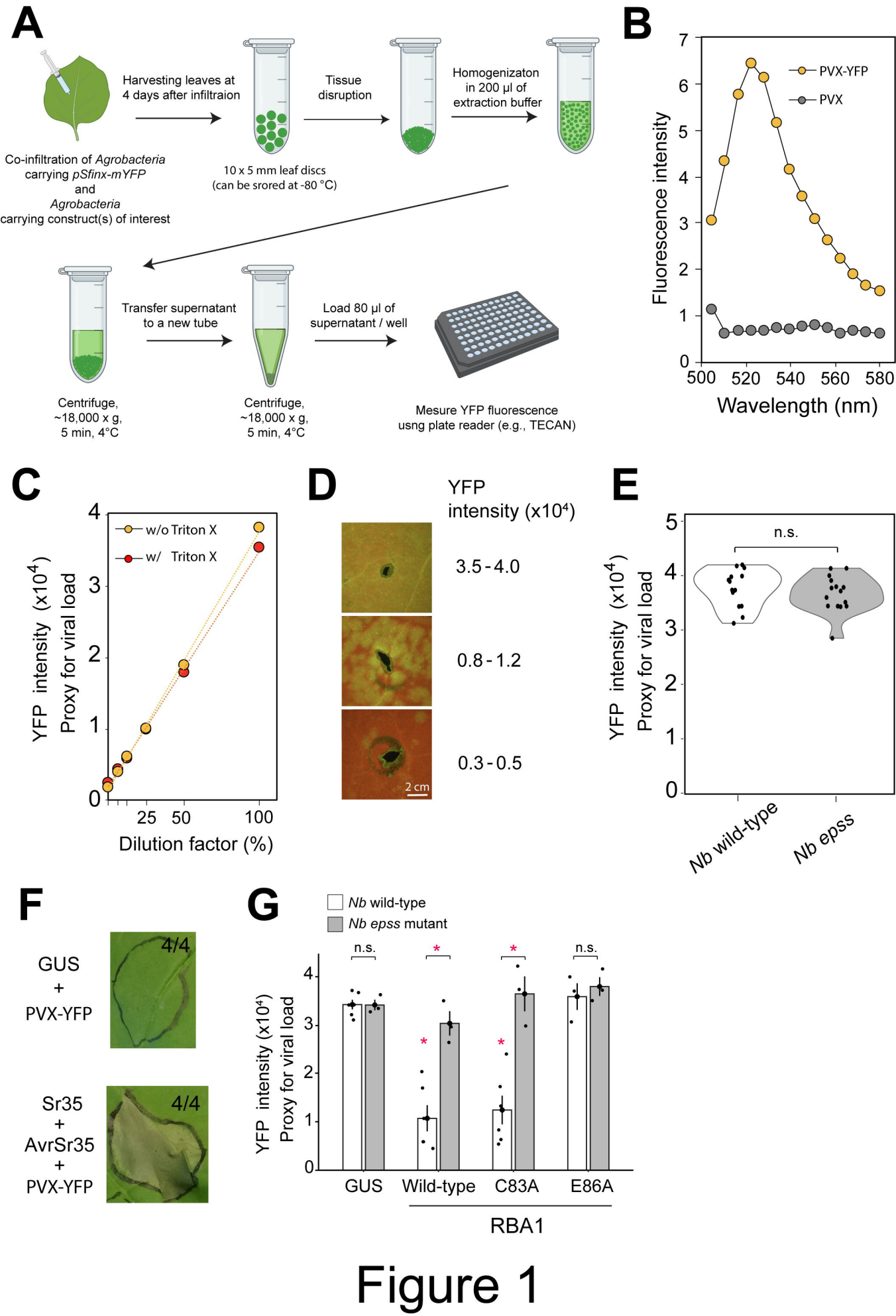
A
Co-infiltration of Agrobacteria carrying pSfinx-mYFP and Agrobacteria carrying construct(s) of interest
Harvesting leaves at 4 days after infiltraion
10 x 5 mm leaf discs (can be srored at -80 °C)
Tissue disruption
Homogenizaton in 200 µl of extraction buffer
Centrifuge, ~18,000 x g, 5 min, 4°C
Transfer supernatant to a new tube
Centrifuge, ~18,000 x g, 5 min, 4°C
Load 80 µl of supernatant / well
Mesure YFP fluorescence usng plate reader (e.g., TECAN)
B
PVX-YFP
PVX
Fluorescence intensity
Wavelength (nm)
C
w/o Triton X
w/ Triton X
YFP intensity (x10⁴) Proxy for viral load
Dilution factor (%)
D
YFP intensity (x10⁴)
3.5 - 4.0
0.8 - 1.2
0.3 - 0.5
2 cm
E
n.s.
YFP intensity (x10⁴) Proxy for viral load
Nb wild-type
Nb epss
F
GUS + PVX-YFP
4/4
Sr35 + AvrSr35 + PVX-YFP
4/4
G
Nb wild-type
Nb epss mutant
n.s.
YFP intensity (x10⁴) Proxy for viral load
GUS
Wild-type
C83A
E86A
RBA1

Figure 1

Title: Cytoplasmic Calcium influx mediated by plant MLKLs confers TNL-triggered immunity

Authors: Qiaochu Shen[1,7], Keiichi Hasegawa[2,7], Nicole Oelerich[3], Anna Prakken[1], Lea Weiler Tersch[1], Frowin Reichhardt[1], Alexandra Tersch[1], Ton Timmers[4] Kay Hofmann[3], Jijie Chai[2,4,5,6] and Takaki Maekawa[1,5,8 *]

[1]Institute for Plant Sciences, University of Cologne, Cologne, 50674, Germany.
[2]Institute for Biochemistry, University of Cologne, 50674 Cologne, Germany
[3]Institute for Genetics, University of Cologne, 50674 Cologne, Germany
[4]Max Planck Institute for Plant Breeding Research, 50829 Cologne, Germany
[5]Cluster of Excellence on Plant Sciences (CEPLAS), Cologne, Germany
[6]Current address: School of Life Sciences, Westlake University, Zhejiang China
[7] These authors contributed equally
[8]Lead Contact
[*]Correspondence: tmaekawa@uni-koeln.de (T.M.)

Summary [147/150 words]

The plant homologue of vertebrate necroptosis inducer MLKL (mixed lineage kinase domain-like) contributes to downstream steps in TNL (Toll-interleukin 1-receptor domain NLR) receptor-triggered immunity. Here, we show that *Arabidopsis* MLKL1 (*At*MLKL1) clusters into puncta at the plasma membrane upon TNL activation and that this sub-cellular reorganization is dependent on the TNL signal transducer, EDS1. We find that *At*MLKLs confer TNL-triggered immunity in parallel with RNLs (RPW8-like HeLo-domain containing NLRs) and that the *At*MLKL N-terminal HeLo domain is indispensable for both immunity and clustering. We show that the *At*MLKL HeLo domain mediates cytoplasmic Ca^{2+} ($[Ca^{2+}]_{cyt}$) influx in plant and human cells, and *At*MLKLs are responsible for sustained $[Ca^{2+}]_{cyt}$ influx during TNL-triggered but not CNL-triggered immunity. Our study reveals parallel immune signaling functions of plant MLKLs and RNLs as mediators of $[Ca^{2+}]_{cyt}$ influx and a potentially common role of the HeLo domain fold in Ca^{2+}-signal relay of diverse organisms.

- *Arabidopsis* MLKL1 clusters into puncta at the plasma membrane upon TNL activation in an EDS1-dependent manner.
- *Arabidopsis* MLKLs (*At*MLKLs) confer immunity in parallel with RPW8-type helper NLRs.
- *Arabidopsis* MLKLs promote a sustained $[Ca^{2+}]_{cyt}$ influx after activation of TNL receptor but not CNL receptor immunity.
- The N-terminal HeLo domain of *At*MLKL1 is indispensable for $[Ca^{2+}]_{cyt}$ influx in plant and human cells, and for TNL-induced MLKL1 clustering at the plasma membrane.

Introduction

In plants, a two-layered immune mechanism comprising pathogen-associated molecular pattern (PAMP)-triggered immunity (PTI) and effector-triggered immunity (ETI)[1-6] effectively detects and combats pathogenic microbes. In many cases, ETI is initiated by intracellular nucleotide-binding leucine-rich repeat (NLR) receptors upon detection of pathogen race-specific effectors.[7,8] Three major classes of plant NLRs – TNLs, CNLs, and RNLs – are defined by the presence of either a Toll/interleukin 1 receptor (TIR)-like domain, a coiled-coil (CC) domain or an RPW8-like CC domain (also known as HeLo domain) at the N-terminus, respectively.[8-10] Activation of NLRs involves conformational changes in these multi-domain proteins, leading to the assembly of supramolecular complexes called "resistosomes".[11-15] Activated CNLs such as ZAR1 form pentameric resistosomes which function as non-selective calcium ion (Ca^{2+})-permeable channels at the plasma membrane (PM).[11,16] By contrast, pathogen-activated TNLs such as *Arabidopsis* RPP1 and *N. benthamiana* Roq1 form tetrameric resistosomes which have TIR-encoded nicotinamide adenine dinucleotide hydrolase (NADase) activity producing nucleotide signaling intermediates for defense promotion.[17-21] Besides TNLs, plant genomes encode a number of shorter TIR-NB-ARC domain-containing (TIR-NB) and TIR-only proteins.[7] Accumulating evidence suggests that TIR domain-containing enzymes, which are often transcriptionally upregulated during PTI and ETI, amplify immune signals at sites of pathogen infection and/or propagate signals from a pathogen infection site to distal tissues.[3,4,22,23] Therefore, TIR-mediated enzymatic activity plays a pivotal role in plant innate immunity.

The execution of TNL and TIR enzyme-triggered immune signaling requires the lipase-like proteins EDS1(Enhanced Disease Susceptibility 1), SAG101 (Senescence Associated gene 101) and PAD4 (Phytoalexin Deficient4) and ADR1(Activated Disease Resistant 1)- or NRG1(N Requirement Gene 1)-family RNLs.[24-26] Two sets of non-cyclic ribosylated nucleotide products of the TIR enzymes are bound by two distinct receptors EDS1-SAG101 and EDS1-PAD4 heterodimer complexes.[27,28] This promotes EDS1-SAG101 and EDS1-PAD4 facilitated conformational changes in ADR1 and NRG1, respectively, leading to their oligomerization.[24-28] Oligomerized RNLs are enriched in puncta on the PM and mediate cytoplasmic Ca^{2+} ($[Ca^{2+}]_{cyt}$) influx in plant and human cells.[29-31] In plant innate immunity, the signatures of cytoplasmic Ca^{2+} influx are eventually decoded into distinct downstream outputs including host cell death.[22,32] We recently showed that the plant homologue of animal necroptosis inducer MLKL (mixed lineage kinase domain-like) contributes to TNL-triggered immunity.[10] Despite their roles in TNL-mediated EDS1-dependent immunity, the functional relationship between RNLs and MLKLs is not known.

Plant MLKLs and RNLs share a characteristic N-terminal four-helix bundle in a coiled-coil arrangement, which is structurally similar to the N-terminal HeLo executor domain (named after the fungal Het and LopB proteins) of animal MLKL, an inducer of lytic cell death.[10,29,33,34] HeLo domain containing proteins occur in diverse organisms, exemplified by fungal HET-S[35,36] and a viral MLKL-like protein.[37] Plant and animal MLKLs have an N-terminal HeLo domain followed by a brace region and a pseudokinase domain.[10,38,39] Plant MLKLs additionally possess a C-terminal intrinsically disordered (ID) region that is missing in animal counterparts.[10] The Cryo-

EM structures of wild-type *At*MLKLs revealed a tetrameric configuration, in which the N-terminal HeLo domains are completely buried (Figure 1A), suggesting that the tetrameric structure represents an auto-repressed configuration of plant MLKLs.[10] However, the mode of MLKL activation and its immune activity remain obscure.

Here, we describe N-terminal HeLo domain-dependent clustering of *Arabidopsis* MLKL1 (*At*MLKL1) at the PM upon TNL activation in *Arabidopsis* and *Nicotiana benthamiana*. Genetic and functional studies indicate that *At*MLKLs and RNLs confer TNL-mediated immunity in a parallel manner and that the *At*MLKL N-terminal HeLo domain, which can self-oligomerize, is indispensable for *At*MLKL-mediated immunity. Furthermore, we detect a TNL activation-dependent interaction between the EDS1-SAG101 dimer and *At*MLKL1, suggesting a mechanistic explanation for the lack of *At*MLKL1 clustering on the PM in an *eds1* null mutant. Finally, we show that the HeLo domain of plant MLKL mediates cytoplasmic Ca^{2+} influx in plant and human cells and that plant MLKLs facilitate sustained cytoplasmic Ca^{2+} influx during TNL-triggered immunity but not CNL-triggered immunity.

Results

Arabidopsis MLKL1 clusters at the plasma membrane (PM) during TNL-triggered immunity in a HeLo domain-dependent manner

As *Arabidopsis* MLKLs (*At*MLKLs) confer TNL-triggered immunity,[10] we investigated the subcellular dynamics of *At*MLKLs during TNL-mediated immunity (Figure 1). We utilized a previously established *Arabidopsis* complementation line expressing *At*MLKL1-GFP under the native *cis*-regulatory sequence in an *Atmlkl1* background[10] and *Nicotiana benthamiana* transiently expressing *At*MLKL1-GFP under a constitutive cauliflower mosaic virus 35S promoter. We chose *At*MLKL1 for subsequent experiments due to the lower expression of *AtMLKL2* and 3 under native conditions[10,40], which hinders microscopic examination. We detected a greater number of clustered GFP signals (i.e., GFP puncta) in leaf epidermal cells of the *Arabidopsis* line and *N. benthamiana* upon infiltration with *Pseudomonas fluorescens* Pf0-1 (Pf0-1) expressing bacterial effectors AvrRps4 and XopQ, respectively (Figures 1B, 1C and Figure S1A). AvrRps4 is recognized by the TNL pair RRS1/RPS4 in *Arabidopsis* and XopQ by TNL Roq1 in *N. benthamiana*[41,42]. In addition to the leaf epidermis, *At*MLKL1-GFP formed clusters in leaf mesophyll cells upon expression of AvrRps4 in protoplasts derived from the *Arabidopsis* complementation line (Figures S1B and S1C). Clustered *At*MLKL1-GFP signals overlapped with fluorescence signals of the plasma membrane (PM) tracer, FM4-64[43] in plasmolyzed epidermal cells, indicating that *At*MLKL1 clusters into puncta at the plasma membrane (Figure 1D). Furthermore, the localization of the *At*MLKL1-GFP signals in the brefeldin A (BFA)-induced vesicle compartment known as the BFA body[44] (Figure S1D), implies that *Arabidopsis* MLKLs are trafficked to and endocytosed from the PM by the Golgi and trans-Golgi network/early endosome-mediated secretory pathway.[45] We noted a transient and slight increase of puncta formation upon infiltration with the Pf0-1 strain without effectors (Figure 1E), suggesting that PAMP-triggered immunity also facilitates *At*MLKL1 puncta formation. *At*MLKL1-GFP accumulation in leaves of the *Arabidopsis* line were comparable at each time point upon infiltration with the Pf0-1 strain expressing AvrRps4, Pf0-1 without an effector or mock treatment (Figure 1F). Therefore, altered *At*MLKL protein abundance does not explain induced localization and clustering of *At*MLKL1-GFP at the PM in the TNL-triggered immune response.

.

Plant MLKL is a multi-domain protein comprising an N-terminal HeLo domain followed by the brace, pseudokinase, and intrinsically disordered (ID) regions[10] (Figure 1A). To determine which domain(s) are responsible for *At*MLKL1 self-oligomerization (potentially explaining induced puncta formation) and/or PM localization, we transiently expressed a series of C-terminally GFP-tagged *At*MLKL1 truncated variants in *N. benthamiana* without an immune trigger (Figure 1G). We found that the HeLo domain alone (H) and the HeLo domain with brace (H+B) variants appeared as puncta at the PM, while neither the HeLo domain with brace and pseudokinase (H+B+P) variant, a variant lacking the HeLo domain (B+P+ID), nor full length *At*MLKL1 formed puncta (Figure 1G). As the *At*MLKL1 variants were barely detectable upon heterologous expression by immunoblotting (data not shown), we verified their expression by transfecting them into *Arabidopsis* protoplasts followed and immunoblotting (Figure S1E). Consistent with previous observations,[10] full-length *At*MLKL1 and the H+B+P variants associated with microtubules (Figures 1G and S1F). Taken together, these results

demonstrate that the N-terminal HeLo domain is necessary and sufficient for the puncta formation and PM localization of *At*MLKL1.

We next sought to determine which domain(s) of *At*MLK1L are responsible for disease resistance activity. Overexpression of helper NLRs (e.g., ADR1 and NRG1) that contain the HeLo domain at their N-terminus conferred disease resistance against potato virus X (PVX) in the absence of host cell death.[46,47] Therefore, we tested whether *At*MLKL is able to suppress PVX proliferation by co-expressing C-terminally HA-tagged *At*MLKL1 or its truncated variants with a PVX variant expressing YFP. We measured the YFP intensity of the leaf lysates as a proxy for viral accumulation and thus disease resistance activity of *At*MLKL1 forms (Figure 1H). The HeLo domain alone (H) and the HeLo with brace (H+B) variants produced a lower YFP intensity compared to full-length *At*MLKL1 protein, indicating these variants have disease resistance activity (Figure 1H). By contrast, the HeLo with brace and pseudokinase (H+B+P) variant, the variant lacking the HeLo domain (B+P+ID) and the variant lacking the HeLo domain and brace (P+ID) did not limit PVX-YFP proliferation (Figure 1H). The HeLo domain also conferred disease resistance against *Pst* DC3000 in the *Atmlkl123* mutant background (Figure 1I). Taken together, our data suggest that the tetrameric configuration of wild-type *At*MLKLs, in which the HeLo domains are buried (Figure 1A), represents an auto-repressed state of this protein family and that *At*MLKLs undergo a drastic conformational change which exposes the HeLo domains for resistance signaling activity.

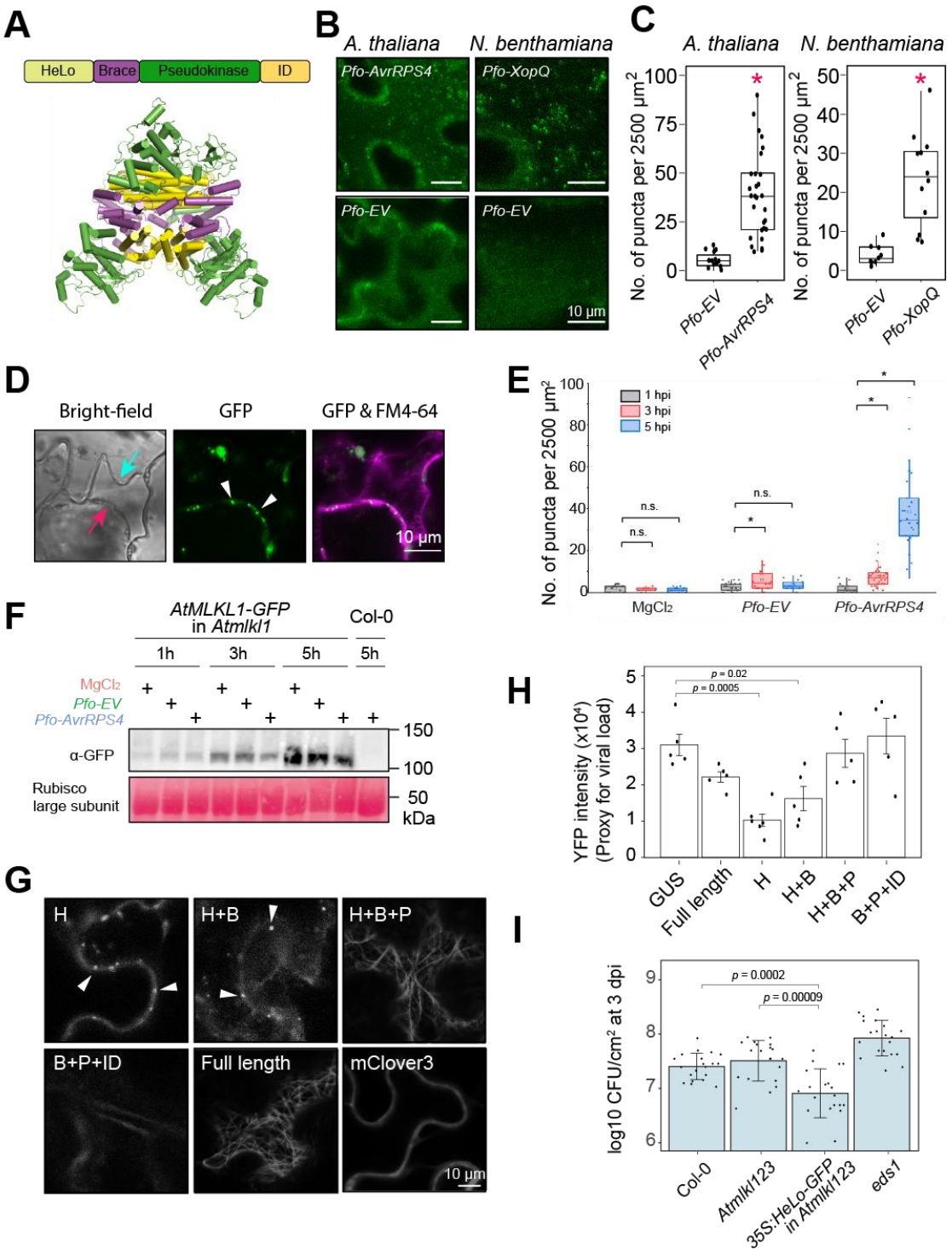

Figure 1. *Arabidopsis* MLKL1 form clusters at the plasma membrane (PM) during TNL-triggered immunity in a HeLo domain-dependent manner.

(A) Top panel: Schematic representations of *At*MLKLs. Bottom panel: Cryo-EM structure of a protomer of the *At*MLKL3 tetramer (PDB: 6KA4). Subdomains of *At*MLKLs are shown in different colors. Yellow: HeLo domain, Purple: Brace region, Green: pseudokinase domain, dark yellow: the intrinsically disordered (ID) region. The ID region does not appear in the Cryo-EM structures likely due to its instability.

(B) Left panels: Top-view of leaf epidermal cells of *Arabidopsis* complementation line expressing *AtMLKL*1-GFP under the native *cis*-regulatory sequence in *Atmlkl1* background[10] upon challenge of *P. fluorescens* Pf0-1 expressing AvrRPS4 (Pf0-AvrRps4) or *P. fluorescens* Pf0-1 carrying empty vector (Pf0-EV) at 5 hours post infiltration (hpi). Right panels; Top-view of leaf epidermal cells of *N. benthamiana* transiently expressing *At*MLKL1-GFP under the constitutive 35S promoter upon challenge of *P. fluorescens* Pf0-1 expressing XopQ or *P. fluorescens* Pf0-1 carrying empty vector (EV) at 5 hpi.

(C) Left: Quantification of *At*MLKL1-GFP puncta number in the *Arabidopsis* complementation line at 5 hpi upon the infiltration of Pf0-AvrRPS4 (n=29) or Pf0-EV (n=15). Right: Quantification of *At*MLKL1-GFP puncta number in *N.*

benthamiana at 7hpi upon infiltration of Pf0-XopQ (n=12) and Pf0-EV (n=9). Asterisks indicate significant differences at $p < 0.001$ which were determined with single-factor ANOVA followed by Tukey's test.
(D) Clustered *At*MLKL1-GFP signals overlapping with the fluorescence signals of the plasma membrane (PM) tracer, FM4-64 in the plasmolyzed epidermal cells. The red and light blue arrows indicate PM and cell wall, respectively. White arrowheads indicate the *At*MLKL1-GFP puncta.
(E) A time-course quantification of *At*MLKL1-GFP puncta number in the *Arabidopsis* complementation line.
(F) Steady-state levels of *At*MLKL1-GFP were comparable at each examined time point upon infiltration with the Pf0-1 strain expressing AvrRps4, *P. fluorescens* Pf0-1 carrying empty vector (EV), and the mock treatment in total cell lysate from the *Arabidopsis* complementation line.
(G) The N-terminal HeLo-domain is sufficient and necessary for puncta formation in *N. benthamiana*. The C-terminally mClover3-tagged truncated *At*MLKL1 variants were expressed under the constitutive 35S promoter in *N. benthamiana*. No avirulent pathogens were challenged. The images were taken at 48 hours post Agrobacterium infiltration. White arrowheads indicate the *At*MLKL1-GFP puncta. H: HeLo domain alone, H+B: HeLo with brace, H+B+P: HeLo with brace and pseudokinase, B+P+ID: *At*MLKL1 lacking the HeLo domain.
(H) The N-terminal HeLo-domain of *At*MLKL1 exhibited disease resistance activity against YFP expressing Potato virus X (PVX) in *N. benthamiana*. All *At*MLKL1 variants were C-terminally tagged with HA epitope. The YFP intensity of the leaf lysate was measured as a proxy of the disease resistance activity.
(I) The N-terminal HeLo-domain of *At*MLKL1 conferred disease resistance against *Pst* DC3000 in *A. thaliana mlkl123* triple mutant background.

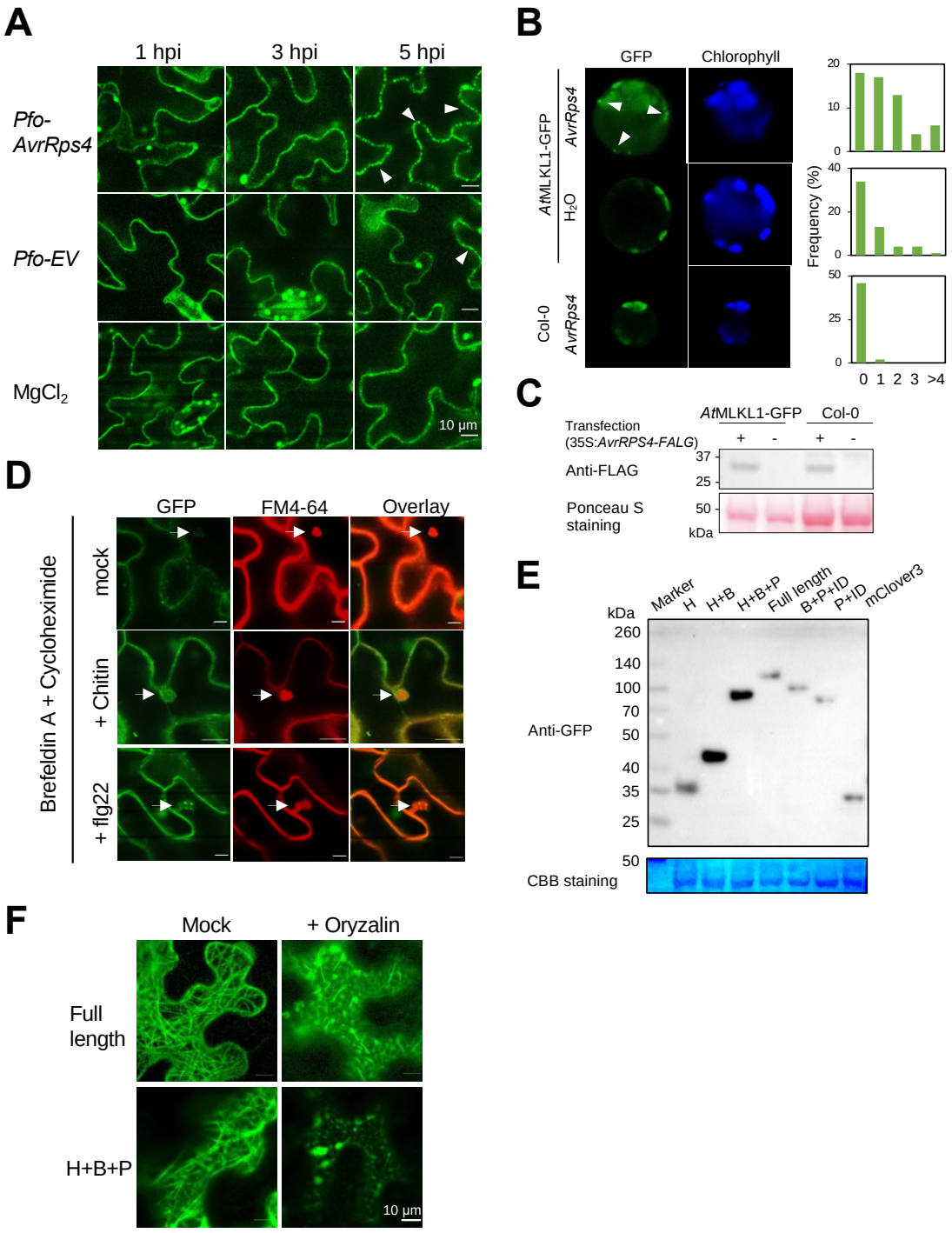

Figure S1. Subcellular localization of monomeric GFP-tagged *AtMLKL*1, related to Figure 1.

(A) A time-course imaging of leaf epidermal cells of the *Arabidopsis* complementation line expressing *AtMLKL*1-GFP under the native *cis*-regulatory sequence in *Atmlkl1* background (Mahdi et al., 2020) upon challenge of *P. fluorescens* Pf0-1 expressing AvrRPS4 (Pf0-AvrRps4) or *P. fluorescens* Pf0-1 carrying empty vector (Pf0-EV) and treated with $MgCl_2$. hpi; hours post infiltration. White arrowheads indicate the *At*MLKL1-GFP puncta. The brightness of images was adjusted.

(B) Left: formation of *At*MLKL1-GFP puncta in leaf mesophyll cells upon transfection of the C-terminally FLAG-tagged AvrRps4 expression plasmid into protoplasts derived from the *Arabidopsis* complementation line. The images were taken at 6–8 hours post transfection. Right: frequency of protoplasts with the GFP puncta. The number of the GFP puncta are varied from 0 to > 4 per protoplast. White arrowheads indicate the *At*MLKL1-GFP puncta.

(C) Immunoblotting of AvrRps4-FLAG in protoplasts. The samples were collected at 4 hours post transfection.

(D) Trafficking of *At*MLKL1 to PM by the Golgi and trans-Golgi network/early endosome-mediated secretory pathway. The localization of *At*MLKL1-GFP signals in the Brefeldin A (BFA)-induced compartment known as the BFA body implies that the *Arabidopsis* MLKLs are trafficked to the PM by the Golgi and trans-Golgi network/early endosome-mediated secretory pathway and can be endocytosed from PM. Furthermore, the presence of the *At*MLKL1-GFP signals in BFA bodies upon co-application of BFA and CHX (cycloheximide) implies that the PM-

localized *At*MLKL1 can be endocytosed from PM. BFA: brefeldin A, an inhibitor of exocytosis. CHX: cycloheximide. White arrows indicate the GFP signals overlapping with BFA bodies.
(E) Immunoblotting of the *At*MLKL1 truncated variants used in Figure 1E. The constructs were transfected into protoplasts prepared from the *Atmlkl123* triple mutant and samples were collected at 8 hours post transfection.
(F) The C-terminally mClover3-tagged full length *At*MLKL1 and the H+B+P variants associate with microtubules in *N. benthamiana*. The filamentous structures were undetectable at 30 minutes after application of 20 μM of the microtubule inhibitor oryzalin.

Arabidopsis MLKL structure-guided mutagenesis reveals an *EDS1*-dependent and RPW8-type helper NLR-independent disease resistance activity

As the disease resistance assay with the truncated *At*MLKl1 variants (Figure 1 H and I) suggests that exposure of the HeLo domains from the tetramer is a pivotal step in plant MLKL activation, we next performed structure-guided mutagenesis in an attempt to disrupt the autorepression. A closer inspection of the cryo-EM structure identified two intra-domain interactions (Figures 2A and 2B) and one inter-domain interaction (Figures 2C and 2D) that could be a direct cause of the burial of the HeLo domains in the tetramer (Figure 1A). Two intra-domain interactions are mediated by an interface between the HeLo domain and brace region and between the HeLo domain and the pseudokinase, which were named the HP interface and the HB interface, respectively, while one inter-domain interaction mediated by an interface between HeLo domains is named the HH interface. Among residues involved in the interactions, we substituted the hydrophobic residues with charged glutamate or aspartate.

Consistent with our *At*MLKL activation model, the combinatorial mutation in the HP + HH interfaces exhibited an increased disease resistance to YFP-expressing PVX compared to the wild type *At*MLKL1 in *N. benthamiana* (Figure 2E). Similar to the above mutation, mutation in the HP + HB interfaces also resulted in increased disease resistance. Phosphorylation in the activation loop of the pseudokinase domain is an initial step in MLKL-dependent necroptosis in animals. Furthermore, the previously identified gain-of-function variant carrying a phosphomimetic mutation in the activation loop of the pseudokinase domain[10] (S393D) also showed increased disease resistance activity in this assay (Figure 2E). These gain-of function variants conferred disease resistance against PVX in the absence of host cell death (Figure S2A).

Pathogen-activated TNL receptors recruit EDS1 dimers with RPW8-type helper NLRs (RNLs) of the ADR1 and NRG1 families for downstream signaling.[10,27,28,47-49]However, the genetic relationship between RNLs and MLKLs as well as between EDS1 and MLKLs in immunity remains unclear. Therefore we next tested whether the gain-of function variants of *At*MLKL1 confer immunity in *adr1 nrg1* knockout mutant[50] and *eds1 pad4 sag101ab* (*Nb-epss*) mutant of *N. benthamiana*[51] using the PVX-based disease resistance assay. We found that the disease resistance activity of the gain-of function variants was largely retained in the *adr1 nrg1* mutant background, while the resistance activity was barely detected in the *Nb-epss* mutant background (Figure 2E). Notably, the N-terminal HeLo domain of human MLKL confers resistance in plants, suggesting the conserved *in vivo* activity of plant and animal MLKLs (Figure S2B). Taken together, our structure-guided analysis further supports the idea that *At*MLKL tetramers represent an auto-repressed conformation of plant MLKLs. Moreover, these data imply that RNLs and plant MLKLs can function in signaling downstream of TNL in a parallel fashion.

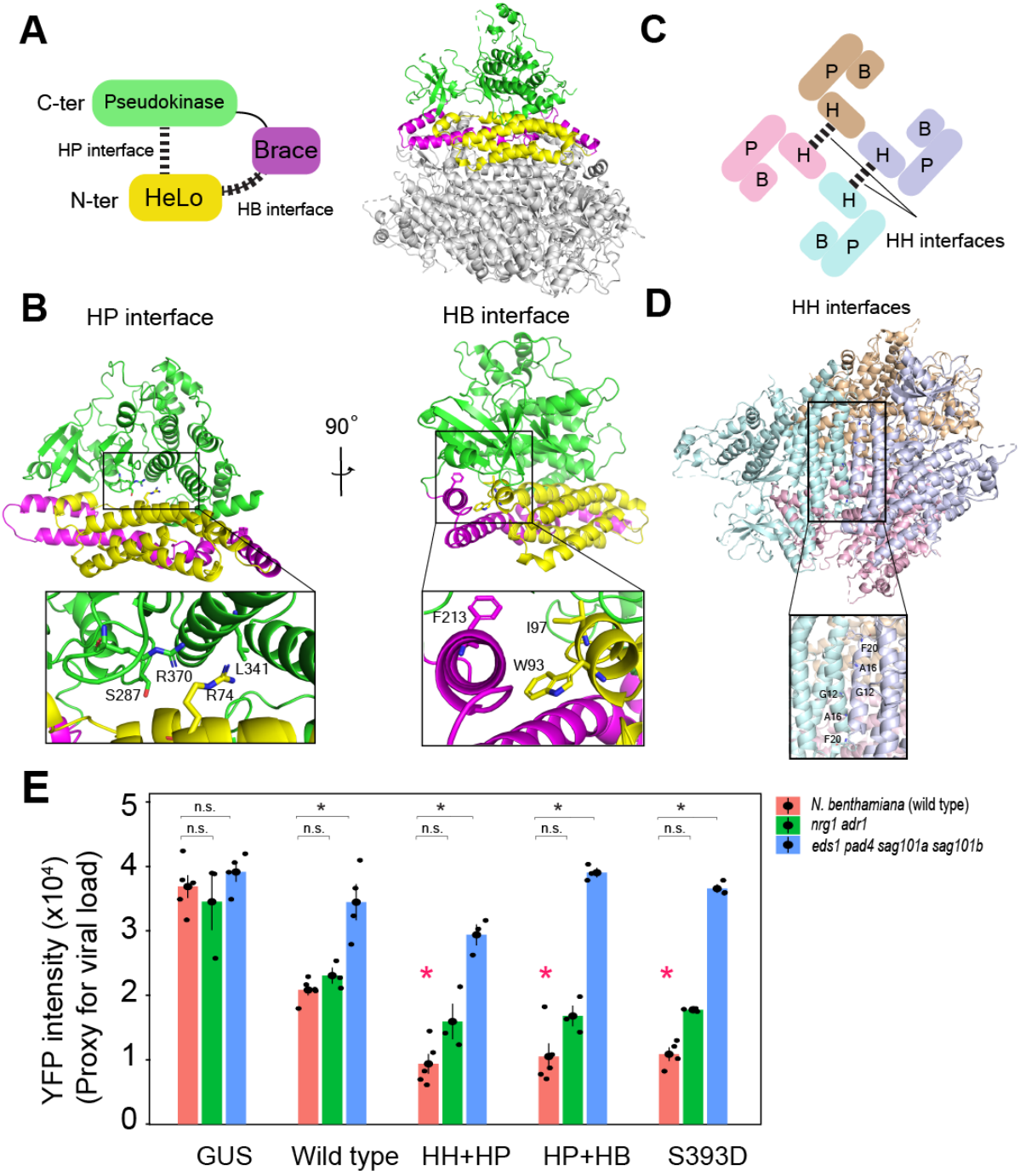

Figure 2. Structure-guided mutagenesis reveals distinctive contributions of the EDS1 family and helper NLRs to the disease resistance activity mediated by the gain-of-function variants of *At*MLKL1.

(A) Left: Schematic representation of the intra-domain interfaces indicated by blue dashed lines. Right: Tertiary structure of the *At*MLKL1 tetramer modeled by Alfafold2.[52] The color code is identical to A. One of four protomers is shown in color. As the cryo-EM structures of *At*MLKL2 and *At*MLKL3 are nearly identical and the protein sequences of *At*MLKL1, 2, and 3 are highly conserved, it is conceivable that *At*MLKL1 also forms an *At*MLKL3 like tetramer.

(B) The position of amino acid residues in the intra-domain interfaces in *At*MLKL1 protomer

(C) Schematic representation of the inter-domain interfaces indicated by black dashed lines.

(D) The position of amino acid residues in the inter-domain interfaces in *At*MLKL1 tetramer.

(E) Disease resistance activity of *At*MLKL1 variants carrying mutations at either intra- or inter-domain interfaces against YFP-expressing PVX. All *At*MLKL1 variants were C-terminally tagged with HA epitope. The YFP intensity of the leaf lysate was measured as a proxy for the disease resistance activity. HH+HP and HP+HB indicate the mutant *At*MLKL1 variants harboring mutations at the HH+HP interfaces and HP+HB interfaces, respectively. The previously identified gain-of-function variant carrying a phosphomimetic mutation (S393D from Mahdi et al.[10]) in the activation loop of the pseudokinase domain was used as a control. The red asterisks indicate significant differences

from the *At*MLKL1 wild type at $p < 0.02$ determined with Dunnett's test. Black asterisks indicate significant differences at $p < 0.01$ which were determined with Kruskal–Wallis H test.

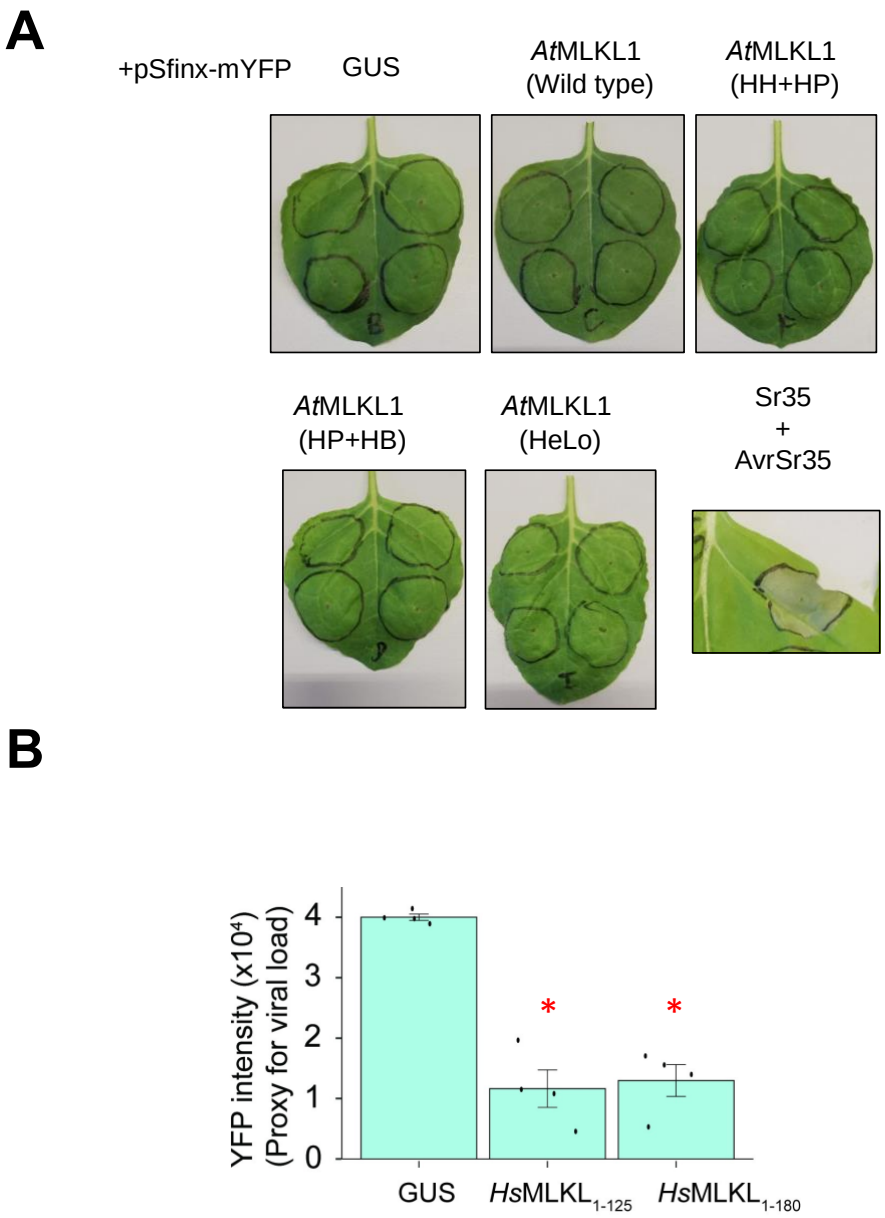

Figure S2. Expression of *Hs*MLKL and *At*MLKL1 variants in *N. benthamiana*, related to Figure 2.
(A) Expression of *At*MLKL1 variants with YFP-expressing potato virus X (PVX) did not cause host cell death in *N. benthamiana* (wild type). GUS and *At*MLKl1 variants were expressed under a constitutive 35S promoter. PVX was expressed using the pSfincs vector.[53]). The cell death mediated by co-expression of Sr35 and AvrSr35[54] was not suppressed by PVX. The images were taken at 4 days after infiltration of *Agrobacteria*.
(B) Expression of *Hs*MLKL variants under a constitutive 35S promoter confer resistance to YFP-expressing potato virus X (PVX). Red asterisks indicate significant differences at $p < 0.01$, which were determined with Dunnett's test.

The EDS1 circuit is required for *At*MLKL1 clustering during TNL-triggered immunity

As the disease resistance activity of *At*MLKL1 is dependent on EDS1 family in *N. benthamiana* (Figure 2E), we next investigated whether *EDS1* is required for the subcellular relocalization and oligomerization of *At*MLKL1 during TNL-mediated immunity. For this we transformed the *Arabidopsis eds1-12*[55] mutant with a construct that complements the *Atmlkl1* mutation,

restoring endogenous levels of the C-terminally GFP-tagged *At*MLKL1.[10] Upon infiltration with the Pf0-1 strain expressing *AvrRps4*, no clustered GFP signals were observed in the *eds1* mutant background in six transgenic lines (Figure 3A), despite comparable steady-state levels of *At*MLKL1-GFP protein in the wild type and *eds1* background (Figure 3B). In contrast with the full-length protein, the GFP-tagged HeLo domain alone clustered around the PM in the *Nb-epss* mutant background (Figure 3C). We attributed this EDS1-independent clustering to autonomous self-association of the *At*MLKL1 HeLo domain as in size-exclusion chromatography, a recombinantly expressed HeLo domain eluted at an estimated molecular weight corresponding to approximately 15 protomers (Figures 3D and 3E). These results prompted us to test an interaction between *At*MLKL1 and the EDS1-SAG101 functional dimer in *N. benthamiana* using bimolecular fluorescence complementation (BiFC) and co-immunoprecipitation (co-IP) assays. As *Arabidopsis* EDS1 and SAG101 do not co-function with *N. benthamiana* native NRG1 [24]and both ADR1 and NRG1 helper NLRs are dispensable for *At*MLKL1 resistance activity (Figure 2E), we minimized interference by activated *Nb*NRG1 (leading to cell death), by transiently co-expressing C-terminally tagged *At*MLKL1, *At*SAG101, and *At*EDS1 in the *Nb-epss* mutant.

The BiFC assay using *At*MLKL1-cYFP, *At*SAG101-nYFP and EDS1-FLAG constructs detected YFP signals around the PM and at nuclei upon infiltration with the Pf0-1 strain expressing XopQ, whereas no marked YFP signal was detected upon infiltration with the Pf0-1 strain without effectors (Figure 3F). The co-immunoprecipitation experiment supports an *in planta* interaction between *At*SAG101 and *At*MLKL1 (Figures S3B and S3C). Further, co-expression of *At*EDS1, *At*SAG101, and *At*MLKL1 restored some Roq1-mediated resistance to *Xanthomonas campestris pv vesicatoria* that natively carry XopQ[42] in the *Nb-epss* mutant background (Figure 3I). Therefore, it is conceivable that the BiFC and Co-IP experiments were conducted under a biologically relevant condition. Unexpectedly, disease resistance inducing activity of *At*MLKL1 HeLo domain alone was impaired in *Nb-epss* (Figure 3H). These results suggest that an EDS1-dependent feedback circuit likely further contributes to signaling downstream of activated MLKLs (see also discussion).

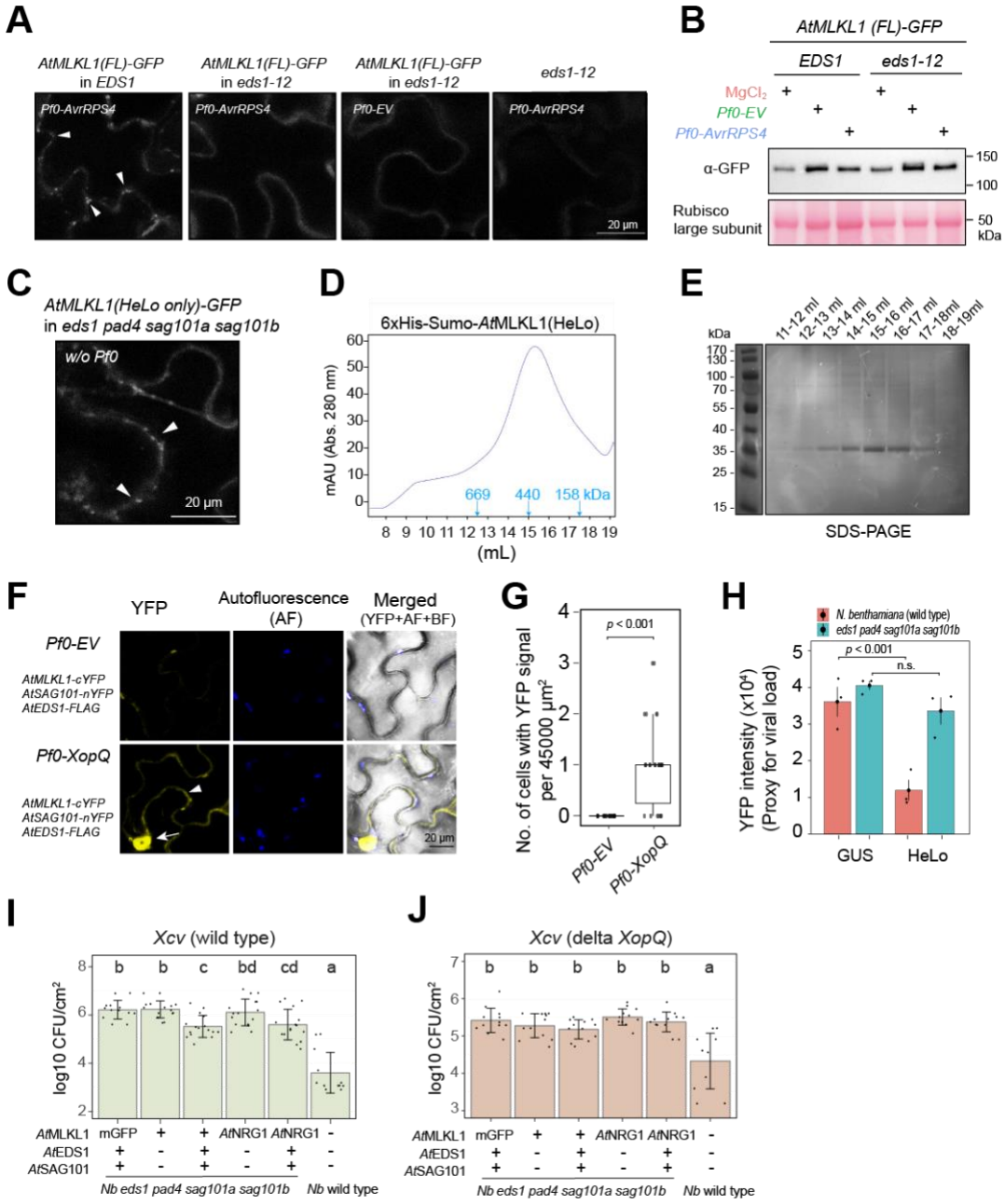

Figure 3. EDS1 facilitates *At*MLKL1 clustering during TNL-triggered immunity.

(A) Confocal images of leaf epidermal cells of *Arabidopsis* wild type or *eds1-12* mutant expressing *AtMLKL*1-GFP under the native *cis*-regulatory sequence. White arrowheads indicate the *At*MLKL1-GFP puncta. Images were taken at 5-6 hours post infiltration of *Pf0-AvrRps4*.

(B) Steady-state levels of *At*MLKL1-GFP in total cell lysate from the indicated *Arabidopsis* lines were comparable upon infiltration with the Pf0-1 strain expressing AvrRps4, *P. fluorescens* Pf0-1 carrying empty vector (EV), and $MgCl_2$. The samples were collected at 5 hours post infiltration.

(C) Confocal images of leaf epidermal cells of the *eds1 pad4 sag101a sag1101b* mutant of *N. benthamiana* expressing the C-terminally mClover3-tagged HeLo domain of *At*MLKL1. No avirulent pathogens were challenged. White arrowheads indicate the *At*MLKL1-GFP puncta. The images were taken at 48 hours post agrobacterium infiltration.

(D) Size-exclusion chromatography profile of the 6xHis-Sumo-tagged HeLo domain of *At*MLKL1. Position of standard molecular weight marker is indicated.

(E) Peak fractions in the size-exclusion chromatography were verified by SDS-PAGE.

(F) Bimolecular fluorescence complementation assays. *At*MLKL1-cYFP, *At*SAG101-nYFP, and *At*EDS1-FLAG were co-expressed under a constitutive 35S promoter in the *eds1 pad4 sag101ab* (*Nb-epss*) mutant of *N. benthamiana*. Enhanced YFP signals around PM and at nuclei indicated by the white arrowhead and arrow, respectively, were detected upon infiltration with the Pf0-1 strain expressing XopQ.

(G) Quantification of number of cells with YFP signals at 48 hpi upon infiltration of Pf0-EV (n=18) or Pf0-XopQ (n=22). Asterisks indicate significant differences at $p < 0.001$, which were determined with single-factor ANOVA followed by Tukey's test.
(H) Disease resistance activity against YFP-expressing PVX by the C-terminally HA-tagged HeLo domain of *At*MLKL1 was impaired in the *eds1 pad4 sag101a sag101b* mutant of *N. benthamiana*. The proteins were expressed under the constitutive 35S promoter.
(I and **J)** Reconstitution of *At*EDS1-, *At*SAG101- and *At*MLKL1-mediated immunity in the *eds1 pad4 sag101a sag101b* mutant of *N. benthamiana* in response to the *Xcv* strain carrying *XopQ* that is recognized by the Roq1 TNL. Different letters indicate statistically significant difference at $p < 0.05$, which was determined with single-factor ANOVA followed by Tukey's test.

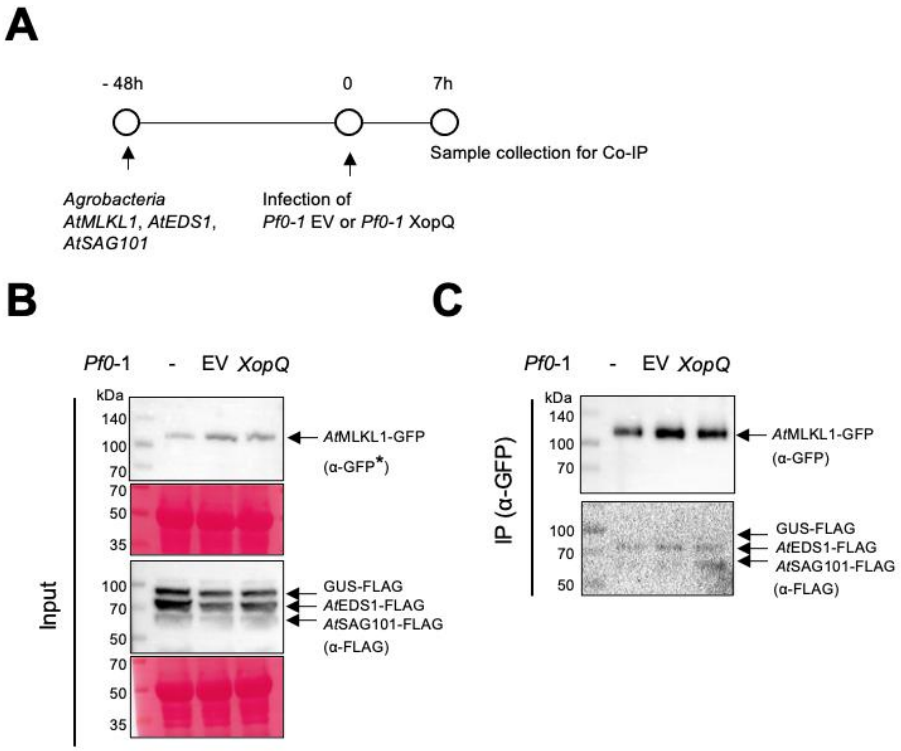

Figure S3. Co-immunoprecipitation of a protein complex containing *At*EDS1, *At*SAG101, and *At*MLKL1 and restoration of *At*EDS1-, *At*SAG101- and *At*MLKL1-mediated immunity upon XopQ recognition by TNL Roq1 in *N. benthamiana,* related to Figure 3. (A) The experimental procedure of the co-immunoprecipitation experiment**.** *At*MLKL1-mClover3, *At*EDS1-FLAG, *At*SAG101-FLAG and GUS-FLAG were co-expressed in the *eds1 pad4 sag101a sag101b* mutant of *N. benthamiana*. Two days after infiltration of Agrobacteria, Pf0-1 EV, Pf0-1 XopQ1 strains were infiltrated. Non- infiltrated leaves were used a control. The leaf samples were collected at 7 hours after Pf0-1 challenge. **(B)** Immunoblotting of the input samples. Due to the overlap with the Rubisco large subunit around 50 kDa, the *At*SAG101-FLAG single was partially masked. *Because of the lower expression, the input *At*MLKL1-mClover3 was enriched with Anti-GFP beads prior to immunoblotting, which is independent from the Co-IP shown in **(C)**. **(C)** Immunoprecipitation with anti-GFP beads followed by immunoblotting. The indicated antibodies were used for the immunoblotting. Lack of GUS-FLAG signal suggests a specific co-immunoprecipitation of *At*MLKL1-*At*EDS1-*At*SAG101.

Plant MLKLs mediate cytoplasmic calcium ion influx in plant and human cells

Plant MLKLs and RNLs share the N-terminal HeLo four-helix bundle[10,29,33,34] and the latter was shown to mediate cytoplasmic Ca^{2+} ($[Ca^{2+}]_{cyt}$) influx in TNL immunity.[29] Therefore, we examined the role of plant MLKLs in $[Ca^{2+}]_{cyt}$ influx in TNL immunity .[32] Using minimally invasive microscopic analysis, we monitored dynamic changes in $[Ca^{2+}]_{cyt}$ in leaves of wild type and *Atmlkl123* mutant plants expressing the GFP-based Ca^{2+} sensor GCaMP3 [56,57] during TNL and

CNL-triggered immune signaling. Unlike in wild type plants, the *Atmlk123* mutant plants failed to mount a sustained $[Ca^{2+}]_{cyt}$ increase at 10–14 h post infiltration with the Pf0-1 strain expressing *AvrRps4* (Figure 4A), while a transient $[Ca^{2+}]_{cyt}$ increase at around 4 h was detectable in both genotypes (Figure 4A). The transient and sustained $[Ca^{2+}]_{cyt}$ increases were a host response specific to the Pf0-*AvrRps4* strain that activates the TNL pair RRS1/RPS4, as the $[Ca^{2+}]_{cyt}$ increases were undetectable upon infiltration of the Pf0-1 strain without effectors (Figure 4A). In agreement with the limited contribution of *At*MLKLs to CNL-triggered immunity,[10] the $[Ca^{2+}]_{cyt}$ increase upon challenge with a Pf0-1 strain expressing *AvrRpm1*(*Pf0*-AvrRpm1) that activates the RPM1 receptor[58] were similar between the wild type and the *Atmlk123* mutant backgrounds (Figure 4B). We noted that in wild type the patterns of $[Ca^{2+}]_{cyt}$ influx were markedly different in response to the Pf0-AvrRps4 and Pf0-AvrRpm1 strains, implying distinctive impacts of these TNL and CNL receptors on $[Ca^{2+}]_{cyt}$ influx.

As the N-terminal HeLo domain of *At*MLKL1 is indispensable for both immunity and clustering at the PM (Figure 1), we tested whether the N-terminal HeLo domains of *At*MLKLs are able to elicit $[Ca^{2+}]_{cyt}$ influx in human HEK 293 cells. We took an advantage of an experimental system that enables chemical (i.e., rapamycin)-induced de-repression of HeLo domain activity (Figure 4E and S4A-C). Upon rapamycin treatment, the N-terminal HeLo domain and HeLo domain plus the brace region of *At*MLKL1 induced $[Ca^{2+}]_{cyt}$ influx in human HEK293T cells (Figures 4C, 4D). Notably, the HeLo domain plus the brace region of human MLKL (*Hs*MLKL) also elicited $[Ca^{2+}]_{cyt}$ influx in human HEK293T (Figures 4C and 4D). Whereas the HeLo domain plus the brace region of *Hs*MLKL caused necroptotic cell death, neither the HeLo domain of *At*MLKL1 nor the HeLo domain plus the brace region of *At*MLKL 1, 2, 3 caused cell death in HEK293T cells (Figures S4D and4E). Therefore, plant MLKL mediated $[Ca^{2+}]_{cyt}$ influx in human HEK293T cells is not a consequence of cell death. We detected an induced GCaMP3 signal in the stable transgenic *N. benthamiana* plants expressing GCaMP3[59] upon expression of the *At*MLKL1 HeLo domain (Figures 4E and S4F). Taken together, the data suggest that plant MLKLs are recruited by TNL but not CNL receptors for downstream signaling leading to pathogen resistance and that plant MLKLs contribute to TNL immunity through HeLo domain-mediated $[Ca^{2+}]_{cyt}$ influx.

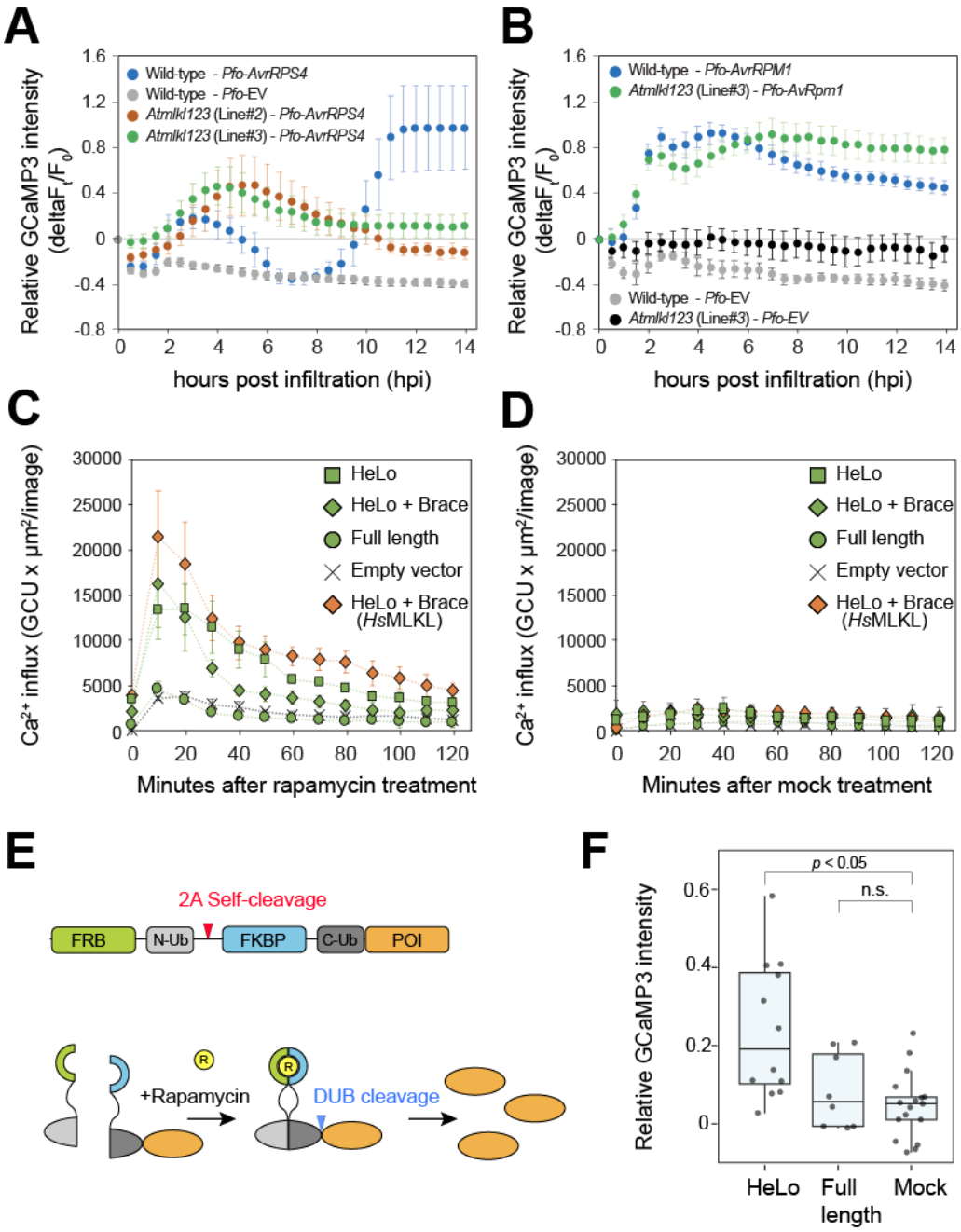

Figure 4. Plant MLKLs are mediators of cytoplasmic calcium ion influx.

(A and **B)** A time course signal analysis of GCaMP3 in the leaves of Col-0 expressing GCaMP3[59] and two independent *Atmlkl12*3 transgenic lines expressing GCaMP3 generated in this study. Average and SE at each time points upon infiltration with Pf0-1 expressing AvrRPS4 (Pf0-AvrRps4) or b, Pf0-1 expressing AvrRpm1 (Pf0-AvrRpm1) are shown. Pf0-1 carrying empty vector (Pf0-EV) was used as a negative control.

(C and **D)** The N-terminal HeLo domain alone and the HeLo domain plus the brace region of *At*MLKL1 induced $[Ca^{2+}]_{cyt}$ influx in human HEK293T cells. **(D)** mock control. **A-D**, the mean and the standard error of the replicates are shown.

(E) Schematic representation of the rapamycin-induced release of the N-terminal tag-free protein of interest (POI) used in **C** and **D**. After transfection of the construct the N-terminal FRB-N-Ub and the C-terminal FKBP-C-Ub-POI are separated by the 2A self-cleaving peptides. Rapamycin treatment leads to dimerization of FRB/FKBP, by which the formerly bisected ubiquitin can fuse together allowing deubiquitinases to cleave and release a protein of interest (POI).

(F) GCaMP3 signal in *N. benthamiana* upon expression of the HeLo domain and the full length *At*MLKL1 under a ß-estradiol inducible promoter. The average and ± SE are indicated ((HeLo (n=13), full length (n=8), Mock (n = 17)). For the mock control, non-transformed agrobacteria were used. A one-way ANOVA followed by a post-hoc Tukey's HSD test (p = 0.05) was conducted.

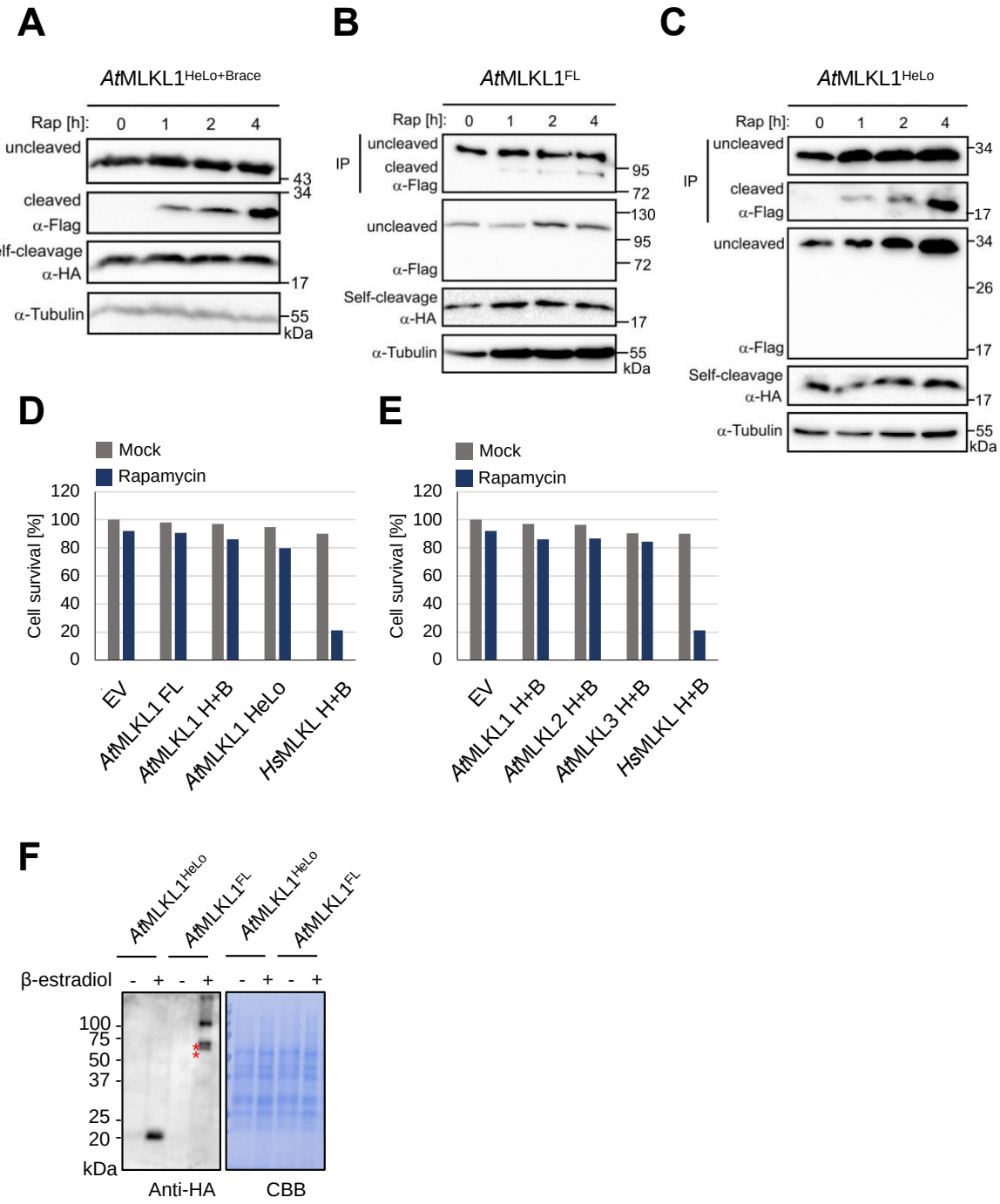

Figure S4. Protein accumulation in HEK293T cells and *N. benthamiana* cells and cell death assay in HEK293T cells, related to Figure 4

(A-C) Immunoblotting of the C-terminally FLAG-tagged *At*MLKL1 variants expressed in human HEK293T cells. Those variants were expressed as fusion proteins with an inhibitory domain at the N-terminus, which is removed by rapamycin-induced split-ubiquitin dimerization. Due to the lower level of cleaved full length *At*MLKL1 (**B**) and the HeLo domain of *At*MLKL1 (**C**), proteins were enriched by immunoprecipitation with FLAG-antibody prior to the immunoblotting. Rap: rapamycin.

(D-E) Human HEK293T cells were transfected with the different *At*MLKLs or *Hs*MLKL constructs as indicated. 24h post transfection cells were treated with rapamycin. Twenty-four hours post rapamycin treatment, cell survival was determined using the Neutral Red assay in a plate reader. Only *Hs*MLKL (HeLo-Brace) elicited cell death.

(F) Steady-state levels of the C-terminally HA-tagged HeLo domain and the full length *At*MLKL1 signal in the stable transgenic *N. benthamiana* plants expressing GCaMP3[59]. The samples were collected at 6 days after infiltration with agrobacteria carrying the expression constructs and 4 days after spraying with ß-estradiol (+) or with a mock-solution (-). The red asterisk indicates protein bands with sizes smaller than expected for full-length *At*MLKL1.

Discussion

We have shown here that PM-localized plant MLKLs are mediators of cytoplasmic Ca^{2+} influx. *At*MLKLs are preferentially engaged by TNL- but not CNL-triggered immunity.[10] Consistent with the disease resistance phenotype, the *Atmlkl* null mutant is defective in mediating sustained Ca^{2+} influx during TNL (i.e., RPS4)-triggered immunity and not CNL (i.e., RPM1)-triggered immunity (Figures 4A and 4B). The involvement of plant MLKLs in TNL-triggered immunity is well supported by the observation that the EDS1 receptor complex that is targeted by TIR enzyme-generated products is required for *At*MLKL1 clustering at the PM (Figures 3A and 3B). In animals, the upstream kinase RIPK3 phosphorylates the activation loop of the pseudokinase domain, inducing oligomerization of MLKL monomers.[39,60-63] Therefore, the EDS1 receptor complex might recruit upstream kinase(s) to trigger conformational changes in plant MLKLs leading to the exposure of the HeLo signaling domains, which possess a propensity for self-oligomerization (Figures 3D and 3E) as well as for triggering Ca^{2+} influx in plant and human cells (Figures 4C–F).

In necroptosis, the oligomerized MLKL permeabilizes the PM via incompletely characterized mechanisms,[64-66] although it is clear that the N-terminal HeLo domain is indispensable.[67,68] Various oligomeric states of activated MLKL have been reported (trimers, tetramers, hexamers, higher-order oligomers, or disulfide-bond dependent amyloid polymers).[61,63,68-72] The HeLo-domain helices of mouse, human, and plant MLKLs can be classified as amphipathic helices, carrying segregated hydrophilic and hydrophobic surfaces.[8,65] Oligomerization of amphipathic helical proteins is often linked to their activities in membrane lysis.[73-75] In ferroptosis, another type of programmed cell death in animals,[8] partial PM damage results in formation of a transient pore that causes cytosolic Ca^{2+} influx[76]. A similar mechanism might underlie plant MLKL-mediated cytosolic Ca^{2+} influx. The *Atmlkl*123 mutant exhibits a pronounced sensitivity to filamentous pathogens (e.g., powdery mildew) in comparison to bacterial pathogens,[10] suggesting that the contribution of plant MLKLs to TNL-triggered immunity varies depending on the mode of pathogen transmission.[77,78] Our minimally invasive microscopy-based monitoring of $[Ca^{2+}]_{cyt}$ using GCaMP3 revealed two distinctive AvrRPS4-dependent $[Ca^{2+}]_{cyt}$ increases; a transient $[Ca^{2+}]_{cyt}$ increase and a sustained $[Ca^{2+}]_{cyt}$ increase (Figure 4A). Intriguingly, the transient $[Ca^{2+}]_{cyt}$ increase peaks at 4 hours post pathogen challenge in both wild type and the *Atmlkl* null mutant, while the sustained $[Ca^{2+}]_{cyt}$ increase starting at 10 hours post pathogen challenge is absent in the *Atmlkl*123mutant (Figure 4A). Instead, the transient $[Ca^{2+}]_{cyt}$ increase is rather retained in the *Atmlkl123* mutant (Figure 4A), which may partially compensate for the lack of the sustained $[Ca^{2+}]_{cyt}$ increase. Therefore, the defect in sustaining cytoplasmic Ca^{2+} influx in the *Atmlkl*123 mutant may account for the varying susceptibility of the *Atmlkl* mutant to different types of pathogenic microbes. Additionally, our data may suggest that the transient $[Ca^{2+}]_{cyt}$ increase peaking at 4 hours is mediated by RNLs.

Taken together, we propose a model for how two distinct HeLo domain-containing protein families, namely plant MLKL and RNL, cooperatively participate in TNL-mediated immune signaling (Figure 5). Recent studies showed that TIR domain-containing proteins, which are often transcriptionally upregulated during ETI, amplify immune signals at the sites of pathogen infection and/or propagate the signals from the pathogen infection site to distal

tissues.[3,4,22] Therefore, TNL-mediated immunity can be separated into two phases: i) signal initiation phase (Figure 5A) and ii) signal amplification phase (Figure 5B). We show that *At*MLKLs and RNLs confer TNL-mediated immunity in a parallel manner (Figure 2E). This is also supported by the reconstitution experiment of *Arabidopsis* MLKL-EDS1 signaling in *N. benthamiana* (Figures 3I and J). As *Arabidopsis* EDS1-SAG101 receptor complex does not substitute the function of *Nb* EDS1-SAG101 receptor complex that activates endogenous helper *Nb*NRG1 in *N. benthamiana*,[24] the *At*MLKL1-mediated immunity to *Xcv* carrying *XopQ* effector in the *eds1 pad4 sag101a sag101b* (Figure 3I) is independent from *Nb*NRG1.

Plant MLKLs and RNLs mediate cytoplasmic Ca^{2+} influx in TNL-mediated immunity but MLKLs contribute to the sustained and intensified $[Ca^{2+}]_{cyt}$ influx (Figure 4A). A propagated TIR-derived signal(s) to the neighboring cells [22,79] could increase the sum of GCaMP3 fluorescence in examined regions, which might explain why the *Atmlkl*123 mutant is much more susceptible to filamentous pathogens (e.g., powdery mildew) which actively spread from infected cells to neighboring healthy cells, than a leaf-infiltrating bacterial pathogen, (e.g., *P. syringae*) that localizes at infection site in a time frame of experiment.[10] Increased levels of MLKL proteins (Figure 2F) would contribute to the MLKL-dependent sustained $[Ca^{2+}]_{cyt}$ increase during RPS4-triggered immunity (Figure 4A). Beside the elevation of protein levels, another, non-mutually exclusive explanation for the MLKL-dependent sustained $[Ca^{2+}]_{cyt}$ increase (Figure 4A) is that structural variations in the TIR-produced metabolites may allow distinctive EDS1 receptor complexes to preferentially activate MLKLs over RNLs. The plant TIR-produced metabolites pRib-AMP and ADPr-ATP promote association of EDS1 receptors with the downstream RNLs NRG1 and ADR1,[27,28] while plant TIR-only proteins like *Bd*TIR generate ~100-fold more v-cADPR (2'cADPR) *in planta* relative to TIR domains from TNL proteins.[18] Lastly, plant TIR-only proteins also linked with the abiotic stress response.[80,81] Consistently, a recent study showed that *At*MLKL1 confers an abiotic stress response (i.e. salt stress),[82] further supporting that plant MLKLs are an integral signaling component for the TIR pathway.

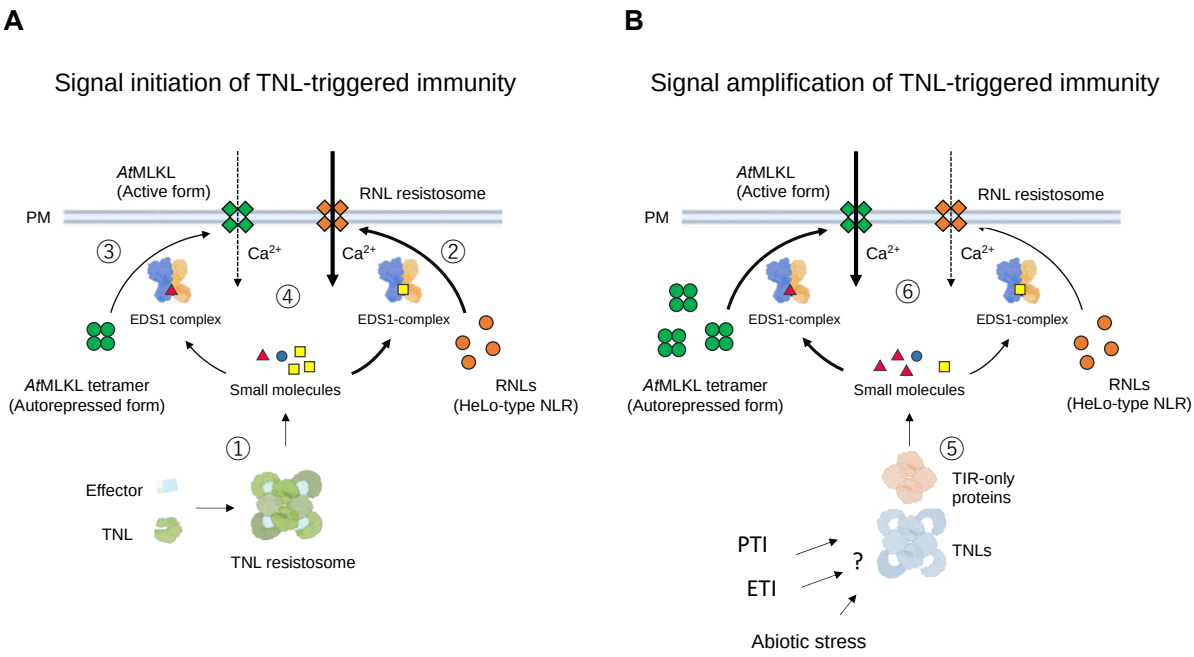

Figure 5. Model for plant MLKL-mediated cytoplasmic calcium ion influx during TNL-triggered immunity.

TNL-mediated immunity can be classified into two phases: **(A)** signal initiation phase upon recognition of pathogen effector and **(B)** signal amplification phase ① TNL resistosomes generate NAD^+-derived small molecules. ② Binding of small molecules by EDS1-SAG101 dimers leads to a conformational change in SAG101, which promotes NRG1 association and formation of the NRG1 resistosome, a calcium-permeable cation channel. ③ Plant MLKLs form EDS1-dependent higher-order oligomers at the PM. ④ MLKLs and NRG1 confer cytoplasmic Ca^{2+} influx during TNL-mediated immunity in a parallel manner. ⑤ Several genes encoding TNLs and TIR-only proteins, which are transcriptionally upregulated during immunity contribute to an EDS1-dependent feedback amplification of the defense signal. ⑥ The increased amount of MLKL proteins would contribute to MLKL-dependent sustained $[Ca^{2+}]_{cyt}$ increase during RPS4-triggered immunity. Beside protein levels, another, non-mutually exclusive explanation for the MLKL-dependent sustained $[Ca^{2+}]_{cyt}$ increase is that structural variations in the TIR products may allow distinctive EDS1 receptor complexes to preferentially activate MLKLs over RNLs.

Acknowledgments: We thank Uyen Nguyen, Leonie Schroers, and Dennis Mahr for technical assistance and Neysan Donnelly for editing the manuscript. We also thank Jane Parker, Frank Takken, Dale Sanders, Keiko Yoshioka, Johannes Stuttmann, Martin Hartmut Schattat, Aaron Lawson/Paul Schulze-lefert for *At*EDS1/*At*SAG101 plasmids, pSfinx plasmid, pBIN20-35s-GCaMP3 plasmid/GCaMP3 *Arabidopsis* line, GCaMP3 *Nicotiana* line, *Nbeds1*, *Nbadr1nrg1 Nbeds1 sag101a sag101b pad4* mutant, CMV2b/P19 plasmids, respectively. We also thank Jane Parker for constructive criticism of the manuscript. This work was supported by the Deutsche Forschungsgemeinschaft (DFG, German Research Foundation, SFB-1403–414786233 to Q.S., K.H., N.O., K.H., J.C., and T.M.), a grant from the University of Cologne Centre of Excellence in Plant Sciences (T.M.), and the Alexander von Humboldt Foundation (a Humboldt professorship to J.C.). A part of Figure 5 was prepared with BioRender.com.

Author contributions: J.C. and T.M. conceptualized the project; Q.S., K.H., N.O., A.P., L.W.T., F.R., and A.T. performed the investigations. Q.S., K.H., N.O., A.P. L.W.T. F.R., A.T., K.H., J.C., and T.M. validated the data, T.T., K.H., J.C., T.M. supervised the work, Q.S., K.H., and T.M. wrote the paper with co-author contributions. The first two authors should be regarded as joint first authors. Co-first authors can prioritize their names when adding this paper's references to their resumes.

Declaration of interests:

The authors declare no competing interests.

Methods

Plant material and growth conditions

The *Arabidopsis thaliana* complementation line expressing *AtMLKL*1-GFP under the native *cis*-regulatory sequence in *Atmlkl1* background was described previously.[10] Using the floral dip method,[83] *Arabidopsis* Col-0 (wild type) and the *eds1-12* mutant[55] were transformed by *Agrobacterium tumefaciens* strain GV3101 pMP90RK[84] carrying the above *AtMLKL*1-GFP complementation construct. Similarly, the *Atmlkl123* triple mutant[10] were transformed by *A. tumefaciens* strain GV3101 pMP90Rgent[84] carrying pBIN20::CaMV35S:GCaMP3.[57] Wild type *A. thaliana* and *Nicotiana benthamiana* plants transformed with pBIN20::CaMV35S:GCaMP3 were generated previously.[57,59] Plant growth conditions were described previously.[40]

Ca^{2+} imaging in leaves

The GCaMP3 signal was acquired in a temperature-controlled (22°C) dark room by a motorized fluorescence stereo microscope Nikon SMZ25 equipped with an 0.5 x objective lens (SHR Plan Apo, WD:71, Nikon) and a high-resolution Nikon DS-Ri2 camera. GCaMP3 was excited using a Nikon GFP-BP filter cube, EX: 470/40 and EM: 525/50. Every 5 min, the GCaMP3 signal was acquired and analyzed by the NIS-Elements Advanced Research microscope imaging software. In the figure, data from every 30 min were shown. For the time-lapse measurement for *A. thaliana* 4–6 old plants were used. Immediately after the infiltration of bacterial suspension, the detached leaves were arranged on a piece of black cardboard that was placed over a wet paper tissue before being placed in a plastic petri dish. After adjustment of exposure time (usually to 5 sec), the measurement was started. During the experiment, the petri dish was closed with a lid. For the image analysis, Fiji software[85] was used to adjust brightness and contrast and to set the LUTs to '16 colors'. Furthermore, for all leaves an individual Region of Interest (ROI) was defined and fluorescence levels were displayed by 'Plot Z-axis profile'. For the bacterial infiltration, the OD_{600} was adjusted to 0.2 with autoclaved milliQ water. The abaxial side of the leaves were infiltrated with the bacterial suspension using a 1-ml needleless syringe. The site wounded by the syringe as well as the infiltrated area -was marked with a permanent marker.

ß-estradiol-based transient protein expression in *N. benthamiana* for Ca^{2+} imaging

The culture of *Agrobacterium* and agro-infiltration was essentially described previously.[86] *A. tumefaciens* strain GV3101 pMP90RK carrying the the ß-estradiol-inducible constructs (pMDC7-GW-3xHA in [87]) of *At*MLKL1 variants or an empty vector (OD_{600} = 0.8) were co-infiltrated into leaves of *N. benthamiana* expressing GCaMP3[59] with *A. tumefaciens* strain GV3101 pMP90RK carrying pGWB517:: CaMV35S:CMV2b (OD_{600} = 0.2) and pGWB517:35S:P19 (OD_{600} = 0.2). A needleless 1-ml syringe was used for infiltrations. One leaf was infiltrated a maximum of six times, without overlap of the infiltration sites. For the ß-estradiol application, the infiltrated leaves were sprayed with 200 µM ß-estradiol solution containing 0.002% [v/v] Silwet L-77 two days after infiltration with *A. tumefaciens*. The GCaMP3 signal was measured as described above.

For immunoblotting, protein samples were collected by harvesting five 6-mm leaf-discs using a biopsy punch from the infiltrated areas avoiding the wounding side and the edge of the infiltration area. Each sample contained leaf discs from five different plants. The collected leaf discs were snap-frozen using liquid nitrogen and kept in a -80°C freezer until protein extraction. For protein extraction, the samples were ground using a pestle or Retsch mill, and 250 µl of 8 M Urea extraction buffer (8 M Urea, 5 mM DTT) were added. All samples were subsequently incubated at room temperature (RT) for 10 min with gentle shaking followed by 20 min at RT without shaking. The resulting lysate was centrifuged for 10 min at 5,000 x g followed by 2 times at 18,000 x g for 30 min, each at RT. After each centrifugation the supernatant was transferred to a new tube. The protein concentration was determined by a Bradford protein assay using BSA (Thermo Scientific Albumin Standard Kit) as a standard and measuring absorbance at 600 nm.

Pathogen infection assays using YFP-expressing potato virus X

The monomeric YFP coding region was amplified from pXCSG-YFP[88] by PCR using the primers containing the *SfiI* recognition sites (*Sfi*IA-mYFPf: TTGGCCATTATGGCCATGGTGAGCAAGGGCGAGGA
, *Sfi*IB-mYFPr: TTGGCCGAGGCGGCCTTACTTGTACAGCTCGTCCA) and the PCR product was digested with *Sfi*I (NEB) and ligated into the *Sfi*IA and *Sfi*IB sites of the binary PVX-based expression vector.[53] The resulting plasmid designated as pSfinx-mYFP was transformed into *A. tumefaciens* strain GV3101 pSoup.[53] The coding regions of GUS (Thermo Fisher Scientific), the HH+HP (G12D, A16D, L20D, R74E, S287E, L341E, R370E) variant of *At*MLKL1, the HP+HB (R74E, W93A, I97E, F213E, S287E, L341E, R370E) variant of *At*MLKL1, and the S393D variants of *At*MLKL1 were cloned into pXCSG-3HA [89] using LR Clonase II (Thermo Fisher Scientific) or In-Fusion cloning (Takara Clontech). The resulting plasmids were transformed into *A. tumefaciens* strain GV3101 pMP90RK.[84] The *A. tumefaciens* strain carrying pSfinx-mYFP (OD_{600} = 0.001) and the *A. tumefaciens* strain carrying either GUS or *At*MLKL1 variants (OD_{600} = 0.6) were co-infiltrated into leaves of wild type, *adr1 nrg1* mutant, [90] or *eds1 pad4 sag101a sag101b* mutant [51] of *N. benthamiana* (*Nbepss*). The *A. tumefaciens* strains each carrying *Sr35* (OD_{600} = 0.075) and AvrSr35 (OD_{600} = 0.5)[54] were used a control.

At 4 days after infiltration, ten 5-mm leaf discs per condition were collected using a biopsy punch from the infiltrated areas. The collected leaf discs were snap-frozen using liquid nitrogen and kept in a -80 °C freezer until use. The leaf discs were ground using a pestle or Retsch mill, and 200 µl of the extraction buffer (50 mM Tris-HCl pH 8.40 150 mM NaCl, proteinase inhibitor (Roche: cOmplet, EDTA-free Protease Inhibitor Cocktail)) were added. The resulting lysate was centrifuged for 5 min at 30,000 x g and 80 µl of the supernatant were loaded into a black 96 well plate (Corning: CLS3915-100EA). The fluorescence microplate reader (TECAN: Tecan infinite 200 pro) was used to measure YFP intensity (Excitation: 516 nm and Emission: 560 nm). YFP intensity was used as a proxy for PVX viral load.

Recombinant protein expression in insect cells and size-exclusion analysis

*At*MLKL1 (residues 1–133) with N-terminal His6-SUMO tag construct in the pFastBac 1 vector (Invitrogen) was generated using a standard PCR-based cloning strategy. The protein was expressed in Sf21 insect cells. One litre of cells was infected with 20 ml baculovirus at 28 °C. After growth at 28 °C for 48 hours, the cells were harvested, re-suspended in a buffer containing 50 mM Tris-HCl pH 8.0 and 300 mM NaCl, and lysed by sonication. The soluble fraction was purified from the cell lysate using cobalt affinity resin (HisPur Cobalt Resin). The protein was subsequently subjected to size-exclusion analysis (Cytiva: Superose 6 Increase 10/300 GL).

SDS-PAGE

Protein samples were mixed with 4×SDS-PAGE loading buffer (Bio-Rad) and subsequently loaded on 12% TGX Stain-Free polyacrylamide gels (Bio-Rad) without a boiling step to avoid aggregation. The electrophoresis was performed at 280 V for 30 minutes. PageRuler Prestained Protein Ladder (Thermo Fisher Scientific) was used as a size standard.

Immunoblotting

Proteins were separated by SDS-PAGE. The samples were mixed with 4×SDS-PAGE loading buffer (Bio-Rad) with 10% 2-mercaptoethanol, then loaded on 10% polyacrylamide gels without a boiling step to avoid aggregation. The electrophoresis was performed at 100 V for 60–90 minutes and proteins were transferred to polyvinylidene fluoride (PVDF) membranes. The membranes were subsequently blocked for 3 h in 5% milk TBS-T before overnight incubation at 4 °C with the corresponding primary antibody in 5% non-fat dry milk TBS-T. The appropriate horseradish (HRP)-conjugated secondary antibody was applied for 2 h in 5% milk TBS-T. Membrane detection was performed using SuperSignal West Femto Maximum Sensitivity Substrate (Thermo Fisher Scientific)) and the ChemiDoc MP imaging system (Biorad). Equal protein transfer was monitored by staining membranes with Ponceau S or Coomassie Brilliant Blue. The following antibodies were used: monoclonal rat anti-HA antibody (Sigma Aldrich, A9037) diluted 1:4,000, goat anti-rat peroxidase antibody (Sigma Aldrich, A5164) diluted 1:5,000, polyclonal rabbit anti-GFP antibody (Abcam, ab6556) diluted 1:4,000, goat anti-rabbit peroxidase antibody (Sigma Aldrich, A9169) diluted 1:5,000, monoclonal mouse anti-FLAG antibody (Sigma Aldrich, F1804) diluted 1:3,000, goat anti-mouse alkaline phosphatase antibody diluted 1:5,000 (Sigma Aldrich, A3562)

Confocal microscopy

Transfected protoplasts in a chamber slide (Nunc Lab-Tek, Thermo Fisher Scientific) with incubation buffer, i.e. WI solution,[91] or 2–5 mm leaf discs prepared form rosette leaves of *Arabidopsis* or *Nicotiana* plants were observed under a confocal microscope (LSM880, Carl Zeiss, Germany) equipped with a 40X water-immersion and a 63X oil-immersion objective. Lambda stack images were obtained for spectral imaging. Images were analyzed and processed with ZEN Software (Carl Zeiss) and Fiji.[85]

Construction of plasmids with *At*MLKL1 variants

Unless otherwise specified, coding sequences (CDS) of *AtMLKL1* variants without stop codons were initially cloned into pENTR/D-TOPO, pDONR221, or pDONR207 (Thermo Fisher Scientific). Entry clones were transferred into the Gateway cloning-compatible pAMPAT-GW-mYFP, pAMPAT-GW-3xHA, or pAMPAT-GW expression vectors.[89] The delineation of domain boundaries of *At*MLKL1 is as follows, HeLo:1–133 aa, Brace: 134–220 aa, Pseudokinase 221–567 aa, Intrinsically disordered (ID) region 568–717 aa.

Transient gene expression in protoplasts

Protoplasts were isolated from the leaves of a 4-week-old *Arabidopsis thaliana* complementation line expressing *At*MLKL1-GFP under the native cis-regulatory sequence in the *Atmlkl1* background. Transfection was as previously described.[91] The *AvrRps4* gene was fused with a FLAG epitope on the pUC19 vector,[92] kindly provided by Dr. Jane Parker. Immunoblotting was essentially as described above for *N. benthamiana*.

Bimolecular fluorescence complementation (BiFC) assays

Agrobacteria delivering BiFC constructs were infiltrated into leaves of *N. benthamiana* quadruple mutant *eds1a pad4 sag101a sag101b* (*Nb epss*).[51] At 48 hpi, Pf0-1 *XopQ* or Pf0-1 (empty vector) (OD_{600} = 0.3) were infiltrated into the same leaf zone. At 6 hpi of Pf0-1, leaf discs were used to observe fluorescence under a confocal microscope (LSM880, Carl Zeiss, Germany).

Pathogen infection assays (*PstDC3000*)

Pseudomonas syringae pv. *tomato* (*Pst*) DC3000 was syringe-infiltrated into *Arabidopsis* leaves at OD_{600} = 0.0005 in 10 mM $MgCl_2$. Bacterial titers were determined at 3 dpi. The released *Pseudomonas* bacteria were diluted and plated onto NYGA plates supplemented with 100 mg/L rifampicin and 25 mg/L kanamycin.

Xanthomonas* growth assay in *N. benthamiana

Xanthomonas campestris pv vesicatoria (*Xcv* 85-10)[93] was provided by Jane Parker. The *Xcv* growth assays in *in N. benthamiana quadruple mutant eds1a pad4 sag101a sag101b (Nb epss)* in the presence of *Agrobacteria*-delivering proteins *At*EDS1-FLAG (OD_{600} = 0.2), *At*SAG101-FLAG (OD_{600} = 0.2), and *At*MLKL-GFP (OD_{600} = 0.8) were performed as described previously[24,26].

Drug treatments

Drugs were used at the following concentrations: 50 µM CHX, 50 µM BFA, 1 mg/ml chitin, 5 mM flg22. *At*MLKL1-GFP seedlings were treated with various mixed working solutions for 1 hour. Before observation under a confocal microscope (LSM880, Carl Zeiss, Germany), samples were immersed in 10 µM FM4-64 for 10 mins.

Immunoprecipitation assays

Protein was purified from 1.0 g infiltrated *N. benthamiana* leaves. Samples were ground to fine powder by a mortar and pestle in liquid nitrogen. Then, 2 ml of extraction buffer (10% glycerol, 50 mM Tris–HCl pH 7.5, 5 mM $MgCl_2$, 150 mM NaCl, 5 mM DTT, 0.25% NP-40, 1% TritonX-100, 0.6mM PMSF, 20mM Mg132, 1x Plant protease cocktail (11873580001, MilliporeSigma)) were added. Lysates were incubated on ice for 10 min and were centrifuged for 10 min at 10000 × *g*, two times. The 50-µl aliquots of the filtered supernatant were taken as input samples. Co-IPs were conducted for 2 h with 25 µl GFP-Trap Agarose (AB_2631357, ChromoTek) under constant rotation. Beads were washed 4 times in extraction buffer without DTT, PMSF and MG132. Immunoblotting was essentially as described for *N. benthamiana*.

Plasmid construction for protein expression in human cell culture

The expression constructs of the C-terminally FLAG-tagged *Hs*MLKL (HeLo+Brace) and *At*MLKL1 truncates (Helo only, HeLo+Brace, and full length) were generated by PCR in combination with In-Fusion cloning (Takara Clontech). Phusion DNA Polymerase (New England Biolabs) was used for PCR with the primers (CIU-At_MLKL1_fw: CGCCTGCGAGGTGGtATGGAGCAATTCAGGCAAATCGGAGAGGTTCTAGGAAG, , At-MLKL1_HeLo_rv:TAGACTCGAGCGGCTTActtgtcatcgtcgtccttgtaatcTGAATTCGCtctagaGGA TCCAAGACCCGAAATCTCACCCGCGGTCTCGATGGCTTCG, At-MLKL1-NT_rv: TAGACTCGAGCGGCTTActtgtcatcgtcgtccttgtaatcTGAATTCGCtctagaGGATCCTCCCGTTA GTTTCTTCAACAGAAAATCAGCTAAACG, AtMLKL1_Fl_rv: TAGACTCGAGCGGCCTTActtgtcatcgtcgtccttgtaatcTGAATTCGCtctagaGGATCCTGTAAGC TCAGAGTCTGAAGCAGGACCAGTTAGTTGTCTACG, pcDNA5_MLKL_fw: TACCGAGCTCGGATCATGGAAAATTTGAAGCATATTATCACCCTTG GCCAGGTCATCCACAAACGGTGTG, pcDNA5_MLKL180_rv: TAGACTCGAGCGGCCCTActtgtcatcgtcgtccttgtaatcTGAATTCGCtctagaGGATCCTAAATAC TGCCTCAAAGTTTCCTTG.

For protein expression in human cell culture, all purified PCR products were cloned into the pcDNA5/FRT/TO vector (ThermoFisher) together with the purified CIUDAD PCR construct (unpublished, AG Hofmann, Figure 4E) using In-Fusion (Takara Clontech).

Human cell culture

Human embryonic kidney (HEK293T; ATCC® CRL-3216™) cells were cultivated in Dulbecco's Modified Eagle Medium (DMEM; Invitrogen) supplemented with 10% fetal-bovine serum (Gibco) and 1% penicillin-streptomycin (Gibco) and maintained at 37 °C, 95% humidity and 5% CO_2.

Plasmid transfection into HEK293T cells

HEK293T cells were transfected using PEI[94]. In brief, 1 µg/µl (PEI:DNA = 2.5:1) transfection mix was added in DMEM supplemented with 5% FBS and 0.5% antibiotics to the cells. Transfection reagent was replaced with DMEM (10% FBS and 1% antibiotics) 5 h after transfection.

Immunoblotting of proteins expressed in human cells

HEK293T cells were lysed in 1x Laemmli sample buffer (125 mM Tris-HCl, pH 6.8, 20% glycerol, 4% SDS, 0.03% bromophenol blue, 20 µl/ml ß-mercaptoethanol). The whole-cell lysates were sonicated, boiled for 10 minutes, and then proteins were resolved by sodium dodecyl sulfate-polyacrylamide gel electrophoresis (SDS-PAGE). After transfer of separated proteins onto PVDF membranes, membranes were blocked in 5% blocking solution (5% milk powder in PBS-T) and then probed for FLAG, HA and tubulin using horseradish peroxidase (HRP)-coupled anti-DYKDDDDK antibody (Miltenyi Biotec, 130-101-572), horseradish peroxidase (HRP)-coupled anti-HA antibody (Miltenyi Biotec, 130-091-972), anti-alpha-tubulin (Sigma Aldrich, T6074) and the appropriate HRP-coupled anti-mouse antibody (Cell Signaling Technology, 7076S). Proteins were detected using enhanced chemiluminescence (ECL; Biozym WesternBright) and signals were collected using GelDoc Imager (BioRad).

Live-cell cytoplasmic Ca^{2+} imaging in human cells

HEK293T cells were seeded into 48 well plates (VWR; 10062-898) and transfected 24 h before live-cell imaging. The medium was supplemented with 1 µM Fluo-4-AM (AAT Bioquest; 20551) a cell-permeable fluorescent Ca^{2+} indicator. Fluo-4 with the AM group is able to cross the plasma membrane by diffusion and intracellular esterases cleave the AM group and trap the dye inside cells. Ca^{2+} binding enhances the fluorescence of Fluo-4. Directly before the measurement, 5 µg/ml rapamycin (Apollo Scientific; 53123-88-9) were added to the transfected cells. Cytoplasmic calcium ions were measured with IncuCyte S3 live-cell imaging. Cells were imaged using the 10x objective and bright-field, green, and red channel settings. Cytoplasmic calcium ions were measured at 10-min intervals. Analysis was performed in Excel by calculating the mean and the standard error of the replicates.

Cell viability assay in human cells

For cell viability assays, HEK293T cells were seeded in 48-well plates and transfected with the various *At*MLKL plasmids. 24 h post transfection, 5 µg/ml rapamycin were added and after a further 24 h the neutral red assay[95] was performed. In brief, 40 µg/ml neural red solution (Fluka; 553-24-2) were added to the cells followed by incubation for 2–3 h at 37 °C, 95% humidity and 5% CO_2. Neural red solution was aspirated, cells were washed once with 1x PBS, and destaining solution (50% ethanol, 1% glacial acetic acid) was added. To extract the neural red, the plate was placed onto a rocker for at least 15 minutes. To evaluate cell viability, the absorbance of neutral red extract at 540 nm was measured in a plate reader (TECAN Infinite F200Pro).

References

1. Ngou, B.P.M., Ahn, H.-K., Ding, P., and Jones, J.D.G. (2021). Mutual potentiation of plant immunity by cell-surface and intracellular receptors. Nature *592*, 110-115. 10.1038/s41586-021-03315-7.
2. Yuan, M., Ngou, B.P.M., Ding, P., and Xin, X.F. (2021). PTI-ETI crosstalk: an integrative view of plant immunity. Current opinion in plant biology *62*, 102030. 10.1016/j.pbi.2021.102030.
3. Tian, H., Wu, Z., Chen, S., Ao, K., Huang, W., Yaghmaiean, H., Sun, T., Xu, F., Zhang, Y., Wang, S., et al. (2021). Activation of TIR signalling boosts pattern-triggered immunity. Nature *598*, 500-503. 10.1038/s41586-021-03987-1.
4. Pruitt, R.N., Locci, F., Wanke, F., Zhang, L., Saile, S.C., Joe, A., Karelina, D., Hua, C., Fröhlich, K., Wan, W.-L., et al. (2021). The EDS1–PAD4–ADR1 node mediates Arabidopsis pattern-triggered immunity. Nature *598*, 495-499. 10.1038/s41586-021-03829-0.
5. Contreras, M.P., Lüdke, D., Pai, H., Toghani, A., and Kamoun, S. (2023). NLR receptors in plant immunity: making sense of the alphabet soup. EMBO reports, e57495. 10.15252/embr.202357495.
6. Yuan, M., Cai, B., and Xin, X.-F. (2023). Plant immune receptor pathways as a united front against pathogens. PLOS Pathogens *19*, e1011106. 10.1371/journal.ppat.1011106.
7. Jacob, F., Vernaldi, S., and Maekawa, T. (2013). Evolution and Conservation of Plant NLR Functions. Frontiers in immunology *4*, 297. 10.3389/fimmu.2013.00297.
8. Maekawa, T., Kashkar, H., and Coll, N.S. (2023). Dying in self-defence: a comparative overview of immunogenic cell death signalling in animals and plants. Cell Death & Differentiation *30*, 258-268. 10.1038/s41418-022-01060-6.
9. Jubic, L.M., Saile, S., Furzer, O.J., El Kasmi, F., and Dangl, J.L. (2019). Help wanted: helper NLRs and plant immune responses. Current opinion in plant biology *50*, 82-94. 10.1016/j.pbi.2019.03.013.
10. Mahdi, L.K., Huang, M., Zhang, X., Nakano, R.T., Kopp, L.B., Saur, I.M.L., Jacob, F., Kovacova, V., Lapin, D., Parker, J.E., et al. (2020). Discovery of a Family of Mixed Lineage Kinase Domain-like Proteins in Plants and Their Role in Innate Immune Signaling. Cell host & microbe *28*, 813-824.e816. 10.1016/j.chom.2020.08.012.
11. Wang, J., Hu, M., Wang, J., Qi, J., Han, Z., Wang, G., Qi, Y., Wang, H.-W., Zhou, J.-M., and Chai, J. (2019). Reconstitution and structure of a plant NLR resistosome conferring immunity. Science (New York, N.Y.) *364*, eaav5870. 10.1126/science.aav5870.
12. Davis, B.K., Wen, H., and Ting, J.P. (2011). The inflammasome NLRs in immunity, inflammation, and associated diseases. Annual review of immunology *29*, 707-735. 10.1146/annurev-immunol-031210-101405.
13. Ma, S., Lapin, D., Liu, L., Sun, Y., Song, W., Zhang, X., Logemann, E., Yu, D., Wang, J., Jirschitzka, J., et al. (2020). Direct pathogen-induced assembly of an NLR immune receptor complex to form a holoenzyme. Science (New York, N.Y.) *370*, eabe3069. doi:10.1126/science.abe3069.
14. Martin, R., Qi, T., Zhang, H., Liu, F., King, M., Toth, C., Nogales, E., and Staskawicz, B.J. (2020). Structure of the activated ROQ1 resistosome directly recognizing the pathogen effector XopQ. Science (New York, N.Y.) *370*, eabd9993. 10.1126/science.abd9993.
15. Li, L., Habring, A., Wang, K., and Weigel, D. (2020). Atypical Resistance Protein RPW8/HR Triggers Oligomerization of the NLR Immune Receptor RPP7 and Autoimmunity. Cell host & microbe *27*, 405-417.e406. https://doi.org/10.1016/j.chom.2020.01.012.
16. Bi, G., Su, M., Li, N., Liang, Y., Dang, S., Xu, J., Hu, M., Wang, J., Zou, M., Deng, Y., et al. (2021). The ZAR1 resistosome is a calcium-permeable channel triggering plant immune signaling. Cell *184*, 3528-3541.e3512. https://doi.org/10.1016/j.cell.2021.05.003.

17. Ma, S., Lapin, D., Liu, L., Sun, Y., Song, W., Zhang, X., Logemann, E., Yu, D., Wang, J., Jirschitzka, J., et al. (2020). Direct pathogen-induced assembly of an NLR immune receptor complex to form a holoenzyme. *370*, eabe3069. doi:10.1126/science.abe3069.
18. Wan, L., Essuman, K., Anderson, R.G., Sasaki, Y., Monteiro, F., Chung, E.-H., Osborne Nishimura, E., DiAntonio, A., Milbrandt, J., Dangl, J.L., and Nishimura, M.T. (2019). TIR domains of plant immune receptors are NAD+-cleaving enzymes that promote cell death. Science (New York, N.Y.) *365*, 799-803. 10.1126/science.aax1771.
19. Nishimura, M.T., Anderson, R.G., Cherkis, K.A., Law, T.F., Liu, Q.L., Machius, M., Nimchuk, Z.L., Yang, L., Chung, E.-H., El Kasmi, F., et al. (2017). TIR-only protein RBA1 recognizes a pathogen effector to regulate cell death in Arabidopsis. Proceedings of the National Academy of Sciences *114*, E2053-E2062. doi:10.1073/pnas.1620973114.
20. Essuman, K., Milbrandt, J., Dangl, J.L., and Nishimura, M.T. (2022). Shared TIR enzymatic functions regulate cell death and immunity across the tree of life. Science (New York, N.Y.) *377*, eabo0001. doi:10.1126/science.abo0001.
21. Bayless, A.M., Chen, S., Ogden, S.C., Xu, X., Sidda, J.D., Manik, M.K., Li, S., Kobe, B., Ve, T., Song, L., et al. (2023). Plant and prokaryotic TIR domains generate distinct cyclic ADPR NADase products. Science Advances *9*, eade8487. doi:10.1126/sciadv.ade8487.
22. Jacob, P., Hige, J., Song, L., Bayless, A., Russ, D., Bonardi, V., El Kasmi, F., Wünsch, L., Yang, Y., Fitzpatrick, Connor R., et al. (2023). Broader functions of TIR domains in Arabidopsis immunity. Proceedings of the National Academy of Sciences *120*, e2220921120. doi:10.1073/pnas.2220921120.
23. Johanndrees, O., Baggs, E.L., Uhlmann, C., Locci, F., Läßle, H.L., Melkonian, K., Käufer, K., Dongus, J.A., Nakagami, H., Krasileva, K.V., et al. (2023). Variation in plant Toll/Interleukin-1 receptor domain protein dependence on ENHANCED DISEASE SUSCEPTIBILITY 1. Plant Physiol *191*, 626-642. 10.1093/plphys/kiac480.
24. Lapin, D., Kovacova, V., Sun, X., Dongus, J.A., Bhandari, D., von Born, P., Bautor, J., Guarneri, N., Rzemieniewski, J., Stuttmann, J., et al. (2019). A Coevolved EDS1-SAG101-NRG1 Module Mediates Cell Death Signaling by TIR-Domain Immune Receptors. The Plant Cell *31*, 2430-2455. 10.1105/tpc.19.00118.
25. Qi, T., Seong, K., Thomazella, D.P.T., Kim, J.R., Pham, J., Seo, E., Cho, M.-J., Schultink, A., and Staskawicz, B.J. (2018). NRG1 functions downstream of EDS1 to regulate TIR-NLR-mediated plant immunity in Nicotiana benthamiana. Proceedings of the National Academy of Sciences *115*, E10979-E10987. doi:10.1073/pnas.1814856115.
26. Sun, X., Lapin, D., Feehan, J.M., Stolze, S.C., Kramer, K., Dongus, J.A., Rzemieniewski, J., Blanvillain-Baufumé, S., Harzen, A., Bautor, J., et al. (2021). Pathogen effector recognition-dependent association of NRG1 with EDS1 and SAG101 in TNL receptor immunity. Nature Communications *12*, 3335. 10.1038/s41467-021-23614-x.
27. Huang, S., Jia, A., Song, W., Hessler, G., Meng, Y., Sun, Y., Xu, L., Laessle, H., Jirschitzka, J., Ma, S., et al. (2022). Identification and receptor mechanism of TIR-catalyzed small molecules in plant immunity. Science (New York, N.Y.) *377*, eabq3297. doi:10.1126/science.abq3297.
28. Jia, A., Huang, S., Song, W., Wang, J., Meng, Y., Sun, Y., Xu, L., Laessle, H., Jirschitzka, J., Hou, J., et al. (2022). TIR-catalyzed ADP-ribosylation reactions produce signaling molecules for plant immunity. Science (New York, N.Y.) *377*, eabq8180. doi:10.1126/science.abq8180.
29. Jacob, P., Kim, N.H., Wu, F., El-Kasmi, F., Chi, Y., Walton, W.G., Furzer, O.J., Lietzan, A.D., Sunil, S., Kempthorn, K., et al. (2021). Plant “helper” immune receptors are Ca2+-permeable nonselective cation channels. Science (New York, N.Y.) *373*, 420-425. 10.1126/science.abg7917.
30. Saile, S.C., Ackermann, F.M., Sunil, S., Keicher, J., Bayless, A., Bonardi, V., Wan, L., Doumane, M., Stöbbe, E., Jaillais, Y., et al. (2021). Arabidopsis ADR1 helper NLR

immune receptors localize and function at the plasma membrane in a phospholipid dependent manner. *232*, 2440-2456. https://doi.org/10.1111/nph.17788.

31. Wang, Z., Liu, X., Yu, J., Yin, S., Cai, W., Kim, N.H., El Kasmi, F., Dangl, J.L., and Wan, L. (2023). Plasma membrane association and resistosome formation of plant helper immune receptors. Proceedings of the National Academy of Sciences of the United States of America *120*, e2222036120. 10.1073/pnas.2222036120.
32. Grant, M., Brown, I., Adams, S., Knight, M., Ainslie, A., and Mansfield, J. (2000). The RPM1 plant disease resistance gene facilitates a rapid and sustained increase in cytosolic calcium that is necessary for the oxidative burst and hypersensitive cell death. The Plant Journal *23*, 441-450. https://doi.org/10.1046/j.1365-313x.2000.00804.x.
33. Fedorova, N.D., Badger, J.H., Robson, G.D., Wortman, J.R., and Nierman, W.C. (2005). Comparative analysis of programmed cell death pathways in filamentous fungi. BMC Genomics *6*, 177. 10.1186/1471-2164-6-177.
34. Maruta, N., Burdett, H., Lim, B.Y.J., Hu, X., Desa, S., Manik, M.K., and Kobe, B. (2022). Structural basis of NLR activation and innate immune signalling in plants. Immunogenetics *74*, 5-26. 10.1007/s00251-021-01242-5.
35. Daskalov, A. (2023). Emergence of the fungal immune system. iScience *26*, 106793. https://doi.org/10.1016/j.isci.2023.106793.
36. Saupe, S.J. (2011). The [Het-s] prion of Podospora anserina and its role in heterokaryon incompatibility. Seminars in Cell & Developmental Biology *22*, 460-468. https://doi.org/10.1016/j.semcdb.2011.02.019.
37. Wang, G., Zhang, D., Orchard, R.C., Hancks, D.C., and Reese, T.A. (2023). Norovirus MLKL-like protein initiates cell death to induce viral egress. Nature *616*, 152-158. 10.1038/s41586-023-05851-w.
38. Murphy, J.M., Czabotar, P.E., Hildebrand, J.M., Lucet, I.S., Zhang, J.G., Alvarez-Diaz, S., Lewis, R., Lalaoui, N., Metcalf, D., Webb, A.I., et al. (2013). The pseudokinase MLKL mediates necroptosis via a molecular switch mechanism. Immunity *39*, 443-453. 10.1016/j.immuni.2013.06.018.
39. Sun, L., Wang, H., Wang, Z., He, S., Chen, S., Liao, D., Wang, L., Yan, J., Liu, W., Lei, X., and Wang, X. (2012). Mixed lineage kinase domain-like protein mediates necrosis signaling downstream of RIP3 kinase. Cell *148*, 213-227. 10.1016/j.cell.2011.11.031.
40. Jacob, F., Kracher, B., Mine, A., Seyfferth, C., Blanvillain-Baufumé, S., Parker, J.E., Tsuda, K., Schulze-Lefert, P., and Maekawa, T. (2018). A dominant-interfering camta3 mutation compromises primary transcriptional outputs mediated by both cell surface and intracellular immune receptors in Arabidopsis thaliana. New Phytologist *217*, 1667-1680. https://doi.org/10.1111/nph.14943.
41. Saucet, S.B., Ma, Y., Sarris, P.F., Furzer, O.J., Sohn, K.H., and Jones, J.D.G. (2015). Two linked pairs of Arabidopsis TNL resistance genes independently confer recognition of bacterial effector AvrRps4. Nature Communications *6*, 6338. 10.1038/ncomms7338.
42. Schultink, A., Qi, T., Lee, A., Steinbrenner, A.D., and Staskawicz, B. (2017). Roq1 mediates recognition of the Xanthomonas and Pseudomonas effector proteins XopQ and HopQ1. The Plant journal : for cell and molecular biology *92*, 787-795. 10.1111/tpj.13715.
43. Rigal, A., Doyle, S.M., and Robert, S. (2015). Live cell imaging of FM4-64, a tool for tracing the endocytic pathways in Arabidopsis root cells. Methods in molecular biology (Clifton, N.J.) *1242*, 93-103. 10.1007/978-1-4939-1902-4_9.
44. Orci, L., Perrelet, A., Ravazzola, M., Wieland, F.T., Schekman, R., and Rothman, J.E. (1993). "BFA bodies": a subcompartment of the endoplasmic reticulum. Proceedings of the National Academy of Sciences of the United States of America *90*, 11089-11093. 10.1073/pnas.90.23.11089.
45. Ponnambalam, S., and Baldwin, S.A. (2003). Constitutive protein secretion from the trans-Golgi network to the plasma membrane. Molecular membrane biology *20*, 129-139. 10.1080/0968768031000084172.
46. Peart, J.R., Mestre, P., Lu, R., Malcuit, I., and Baulcombe, D.C. (2005). NRG1, a CC-NB-LRR Protein, together with N, a TIR-NB-LRR Protein, Mediates Resistance against

Tobacco Mosaic Virus. Current Biology *15*, 968-973. https://doi.org/10.1016/j.cub.2005.04.053.

47. Collier, S.M., Hamel, L.-P., and Moffett, P. (2011). Cell Death Mediated by the N-Terminal Domains of a Unique and Highly Conserved Class of NB-LRR Protein. Molecular Plant-Microbe Interactions® *24*, 918-931. 10.1094/mpmi-03-11-0050.
48. Castel, B., Ngou, P.-M., Cevik, V., Redkar, A., Kim, D.-S., Yang, Y., Ding, P., and Jones, J.D.G. (2019). Diverse NLR immune receptors activate defence via the RPW8-NLR NRG1. New Phytologist *222*, 966-980. https://doi.org/10.1111/nph.15659.
49. Gong, Y., Tian, L., Kontos, I., Li, J., and Li, X. (2023). Plant immune signaling network mediated by helper NLRs. Current opinion in plant biology *73*, 102354. 10.1016/j.pbi.2023.102354.
50. Prautsch, J., Erickson, J.L., Özyürek, S., Gormanns, R., Franke, L., Lu, Y., Marx, J., Niemeyer, F., Parker, J.E., Stuttmann, J., and Schattat, M.H. (2022). Effector XopQ-induced stromule formation in Nicotiana benthamiana depends on ETI signaling components ADR1 and NRG1. Plant Physiology *191*, 161-176. 10.1093/plphys/kiac481.
51. Gantner, J., Ordon, J., Kretschmer, C., Guerois, R., and Stuttmann, J. (2019). An EDS1-SAG101 Complex Is Essential for TNL-Mediated Immunity in Nicotiana benthamiana. The Plant Cell *31*, 2456-2474. 10.1105/tpc.19.00099.
52. Jumper, J., Evans, R., Pritzel, A., Green, T., Figurnov, M., Ronneberger, O., Tunyasuvunakool, K., Bates, R., Žídek, A., Potapenko, A., et al. (2021). Highly accurate protein structure prediction with AlphaFold. Nature *596*, 583-589. 10.1038/s41586-021-03819-2.
53. Takken, F.L.W., Luderer, R., Gabriëls, S.H.E.J., Westerink, N., Lu, R., De Wit, P.J.G.M., and Joosten, M.H.A.J. (2000). A functional cloning strategy, based on a binary PVX-expression vector, to isolate HR-inducing cDNAs of plant pathogens. The Plant Journal *24*, 275-283. https://doi.org/10.1046/j.1365-313x.2000.00866.x.
54. Förderer, A., Li, E., Lawson, A.W., Deng, Y.N., Sun, Y., Logemann, E., Zhang, X., Wen, J., Han, Z., Chang, J., et al. (2022). A wheat resistosome defines common principles of immune receptor channels. Nature *610*, 532-539. 10.1038/s41586-022-05231-w.
55. Ordon, J., Gantner, J., Kemna, J., Schwalgun, L., Reschke, M., Streubel, J., Boch, J., and Stuttmann, J. (2017). Generation of chromosomal deletions in dicotyledonous plants employing a user-friendly genome editing toolkit. The Plant Journal *89*, 155-168. https://doi.org/10.1111/tpj.13319.
56. Tian, L., Hires, S.A., Mao, T., Huber, D., Chiappe, M.E., Chalasani, S.H., Petreanu, L., Akerboom, J., McKinney, S.A., Schreiter, E.R., et al. (2009). Imaging neural activity in worms, flies and mice with improved GCaMP calcium indicators. Nature methods *6*, 875-881. 10.1038/nmeth.1398.
57. Vincent, T.R., Avramova, M., Canham, J., Higgins, P., Bilkey, N., Mugford, S.T., Pitino, M., Toyota, M., and Gilroy, S. (2017). Interplay of Plasma Membrane and Vacuolar Ion Channels, Together with BAK1, Elicits Rapid Cytosolic Calcium Elevations in Arabidopsis during Aphid Feeding. *29*, 1460-1479. 10.1105/tpc.17.00136.
58. Grant, M.R., Godiard, L., Straube, E., Ashfield, T., Lewald, J., Sattler, A., Innes, R.W., and Dangl, J.L. (1995). Structure of the Arabidopsis RPM1 Gene Enabling Dual Specificity Disease Resistance. Science (New York, N.Y.) *269*, 843-846. 10.1126/science.7638602.
59. DeFalco, T.A., Toyota, M., Phan, V., Karia, P., Moeder, W., Gilroy, S., and Yoshioka, K. (2017). Using GCaMP3 to Study Ca2+ Signaling in Nicotiana Species. Plant and Cell Physiology *58*, 1173-1184. 10.1093/pcp/pcx053.
60. Wang, H., Sun, L., Su, L., Rizo, J., Liu, L., Wang, L.F., Wang, F.S., and Wang, X. (2014). Mixed lineage kinase domain-like protein MLKL causes necrotic membrane disruption upon phosphorylation by RIP3. Molecular cell *54*, 133-146. 10.1016/j.molcel.2014.03.003.
61. Liu, S., Liu, H., Johnston, A., Hanna-Addams, S., Reynoso, E., Xiang, Y., and Wang, Z. (2017). MLKL forms disulfide bond-dependent amyloid-like polymers to induce necroptosis. *114*, E7450-e7459. 10.1073/pnas.1707531114.

62. Garnish, S.E., Meng, Y., Koide, A., Sandow, J.J., Denbaum, E., Jacobsen, A.V., Yeung, W., Samson, A.L., Horne, C.R., Fitzgibbon, C., et al. (2021). Conformational interconversion of MLKL and disengagement from RIPK3 precede cell death by necroptosis. Nature Communications *12*, 2211. 10.1038/s41467-021-22400-z.
63. Petrie, E.J., Sandow, J.J., Jacobsen, A.V., Smith, B.J., Griffin, M.D.W., Lucet, I.S., Dai, W., Young, S.N., Tanzer, M.C., Wardak, A., et al. (2018). Conformational switching of the pseudokinase domain promotes human MLKL tetramerization and cell death by necroptosis. Nature Communications *9*, 2422. 10.1038/s41467-018-04714-7.
64. Grootjans, S., Vanden Berghe, T., and Vandenabeele, P. (2017). Initiation and execution mechanisms of necroptosis: an overview. Cell Death & Differentiation *24*, 1184-1195. 10.1038/cdd.2017.65.
65. Flores-Romero, H., Ros, U., and Garcia-Saez, A.J. (2020). Pore formation in regulated cell death. The EMBO Journal *39*, e105753. https://doi.org/10.15252/embj.2020105753.
66. Bi, G., and Zhou, J.M. (2021). Regulation of Cell Death and Signaling by Pore-Forming Resistosomes. Annual review of phytopathology *59*, 239-263. 10.1146/annurev-phyto-020620-095952.
67. Su, L., Quade, B., Wang, H., Sun, L., Wang, X., and Rizo, J. (2014). A plug release mechanism for membrane permeation by MLKL. Structure (London, England : 1993) *22*, 1489-1500. 10.1016/j.str.2014.07.014.
68. Hildebrand, J.M., Tanzer, M.C., Lucet, I.S., Young, S.N., Spall, S.K., Sharma, P., Pierotti, C., Garnier, J.-M., Dobson, R.C.J., Webb, A.I., et al. (2014). Activation of the pseudokinase MLKL unleashes the four-helix bundle domain to induce membrane localization and necroptotic cell death. Proceedings of the National Academy of Sciences *111*, 15072-15077. doi:10.1073/pnas.1408987111.
69. Chen, X., Li, W., Ren, J., Huang, D., He, W.T., Song, Y., Yang, C., Li, W., Zheng, X., Chen, P., and Han, J. (2014). Translocation of mixed lineage kinase domain-like protein to plasma membrane leads to necrotic cell death. Cell research *24*, 105-121. 10.1038/cr.2013.171.
70. Cai, Z., Jitkaew, S., Zhao, J., Chiang, H.C., Choksi, S., Liu, J., Ward, Y., Wu, L.G., and Liu, Z.G. (2014). Plasma membrane translocation of trimerized MLKL protein is required for TNF-induced necroptosis. Nature cell biology *16*, 55-65. 10.1038/ncb2883.
71. Huang, D., Zheng, X., Wang, Z.A., Chen, X., He, W.T., Zhang, Y., Xu, J.G., Zhao, H., Shi, W., Wang, X., et al. (2017). The MLKL Channel in Necroptosis Is an Octamer Formed by Tetramers in a Dyadic Process. Molecular and cellular biology *37*. 10.1128/mcb.00497-16.
72. Davies, K.A., Tanzer, M.C., Griffin, M.D.W., Mok, Y.F., Young, S.N., Qin, R., Petrie, E.J., Czabotar, P.E., Silke, J., and Murphy, J.M. (2018). The brace helices of MLKL mediate interdomain communication and oligomerisation to regulate cell death by necroptosis. Cell Death & Differentiation *25*, 1567-1580. 10.1038/s41418-018-0061-3.
73. Tayeb-Fligelman, E., and Tabachnikov, O. (2017). The cytotoxic Staphylococcus aureus PSMα3 reveals a cross-α amyloid-like fibril. *355*, 831-833. 10.1126/science.aaf4901.
74. Adachi, H., Kamoun, S., and Maqbool, A. (2019). A resistosome-activated 'death switch'. Nature Plants *5*, 457-458. 10.1038/s41477-019-0425-9.
75. Kayagaki, N., Stowe, I.B., Alegre, K., Deshpande, I., Wu, S., Lin, Z., Kornfeld, O.S., Lee, B.L., Zhang, J., Liu, J., et al. (2023). Inhibiting membrane rupture with NINJ1 antibodies limits tissue injury. Nature *618*, 1072-1077. 10.1038/s41586-023-06191-5.
76. Pedrera, L., Espiritu, R.A., Ros, U., Weber, J., Schmitt, A., Stroh, J., Hailfinger, S., von Karstedt, S., and García-Sáez, A.J. (2021). Ferroptotic pores induce Ca2+ fluxes and ESCRT-III activation to modulate cell death kinetics. Cell Death & Differentiation *28*, 1644-1657. 10.1038/s41418-020-00691-x.
77. Antonovics, J. (1994). The interplay of numerical and gene-frequency dynamics in host-pathogen systems. Ecological genetics *129*, 145.
78. Real, L.A., and McElhany, P. (1996). Spatial Pattern and Process in Plant--Pathogen Interactions. Ecology *77*, 1011-1025. https://doi.org/10.2307/2265572.

79. Jacob, P., Hige, J., and Dangl, J.L. (2023). Is localized acquired resistance the mechanism for effector-triggered disease resistance in plants? Nature Plants *9*, 1184-1190. 10.1038/s41477-023-01466-1.
80. Kosmacz, M., Luzarowski, M., Kerber, O., Leniak, E., Gutiérrez-Beltrán, E., Moreno, J.C., Gorka, M., Szlachetko, J., Veyel, D., Graf, A., and Skirycz, A. (2018). Interaction of 2′,3′-cAMP with Rbp47b Plays a Role in Stress Granule Formation. Plant Physiology *177*, 411-421. 10.1104/pp.18.00285.
81. Yu, D., Song, W., Tan, E.Y.J., Liu, L., Cao, Y., Jirschitzka, J., Li, E., Logemann, E., Xu, C., Huang, S., et al. (2022). TIR domains of plant immune receptors are 2′,3′-cAMP/cGMP synthetases mediating cell death. Cell *185*, 2370-2386.e2318. https://doi.org/10.1016/j.cell.2022.04.032.
82. Awlia, M., Alshareef, N., Saber, N., Korte, A., Oakey, H., Panzarová, K., Trtílek, M., Negrão, S., Tester, M., and Julkowska, M.M. (2021). Genetic mapping of the early responses to salt stress in Arabidopsis thaliana. The Plant Journal *107*, 544-563. https://doi.org/10.1111/tpj.15310.
83. Clough, S.J., and Bent, A.F. (1998). Floral dip: a simplified method for Agrobacterium -mediated transformation of Arabidopsis thaliana. The Plant Journal *16*, 735-743. https://doi.org/10.1046/j.1365-313x.1998.00343.x.
84. Koncz, C., and Schell, J. (1986). The promoter of TL-DNA gene 5 controls the tissue-specific expression of chimaeric genes carried by a novel type of Agrobacterium binary vector. Molecular and General Genetics MGG *204*, 383-396. 10.1007/BF00331014.
85. Schindelin, J., Arganda-Carreras, I., Frise, E., Kaynig, V., Longair, M., Pietzsch, T., Preibisch, S., Rueden, C., Saalfeld, S., Schmid, B., et al. (2012). Fiji: an open-source platform for biological-image analysis. Nature methods *9*, 676-682. 10.1038/nmeth.2019.
86. Ma, L., Lukasik, E., Gawehns, F., and Takken, F.L. (2012). The use of agroinfiltration for transient expression of plant resistance and fungal effector proteins in Nicotiana benthamiana leaves. Methods in molecular biology (Clifton, N.J.) *835*, 61-74. 10.1007/978-1-61779-501-5_4.
87. Curtis, M.D., and Grossniklaus, U. (2003). A Gateway Cloning Vector Set for High-Throughput Functional Analysis of Genes in Planta. Plant Physiology *133*, 462-469. 10.1104/pp.103.027979.
88. Feys, B.J., Wiermer, M., Bhat, R.A., Moisan, L.J., Medina-Escobar, N., Neu, C., Cabral, A., and Parker, J.E. (2005). Arabidopsis SENESCENCE-ASSOCIATED GENE101 Stabilizes and Signals within an ENHANCED DISEASE SUSCEPTIBILITY1 Complex in Plant Innate Immunity. The Plant Cell *17*, 2601-2613. 10.1105/tpc.105.033910.
89. Maekawa, T., Cheng, W., Spiridon, L.N., Töller, A., Lukasik, E., Saijo, Y., Liu, P., Shen, Q.-H., Micluta, M.A., Somssich, I.E., et al. (2011). Coiled-Coil Domain-Dependent Homodimerization of Intracellular Barley Immune Receptors Defines a Minimal Functional Module for Triggering Cell Death. Cell host & microbe *9*, 187-199. https://doi.org/10.1016/j.chom.2011.02.008.
90. Prautsch, J., Erickson, J.L., Özyürek, S., Gormanns, R., Franke, L., Lu, Y., Marx, J., Niemeyer, F., Parker, J.E., Stuttmann, J., and Schattat, M.H. (2023). Effector XopQ-induced stromule formation in Nicotiana benthamiana depends on ETI signaling components ADR1 and NRG1. Plant Physiology *191*, 161-176. 10.1093/plphys/kiac481.
91. Yoo, S.-D., Cho, Y.-H., and Sheen, J. (2007). Arabidopsis mesophyll protoplasts: a versatile cell system for transient gene expression analysis. Nature Protocols *2*, 1565-1572. 10.1038/nprot.2007.199.
92. Xing, Y., Xu, N., Bhandari, D.D., Lapin, D., Sun, X., Luo, X., Wang, Y., Cao, J., Wang, H., Coaker, G., et al. (2021). Bacterial effector targeting of a plant iron sensor facilitates iron acquisition and pathogen colonization. Plant Cell *33*, 2015-2031. 10.1093/plcell/koab075.
93. Thieme, F., Koebnik, R., Bekel, T., Berger, C., Boch, J., Büttner, D., Caldana, C., Gaigalat, L., Goesmann, A., Kay, S., et al. (2005). Insights into genome plasticity and pathogenicity of the plant pathogenic bacterium Xanthomonas campestris pv.

vesicatoria revealed by the complete genome sequence. Journal of bacteriology *187*, 7254-7266. 10.1128/jb.187.21.7254-7266.2005.
94. Durocher, Y., Perret, S., and Kamen, A. (2002). High-level and high-throughput recombinant protein production by transient transfection of suspension-growing human 293-EBNA1 cells. Nucleic acids research *30*, E9. 10.1093/nar/30.2.e9.
95. Repetto, G., del Peso, A., and Zurita, J.L. (2008). Neutral red uptake assay for the estimation of cell viability/cytotoxicity. Nature Protocols *3*, 1125-1131. 10.1038/nprot.2008.75.

Figure legends

Figure 1. *Arabidopsis* MLKL1 form clusters at the plasma membrane (PM) during TNL-triggered immunity in a HeLo domain-dependent manner.
(A) Top panel: Schematic representations of *At*MLKLs. Bottom panel: Cryo-EM structure of a protomer of the *At*MLKL3 tetramer (PDB: 6KA4). Subdomains of *At*MLKLs are shown in different colors. Yellow: HeLo domain, Purple: Brace region, Green: pseudokinase domain, dark yellow: the intrinsically disordered (ID) region. The ID region does not appear in the Cryo-EM structures likely due to its instability.
(B) Left panels: Top-view of leaf epidermal cells of *Arabidopsis* complementation line expressing *AtMLKL*1-GFP under the native *cis*-regulatory sequence in *Atmlkl1* background[10] upon challenge of *P. fluorescens* Pf0-1 expressing AvrRPS4 (Pf0-AvrRps4) or *P. fluorescens* Pf0-1 carrying empty vector (Pf0-EV) at 5 hours post infiltration (hpi). Right panels; Top-view of leaf epidermal cells of *N. benthamiana* transiently expressing *At*MLKL1-GFP under the constitutive 35S promoter upon challenge of *P. fluorescens* Pf0-1 expressing XopQ or *P. fluorescens* Pf0-1 carrying empty vector (EV) at 5 hpi.
(C) Left: Quantification of *At*MLKL1-GFP puncta number in the *Arabidopsis* complementation line at 5 hpi upon the infiltration of Pf0-AvrRPS4 (n=29) or Pf0-EV (n=15). Right: Quantification of *At*MLKL1-GFP puncta number in *N. benthamiana* at 7hpi upon infiltration of Pf0-XopQ (n=12) and Pf0-EV (n=9). Asterisks indicate significant differences at $p < 0.001$ which were determined with single-factor ANOVA followed by Tukey's test.
(D) Clustered *At*MLKL1-GFP signals overlapping with the fluorescence signals of the plasma membrane (PM) tracer, FM4-64 in the plasmolyzed epidermal cells. The red and light blue arrows indicate PM and cell wall, respectively. White arrowheads indicate the *At*MLKL1-GFP puncta.
(E) A time-course quantification of *At*MLKL1-GFP puncta number in the *Arabidopsis* complementation line.
(F) Steady-state levels of *At*MLKL1-GFP were comparable at each examined time point upon infiltration with the Pf0-1 strain expressing AvrRps4, *P. fluorescens* Pf0-1 carrying empty vector (EV), and the mock treatment in total cell lysate from the *Arabidopsis* complementation line.
(G) The N-terminal HeLo-domain is sufficient and necessary for puncta formation in *N. benthamiana*. The C-terminally mClover3-tagged truncated *At*MLKL1 variants were expressed under the constitutive 35S promoter in *N. benthamiana*. No avirulent pathogens were challenged. The images were taken at 48 hours post Agrobacterium infiltration. White arrowheads indicate the *At*MLKL1-GFP puncta. H: HeLo domain alone, H+B: HeLo with brace, H+B+P: HeLo with brace and pseudokinase, B+P+ID: *At*MLKL1 lacking the HeLo domain.
(H) The N-terminal HeLo-domain of *At*MLKL1 exhibited disease resistance activity against YFP expressing Potato virus X (PVX) in *N. benthamiana*. All *At*MLKL1 variants were C-terminally tagged with HA epitope. The YFP intensity of the leaf lysate was measured as a proxy of the disease resistance activity.
(I) The N-terminal HeLo-domain of *At*MLKL1 conferred disease resistance against *Pst* DC3000 in *A. thaliana mlkl123* triple mutant background.

Figure 2. Structure-guided mutagenesis reveals distinctive contributions of the EDS1 family and helper NLRs to the disease resistance activity mediated by the gain-of-function variants of *At*MLKL1.
(A) Left: Schematic representation of the intra-domain interfaces indicated by blue dashed lines. Right: Tertiary structure of the *At*MLKL1 tetramer modeled by Alfafold2.[52] The color code is identical to A. One of four protomers is shown in color. As the cryo-EM structures of *At*MLKL2 and *At*MLKL3 are nearly identical and the protein sequences of *At*MLKL1, 2, and 3 are highly conserved, it is conceivable that *At*MLKL1 also forms an *At*MLKL3 like tetramer. **(B)** The position of amino acid residues in the intra-domain interfaces in *At*MLKL1 protomer .**(C)** Schematic representation of the inter-domain interfaces indicated by black dashed lines. **(D)** The position of amino acid residues in the inter-domain interfaces in *At*MLKL1 tetramer. **(E)** Disease resistance activity of *At*MLKL1 variants carrying mutations at either intra- or inter-domain interfaces against YFP-expressing PVX. All *At*MLKL1 variants were C-terminally tagged with HA epitope. The YFP intensity of the leaf lysate was measured as a proxy for the disease resistance activity. HH+HP and HP+HB indicate the mutant *At*MLKL1 variants harboring mutations at the HH+HP interfaces and HP+HB interfaces, respectively. The previously identified gain-of-function variant carrying a phosphomimetic mutation (S393D from Mahdi et al.[10]) in the activation loop of the pseudokinase domain was used as a control. The red asterisks indicate significant differences from the *At*MLKL1 wild type at $p < 0.02$ determined with Dunnett's test. Black asterisks indicate significant differences at $p < 0.01$ which were determined with Kruskal–Wallis H test.

Figure 3. EDS1 facilitates *At*MLKL1 clustering during TNL-triggered immunity.

(A) Confocal images of leaf epidermal cells of *Arabidopsis* wild type or *eds1-12* mutant expressing *AtMLKL*1-GFP under the native *cis*-regulatory sequence. White arrowheads indicate the *At*MLKL1-GFP puncta. Images were taken at 5-6 hours post infiltration of *Pf0-AvrRps4*. **(B)** Steady-state levels of *At*MLKL1-GFP in total cell lysate from the indicated *Arabidopsis* lines were comparable upon infiltration with the Pf0-1 strain expressing AvrRps4, *P. fluorescens* Pf0-1 carrying empty vector (EV), and $MgCl_2$. The samples were collected at 5 hours post infiltration. **(C)** Confocal images of leaf epidermal cells of the *eds1 pad4 sag101a sag1101b* mutant of *N. benthamiana* expressing the C-terminally mClover3-tagged HeLo domain of *At*MLKL1. No avirulent pathogens were challenged. White arrowheads indicate the *At*MLKL1-GFP puncta. The images were taken at 48 hours post agrobacterium infiltration. **(D)** Size-exclusion chromatography profile of the 6xHis-Sumo-tagged HeLo domain of *At*MLKL1. Position of standard molecular weight marker is indicated. **(E)** Peak fractions in the size-exclusion chromatography were verified by SDS-PAGE. **(F)** Bimolecular fluorescence complementation assays. *At*MLKL1-cYFP, *At*SAG101-nYFP, and *At*EDS1-FLAG were co-expressed under a constitutive 35S promoter in the *eds1 pad4 sag101ab* (*Nb-epss*) mutant of *N. benthamiana*. Enhanced YFP signals around PM and at nuclei indicated by the white arrowhead and arrow, respectively, were detected upon infiltration with the Pf0-1 strain expressing XopQ. **(G)** Quantification of number of cells with YFP signals at 48 hpi upon infiltration of Pf0-EV (n=18) or Pf0-XopQ (n=22). Asterisks indicate significant differences at $p < 0.001$, which were determined with single-factor ANOVA followed by Tukey's test. **(H)** Disease resistance activity against YFP-expressing PVX by the C-terminally HA-tagged HeLo domain of *At*MLKL1 was impaired in the *eds1 pad4 sag101a sag101b* mutant of *N. benthamiana*. The proteins were expressed under the constitutive 35S promoter. **(I** and **J)** Reconstitution of *At*EDS1-, *At*SAG101- and *At*MLKL1-mediated immunity in the *eds1 pad4 sag101a sag101b* mutant of *N. benthamiana* in response to the *Xcv* strain carrying *XopQ* that is recognized by the Roq1 TNL. Different letters indicate statistically significant difference at $p < 0.05$, which was determined with single-factor ANOVA followed by Tukey's test.

Figure 4. Plant MLKLs are mediators of cytoplasmic calcium ion influx.

(A and **B)** A time course signal analysis of GCaMP3 in the leaves of Col-0 expressing GCaMP3[59] and two independent *Atmlkl12*3 transgenic lines expressing GCaMP3 generated in this study. Average and SE at each time points upon infiltration with Pf0-1 expressing AvrRPS4 (Pf0-AvrRps4) or b, Pf0-1 expressing AvrRpm1 (Pf0-AvrRpm1) are shown. Pf0-1 carrying empty vector (Pf0-EV) was used as a negative control.
(C and **D)** The N-terminal HeLo domain alone and the HeLo domain plus the brace region of *At*MLKL1 induced $[Ca^{2+}]_{cyt}$ influx in human HEK293T cells. **(D)** mock control. **A-D**, the mean and the standard error of the replicates are shown. **(E**) Schematic representation of the rapamycin-induced release of the N-terminal tag-free protein of interest (POI) used in **C** and **D**. After transfection of the construct the N-terminal FRB-N-Ub and the C-terminal FKBP-C-Ub-POI are separated by the 2A self-cleaving peptides. Rapamycin treatment leads to dimerization of FRB/FKBP, by which the formerly bisected ubiquitin can fuse together allowing deubiquitinases to cleave and release a protein of interest (POI). **(F)** GCaMP3 signal in *N. benthamiana* upon expression of the HeLo domain and the full length *At*MLKL1 under a ß-estradiol inducible promoter. The average and ± SE are indicated ((HeLo (n=13), full length (n=8), Mock (n = 17)). For the mock control, non-transformed agrobacteria were used. A one-way ANOVA followed by a post-hoc Tukey's HSD test ($p = 0.05$) was conducted.

Figure 5. Model for plant MLKL-mediated cytoplasmic calcium ion influx during TNL-triggered immunity.

TNL-mediated immunity can be classified into two phases: **(A)** signal initiation phase upon recognition of pathogen effector and **(B)** signal amplification phase ① TNL resistosomes generate NAD^+-derived small molecules. ② Binding of small molecules by EDS1-SAG101 dimers leads to a conformational change in SAG101, which promotes NRG1 association and formation of the NRG1 resistosome, a calcium-permeable cation channel. ③ Plant MLKLs form EDS1-dependent higher-order oligomers at the PM. ④ MLKLs and NRG1 confer cytoplasmic Ca^{2+} influx during TNL-mediated immunity in a parallel manner. ⑤ Several genes encoding TNLs and TIR-only proteins, which are transcriptionally upregulated during immunity contribute to an EDS1-dependent feedback amplification of the defense signal. ⑥ The increased amount of MLKL proteins would contribute to MLKL-dependent sustained $[Ca^{2+}]_{cyt}$ increase during RPS4-triggered immunity. Beside protein levels, another, non-mutually exclusive explanation for the MLKL-dependent sustained $[Ca^{2+}]_{cyt}$ increase is that structural variations in the TIR products may allow distinctive EDS1 receptor complexes to preferentially activate MLKLs over RNLs.

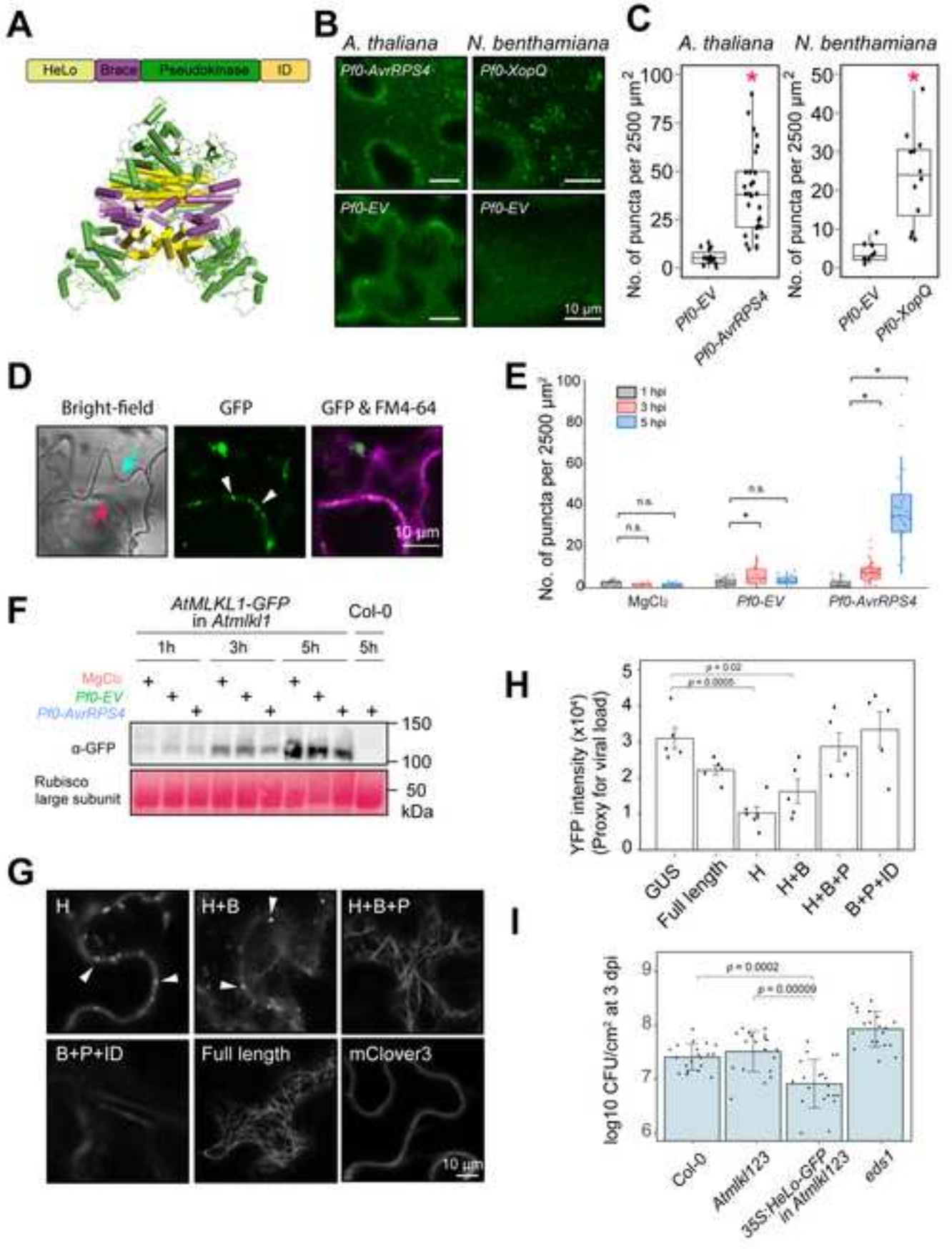

Figure 1

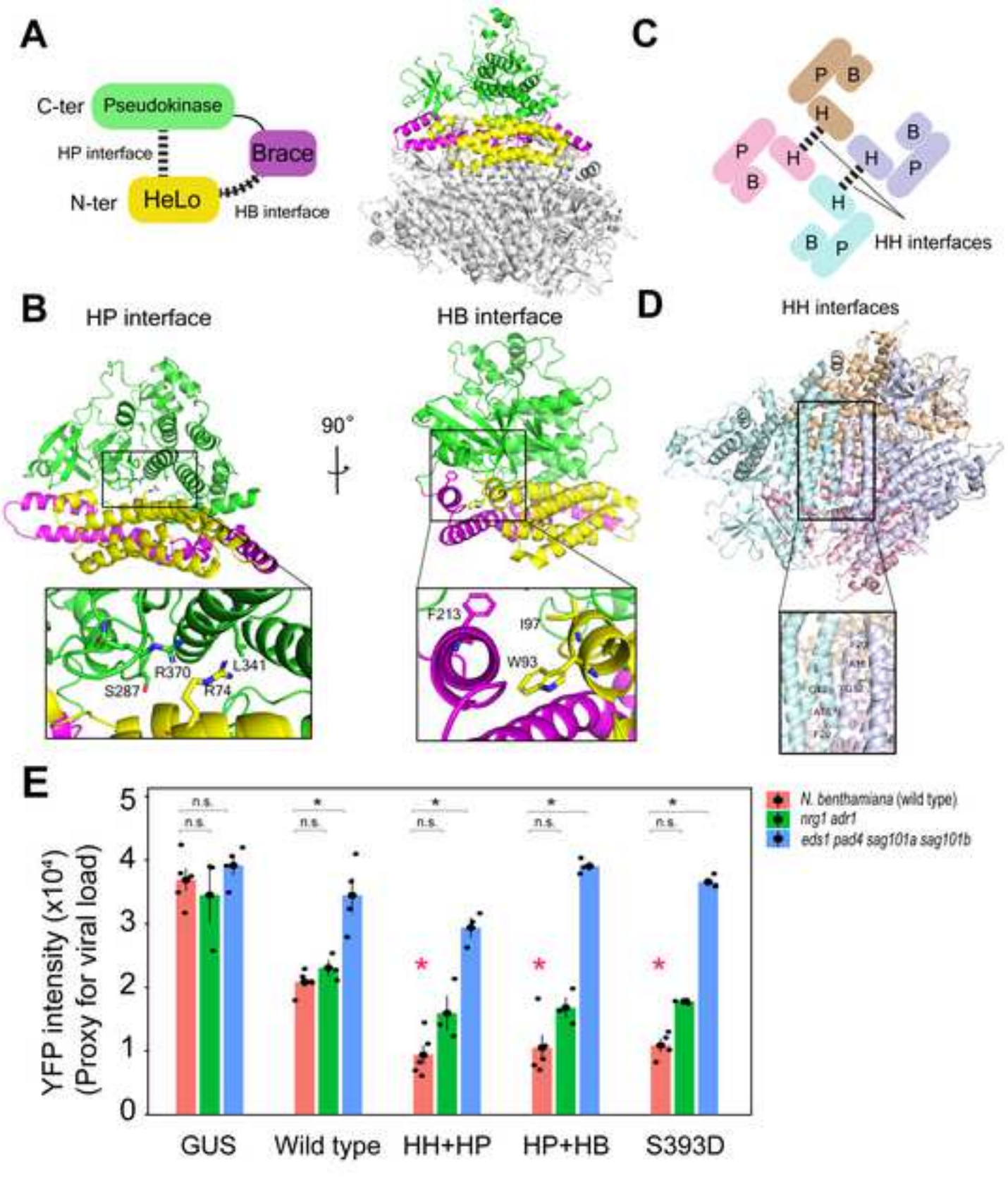

Figure 2

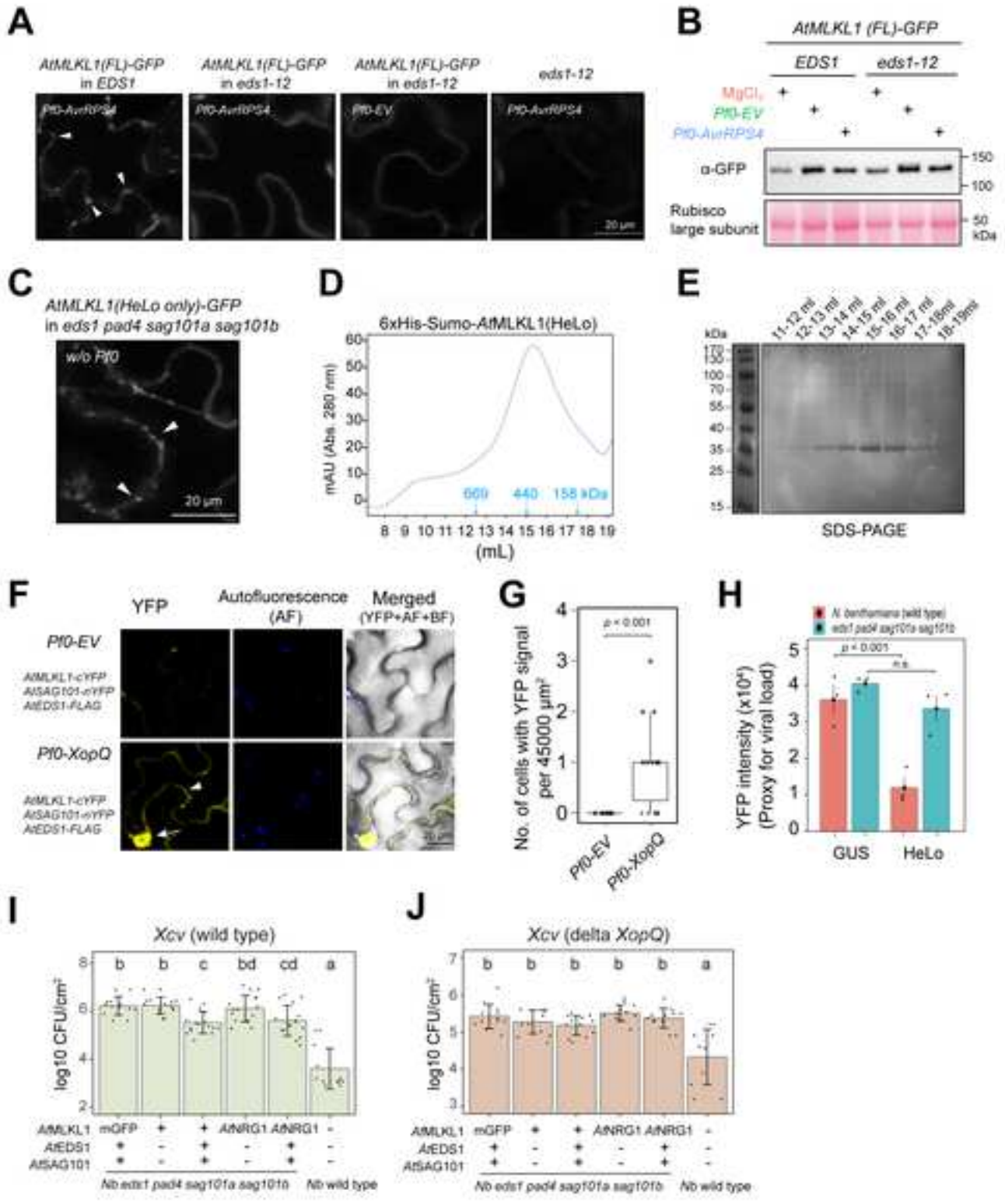

Figure 3

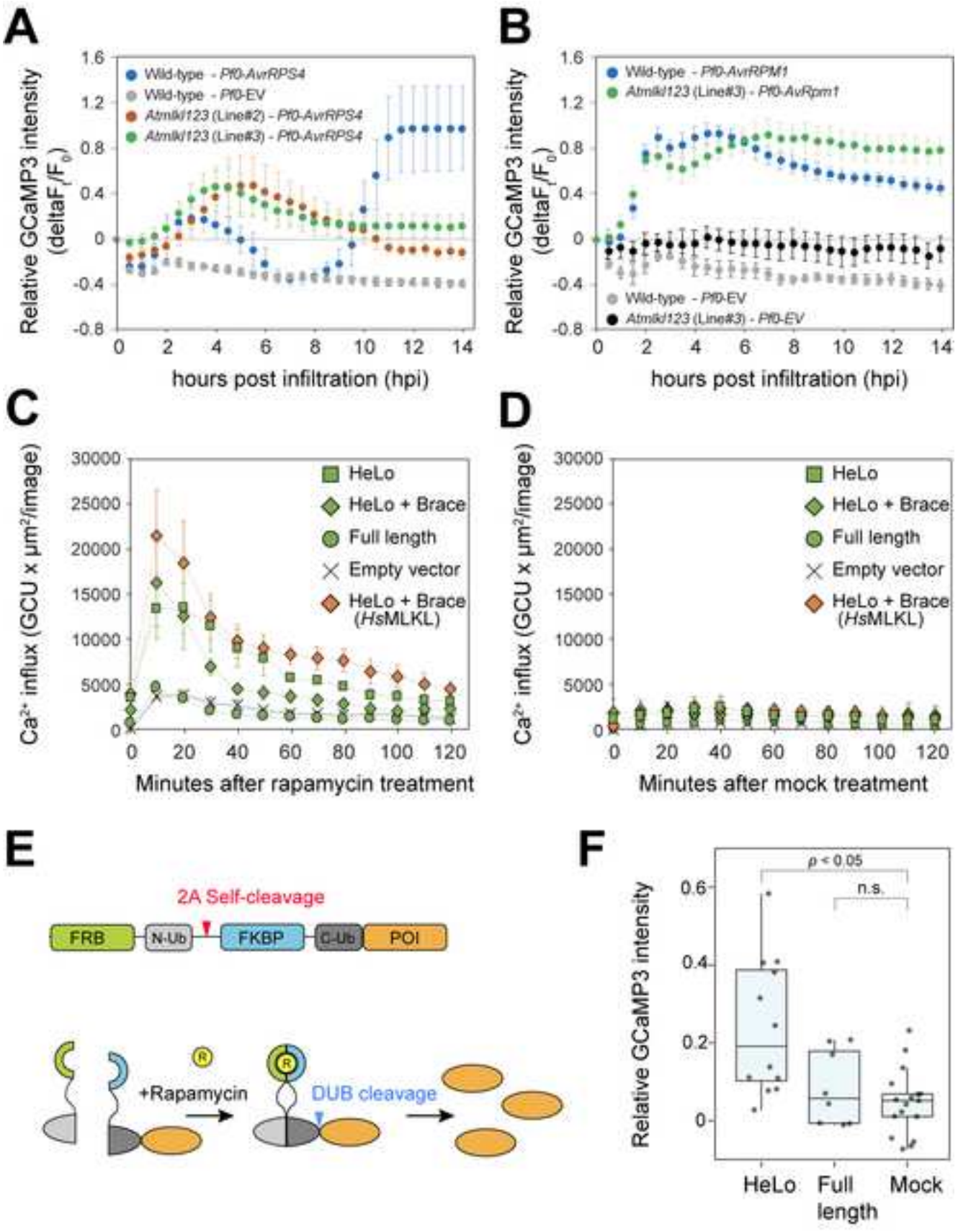

Figure 4

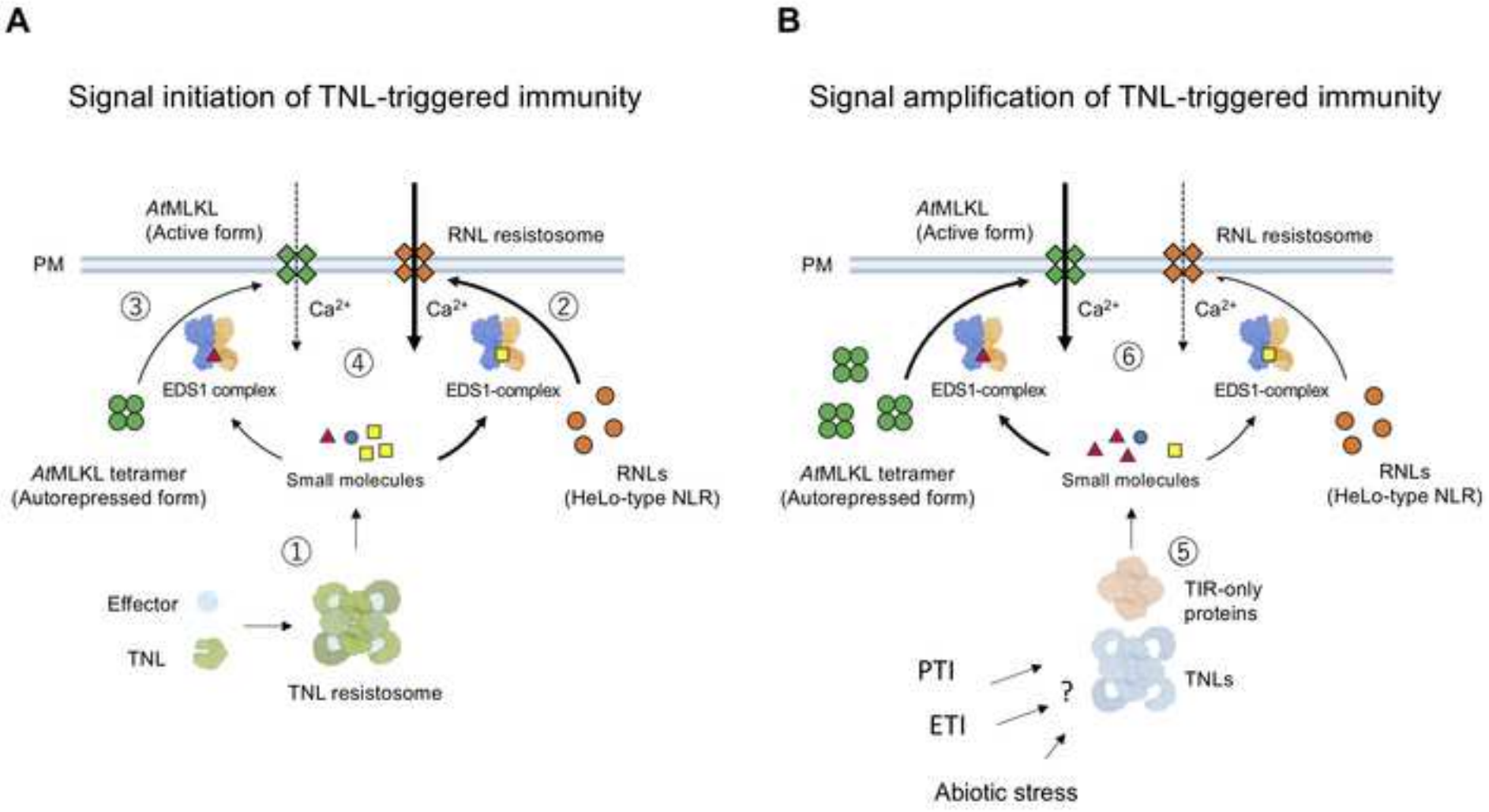

Figure 5

CELL PRESS DECLARATION OF INTERESTS POLICY

Transparency is essential for a reader's trust in the scientific process and for the credibility of published articles. At Cell Press, we feel that disclosure of competing interests is a critical aspect of transparency. Therefore, we require a "declaration of interests" section in which all authors disclose any financial or other interests related to the submitted work that (1) could affect or have the perception of affecting the author's objectivity or (2) could influence or have the perception of influencing the content of the article.

What types of articles does this apply to?

We require that you disclose competing interests for all submitted content by completing and submitting the form below. We also require that you include a "declaration of interests" section in the text of all articles even if there are no interests to declare.

What should I disclose?

We require that you and all authors disclose any personal financial interests (e.g., stocks or shares in companies with interests related to the submitted work or consulting fees from companies that could have interests related to the work), professional affiliations, advisory positions, board memberships (including membership on a journal's advisory board when publishing in that journal), or patent holdings that are related to the subject matter of the contribution. As a guideline, you need to declare an interest for (1) any affiliation associated with a payment or financial benefit exceeding $10,000 p.a. or 5% ownership of a company or (2) research funding by a company with related interests. You do not need to disclose diversified mutual funds, 401ks, or investment trusts.

Authors should also disclose relevant financial interests of immediate family members. Cell Press uses the Public Health Service definition of "immediate family member," which includes spouse and dependent children.

Where do I declare competing interests?

Competing interests should be disclosed on this form as well as in a "declaration of interests" section in the manuscript. This section should include financial or other competing interests as well as affiliations that are not included in the author list. Examples of "declaration of interests" language include:

> "AUTHOR is an employee and shareholder of COMPANY."
> "AUTHOR is a founder of COMPANY and a member of its scientific advisory board."

NOTE: Primary affiliations should be included with the author list and do not need to be included in the "declaration of interests" section. Funding sources should be included in the "acknowledgments" section and also do not need to be included in the "declaration of interests" section. (A small number of front-matter article types do not include an "acknowledgments" section. For these articles, reporting of funding sources is not required.)

What if there are no competing interests to declare?

If you have no competing interests to declare, please note that in the "declaration of interests" section with the following wording:

> "The authors declare no competing interests."

CELL PRESS DECLARATION OF INTERESTS FORM

If submitting materials via Editorial Manager, please complete this form and upload with your initial submission. Otherwise, please email as an attachment to the editor handling your manuscript.

Please complete each section of the form and insert any necessary "declaration of interests" statement in the text box at the end of the form. A matching statement should be included in a "declaration of interests" section in the manuscript.

Institutional affiliations

We require that you list the current institutional affiliations of all authors, including academic, corporate, and industrial, on the title page of the manuscript. ***Please select one of the following:***

☒ All affiliations are listed on the title page of the manuscript.

☐ I or other authors have additional affiliations that we have noted in the "declaration of interests" section of the manuscript and on this form below.

Funding sources

We require that you disclose all funding sources for the research described in this work. ***Please confirm the following:***

☒ All funding sources for this study are listed in the "acknowledgments" section of the manuscript.*

*A small number of front-matter article types do not include an "acknowledgments" section. For these, reporting funding sources is not required.

Competing financial interests

We require that authors disclose any financial interests and any such interests of immediate family members, including financial holdings, professional affiliations, advisory positions, board memberships, receipt of consulting fees, etc., that:

(1) could affect or have the perception of affecting the author's objectivity, *or*
(2) could influence or have the perception of influencing the content of the article.

Please select one of the following:

☒ We, the authors and our immediate family members, have no financial interests to declare.

☐ We, the authors, have noted any financial interests in the "declaration of interests" section of the manuscript and on this form below, and we have noted interests of our immediate family members.

Advisory/management and consulting positions

We require that authors disclose any position, be it a member of a board or advisory committee or a paid consultant, that they have been involved with that is related to this study. We also require that members of our journal advisory boards disclose their position when publishing in that journal. ***Please select one of the following:***

☒ We, the authors and our immediate family members, have no positions to declare and are not members of the journal's advisory board.

☐ The authors and/or their immediate family members have management/advisory or consulting relationships noted in the "declaration of interests" section of the manuscript and on this form below.

Patents

We require that you disclose any patents related to this work by any of the authors or their institutions. ***Please select one of the following:***

☐ We, the authors and our immediate family members, have no related patents to declare.

☐ We, the authors, have a patent related to this work, which is noted in the "declaration of interests" section of the manuscript and on this form below, and we have noted the patents of immediate family members.

Please insert any "declaration of interests" statements in this space. This exact text should also be included in the "declaration of interests" section of the manuscript. If no authors have a competing interest, please insert the text, "The authors declare no competing interests."

The authors declare no competing interests.

☒ **On behalf of all authors, I declare that I have disclosed all competing interests related to this work. If any exist, they have been included in the "declaration of interests" section of the manuscript.**

Erklärung zur Dissertation
gemäß der Promotionsordnung vom 12. März 2020

Diese Erklärung muss in der Dissertation enthalten sein.
(This version must be included in the doctoral thesis)

„Hiermit versichere ich an Eides statt, dass ich die vorliegende Dissertation selbstständig und ohne die Benutzung anderer als der angegebenen Hilfsmittel und Literatur angefertigt habe. Alle Stellen, die wörtlich oder sinngemäß aus veröffentlichten und nicht veröffentlichten Werken dem Wortlaut oder dem Sinn nach entnommen wurden, sind als solche kenntlich gemacht. Ich versichere an Eides statt, dass diese Dissertation noch keiner anderen Fakultät oder Universität zur Prüfung vorgelegen hat; dass sie - abgesehen von unten angegebenen Teilpublikationen und eingebundenen Artikeln und Manuskripten - noch nicht veröffentlicht worden ist sowie, dass ich eine Veröffentlichung der Dissertation vor Abschluss der Promotion nicht ohne Genehmigung des Promotionsausschusses vornehmen werde. Die Bestimmungen dieser Ordnung sind mir bekannt. Darüber hinaus erkläre ich hiermit, dass ich die Ordnung zur Sicherung guter wissenschaftlicher Praxis und zum Umgang mit wissenschaftlichem Fehlverhalten der Universität zu Köln gelesen und sie bei der Durchführung der Dissertation zugrundeliegenden Arbeiten und der schriftlich verfassten Dissertation beachtet habe und verpflichte mich hiermit, die dort genannten Vorgaben bei allen wissenschaftlichen Tätigkeiten zu beachten und umzusetzen. Ich versichere, dass die eingereichte elektronische Fassung der eingereichten Druckfassung vollständig entspricht."

Teilpublikationen:

- A simplified disease resistance assay using YFP expressing Potato Virus X in N. benthamiana revealed a cell death independent immunity of RBA1
- Cytoplasmic Calcium influx mediated by plant MLKLs confers TNL-triggered immunity

Datum, Name und Unterschrift

13.10.2023, Keiichi Hasegawa, Keiichi Hasegawa

Declaration for the doctoral thesis (dissertation)
according to the doctoral regulations published 12th March 2020

Non-official English translation of the "Erklärung zur Dissertation"
(The German version must be included in the doctoral thesis)

"I hereby declare that I have completed the present dissertation independently and without the use of any aids or literature other than those referred to. All passages that have been taken, either literally or in sense, from published and unpublished works, are marked as such. I declare that this dissertation has not been submitted to any other faculty or university; that - apart from the partial publications and included articles and manuscripts listed below - it has not yet been published, and that I will not publish the dissertation before completing my doctorate without the permission of the PhD Committee. I am aware of the terms of the doctoral regulations. In addition, I hereby declare that I am aware of the "Regulations for Safeguarding Good Scientific Practice and Dealing with Scientific Misconduct" of the University of Cologne, and that I have observed them during the work on the thesis project and the written doctoral thesis. I hereby commit myself to observe and implement the guidelines mentioned there in all scientific activities. I assure that the submitted electronic version is identical to the submitted printed version".

Partial publications of the thesis:

- A simplified disease resistance assay using YFP expressing Potato Virus X in N. benthamiana revealed a cell death independent immunity of RBA1
- Cytoplasmic Calcium influx mediated by plant MLKLs confers TNL-triggered immunity

Date, name, and signature

13.10.2023 , Keiichi Hasegawa , Keiichi Hasegawa

Erklärung zum Gesuch um Zulassung zur Promotion

gemäß der Promotionsordnung vom 12. März 2020

1. Zugänglichkeit von Daten und Materialien

Die Dissertation beinhaltet die Gewinnung von Primärdaten oder die Analyse solcher Daten oder die Reproduzierbarkeit der in der Dissertation dargestellten Ergebnisse setzt die Verfügbarkeit von Datenanalysen, Versuchsprotokollen oder Probenmaterial voraus.

☐ Trifft nicht zu

☑ Trifft zu.
In der Dissertation ist dargelegt wie diese Daten und Materialien gesichert und zugänglich sind (entsprechend den Vorgaben des Fachgebiets beziehungsweise der Betreuerin oder des Betreuers).

2. Frühere Promotionsverfahren

Ich habe bereits einen Doktortitel erworben oder ehrenhalber verliehen bekommen.

Oder: Für mich ist an einer anderen Fakultät oder Universität ein Promotionsverfahren eröffnet worden, aber noch nicht abgeschlossen.

Oder: Ich bin in einem Promotionsverfahren gescheitert.

☑ Trifft nicht zu

☐ Zutreffend
Erläuterung:

3. Straftat

Ich bin <u>nicht</u> zu einer vorsätzlichen Straftat verurteilt worden, bei deren Vorbereitung oder Begehung der Status einer Doktorandin oder eines Doktoranden missbraucht wurde.

Ich versichere, alle Angaben wahrheitsgemäß gemacht zu haben.

Datum	Name	Unterschrift
13.10.2023	Keiichi Hasegawa	Keiichi Hasegawa

Declaration on the application for admission to the doctoral examinations
according to the doctoral regulations published 12th March 2020

1. Accessibility of data and materials

The dissertation involves the acquisition of primary data or the analysis of such data or the reproducibility of the results presented in the dissertation requires the availability of data analyses, experimental protocols or sample material.

☐ not applicable

☑ applicable
I have described in the dissertation how these data and materials are secured and accessible (according to the specifications of the subject area or supervisor).

2. Previous doctoral examinations

I have already obtained a doctorate or been awarded an honorary doctoral degree.
Or: A doctoral examination has been opened at another faculty or university, but not yet completed.
Or: I have failed in a doctoral examination.

☑ not applicable

☐ applicable
explanatory note:

3. Criminal offense

I have <u>not</u> been convicted of a deliberate criminal offence in the preparation or commission of which the status as a doctoral candidate was abused.

I declare that all information provided is truthful.

Date	Name	Signature
13.10.2023	Keiichi Hasegawa	Keiichi Hasegawa